

GRANULAR FLOW SIMULATIONS AND EXPERIMENTS FOR THE FOOD INDUSTRY

THÈSE N° 3997 (2007)

PRÉSENTÉE LE 18 JANVIER 2008

À LA FACULTÉ DES SCIENCES DE BASE
CHAIRE DE RECHERCHE OPÉRATIONNELLE SO
PROGRAMME DOCTORAL EN MATHÉMATIQUES

ÉCOLE POLYTECHNIQUE FÉDÉRALE DE LAUSANNE

POUR L'OBTENTION DU GRADE DE DOCTEUR ÈS SCIENCES

PAR

Marco RAMAIOLI

Laurea di Dottore in Ingegneria Chimica, Politecnico di Milano, Italie
et de nationalité italienne

acceptée sur proposition du jury:

Prof. T. Mountford, président du jury

Prof. T. Liebling, directeur de thèse

Prof. C. Ancey, rapporteur

A. Besson, rapporteur

Prof. S. Luding, rapporteur



ÉCOLE POLYTECHNIQUE
FÉDÉRALE DE LAUSANNE

Suisse
2008

Acknowledgements

First, I would like to deeply thank Prof. Th.M.Liebling for his supervision and coaching during the research and the publication of this work. He has been always sharing much more than just science with me, making this PhD a very enriching human experience.

I am thankful to Nestlé for sponsoring this work and for having given me always new opportunities of learning.

I am also extremely thankful to A.Besson. When I was still freshly graduated, he has taught me through his example what being professional means. Some years later he has inspired this work and offered me the opportunity to realize it. He has also "*infected*" me with his passion for traveling and exploring. He did not manage to turn me into a sportsman, but without meeting him I would most probably have become a lazy person by now.

Deep thanks also to all my colleagues at Nestlé PTC Orbe and at EPFL, particularly Ritchie, Laurent, Mathalai and Lionel. Thank you for your day to day support, for all what you taught me and for the nice discussions during which we were almost tempted to change the world.

S.Cerrutti, M.Fetiarison, C.Eminian, C.Kirchofer and A.Petit contributed to this work through their semester or master projects. Supervising them has been for me a very enriching experience.

Much of what I learnt on granular media physics comes from the very open and stimulating atmosphere of the French GdR MIDI. Many thanks to the organizers for their valuable work.

I cannot find words strong enough to say thanks to my parents who always encouraged all my choices as if they were their own. Without the curiosity, the passion for learning and the perseverance that you have always taught me, I would not have started and completed this work.

Final thanks to my friends. You were always there, both to withstand my moments of overflowing energy and to refill my tank when I was almost running on empty. You have been the lenses allowing me to focus and interpret all what has happened in my life. Thanks Carolina, Tanja, Céline, Janine, Cristina, Gautier, Matteo and Teresa, Emma and all the others. Many thanks also to the "*salseras*" friends, Ana, Valerie, Vanessa, Anahide. Even if sometimes only for the duration of a song, you have had the magical power to make me forget work. And naturally also a big thank to my childhood friends, "*I Santangiolini*", and Politecnico friends "*Le Stordite*". You still make me laugh until crying and you are still so close, despite the distance.

Abstract

Granular media are omnipresent in the food industry, whether as raw materials, intermediate or final products. While a lot has been done already in modelling food processes dealing with liquids, solid and gases, very little existed until now in granular flow modelling. The present thesis takes up the challenge of producing realistic granular simulations via DEM and validating them experimentally.

Indeed DEM is one of the most promising granular media simulation approaches, but its wide application is still restrained by the limited number of particles that can be considered and the small collection of comparisons with experimental data. Yet it will be shown in this thesis that DEM is indeed a powerful tool for realistic modelling. We focus on two granular systems relevant to the food industry, for which we carry out in parallel simulations and physical experiments.

First we study the size segregation of cereals in a vertically vibrated cereal box. Three configurations are tested experimentally, and compared with simulations achieving a qualitative validation. The importance of convection rolls and the role of particle and wall friction coefficients is illustrated. We extend the study to the ordering behaviour of elongated grains under vertical vibrations. We show that this phenomenon is intrinsic to elongated grains and takes place also in the absence of help from sidewalls. We study the role of particle geometry and vibration acceleration and we provide a novel interpretation in terms of available kinetic energy and relevant potential energy barriers. Building on these results, we study and interpret the shape segregation of rods from spheres. Experiments and simulations fit together nicely.

The second food application concerns the flow and dosing from vending machine canisters. Our three dimensional DEM simulation unveils a rich microcosm of particle interactions and provides in particular an unexpected explanation for the decreasing dose mass over time. To make this simulation possible we developed an algorithm to detect the collisions between spherical grains and the helix auger. A dosing experiment using glass beads is successfully compared with a simulation in terms of the evolution of both the surface shape and the dosed mass. Good agreement is reached. Further dosing experiments are performed using a cohesive beverage powder. The effect of the dosing screw design on the flow in the canister is quantified and a dosing coil improving the powder withdrawal across the canister is designed and successfully tested.

The quantitative comparisons between experiments and simulations achieved in this work and the insight gained from such simulations show clearly the benefit for the food industry stemming from a coupled use of DEM simulations and experiments.

Keywords

Modelling, Granular flows, Experiments, Validations, Segregation, Ordering, Vibrations, Particles, Dosing.

Résumé

Qu'il s'agisse de matières premières, produits intermédiaires ou produits finis, les milieux granulaires sont omniprésents dans l'industrie alimentaire. Alors que pour les procédés qui traitent les liquides, solides et/ou gaz, la modélisation est déjà bien répandue, très peu a été fait jusqu'à présent dans la modélisation des écoulements granulaires. Cette thèse relève le défi de réaliser des simulations granulaires via DEM et de les valider expérimentalement.

DEM se profile parmi les techniques plus prometteuses pour simuler les flux granulaires. Cependant, sa diffusion est ralentie par le nombre restreint de particules qui peuvent être considérées et par la disponibilité encore trop limitée de comparaisons avec les expériences. Or, il sera montré dans cette thèse que DEM constitue véritablement un puissant outil de simulation réaliste. Nous nous concentrons sur deux systèmes d'intérêt pour l'industrie alimentaire et réalisons en parallèle des simulations et des expériences physiques.

Tout d'abord nous étudions la ségrégation par taille d'un mélange de céréales vibré verticalement. Nous considérons expérimentalement trois configurations que nous comparons avec des simulations, obtenant ainsi une validation qualitative. L'importance des flux convectifs et le rôle des coefficients de frottement sont analysés. L'extension de cet étude à la verticalisation des grains allongés lors d'une vibration verticale constitue un des résultats principaux de cette thèse. Nous montrons que ce phénomène est intrinsèquement lié à la forme allongée est a lieu même sans l'aide des parois latérales. Nous étudions l'effet de la géométrie des particules et de l'intensité des vibrations et développons une nouvelle interprétation des phénomènes basée sur l'énergie cinétique disponible et les barrières d'énergie potentielle rencontrées par les grains. Nous utilisons ultérieurement ces résultats pour étudier et interpréter la ségrégation par forme de mélanges de sphères et bâtonnets. L'accord entre expériences et simulations est très bon.

La deuxième application alimentaire concerne le flux granulaire à l'intérieur d'un bac distributeur de boissons en poudre. Notre simulation DEM tridimensionnelle dévoile le riche microcosme des interactions entre les particules et suggère une explication inattendue de la diminution de la masse dosée au cours du temps. Pour réaliser cette simulation nous avons développé un algorithme pour identifier les contacts entre les grains sphériques et la vis doseuse en forme d'hélice. Une expérience de dosage de billes de verre est comparée avec succès avec la simulation, pour ce qui concerne l'évolution de la surface du produit et de la masse dosée. L'accord est très bon. D'autres expériences utilisant un produit alimentaire en poudre au comportement cohésif, ont été réalisées. L'effet de la géométrie de la vis doseuse sur le flux de la poudre dans le bac a été étudié, permettant de développer une vis doseuse qui améliore l'uniformité d'extraction de la poudre.

Les validations quantitatives entre expériences et simulations obtenues dans le cadre de ce travail et la compréhension que ces simulations ont permis de développer, montrent clairement les avantages que l'industrie agro-alimentaire peut obtenir d'une utilisation couplée des simulations DEM et des expériences.

Mots-clés

Modélisation, Ecoulements Granulaires, Expériences, Validations, Ségrégation, Vibrations, Particules, Dosage.

Contents

Introduction	1
Welcome to the beautiful world of granular media!	1
Outline of this work	3
1 ROSO-EPFL non spherical DEM code	5
1.1 Physical contact model	7
1.2 Contact between a grain and a wall	9
1.3 Updating the state of the medium	10
2 Spherical cereals shaken in a cereal box	11
2.1 Summary	11
2.2 Introduction	12
2.3 A food application: size segregation of spherical cereals in a vibrated box	15
2.4 Experiments	15
2.4.1 Methodology	15
2.4.2 Size segregation results	16
2.4.3 Some observations on convection in mono-sized cereals.	17
2.4.4 Impact tests to assess cereal restitution coefficient.	21
2.4.5 Inferring friction properties.	25
2.5 DEM simulations.	26
2.5.1 Size segregation.	26
2.5.2 Convection in mono-sized cereals.	27
2.6 Next steps	31
2.7 Conclusions	31

3	On the vertical ordering of rods vibrated vertically.	33
3.1	Summary	33
3.2	Introduction	34
3.3	Some preliminary experiments	34
3.4	DEM simulation set-up	38
3.5	DEM simulation results	38
3.6	Is vertical ordering linked to void sizes?	41
3.7	Potential energy barriers	45
3.8	Conclusions	46
4	Shape segregation of mixtures of rods and spheres vibrated vertically.	49
4.1	Summary	49
4.2	Introduction	49
4.3	Simulating shape segregation of iso-volume particles.	50
4.4	Simulation of the shape segregation of particles of different volumes.	54
4.5	Comparison with experiments	54
4.5.1	Experimental setup	54
4.5.2	DEM simulations setup	56
4.5.3	Results	56
4.6	Conclusions	58
5	Flow in vending machine canisters and dosage	61
5.1	Summary	61
5.2	Introduction	61
5.3	Flow and dosage experiments.	62
5.3.1	Experimental set-up	62
5.3.2	Experimental results using a cohesive beverage powder	64
5.4	Angle of repose test and its relevance to the canister dosage	67
5.5	Flow and dosage simulations	68

5.5.1	Contact detection between the dosing coil and spherical grains	68
5.5.2	Simulation set-up	69
5.5.3	Comparing experiments using glass beads and simulations	70
5.5.4	What more can simulation tell us?	73
5.6	Next steps	77
5.7	Conclusions	78
	Conclusions	79
	Bibliography	79

Introduction

Welcome to the beautiful world of granular media!

I could start this thesis report by highlighting the paramount importance of granular media in both industrial and natural environments. However, many reviews (Dur00a),(dG99), (JN92), (JN96), (Cam06) start by describing their importance much better than what I could hope doing myself here. Furthermore, the reader will find in the following pages so many facts, that he can probably excuse me and maybe be also relieved if I start by describing rather my own feelings and emotions and the little background that brought me to this fascinating field of research.

As many Italians, I started very early my summer schools on sand, its more or less dry forms and its fabulous properties as ephemeral building material. Refresher classes were held punctually each summer to better consolidate and develop a solid background of practical skills. In parallel to this experience, another passion that is somehow related to this area was animating my childhood: magic tricks. I used to love these little games that were puzzling both myself and the audience, going against the common intuition.

Many years later came the serious stuff: my chemical engineering studies and the interest for modelling heat, mass transfer and reaction kinetics in industrial processes. But also the amazing mechanics teaching of Prof.Cappi in the "Scienza delle costruzioni" class and finally the work on packed bed reactors with Prof. Morbidelli (GRVM03) during my diploma project. Beads were there already, albeit motionless.

Upon starting working as a modelling research and development engineer at Nestlé, I was straight away given a project involving deformable packed bed of grains, which I tackled with the only tool available in my background at that time, namely continuous mechanics. This was the first sign of what turned out to be a leitmotiv during these years in industry: despite the abundance of powder products and related issues, many people were turning away from this area, somehow labelling it as "quicksand". Indeed, all the tools and methods that allow designing robustly processes involving liquids or gases, hardly have an equivalent for powders, at least in industry. I first came in contact with the technical know-how of the engineering bulk handling community and then, through Dr. M.Sawley and Prof.Liebling to MD-DEM, which was one of the few modelling techniques to simulate granular flows emerging from academia. This technique was recognized as a promising tool for the food industry by A.Besson, who strongly supported its development.

Beside these episodes that were accumulating rational reasons for developing a competence in this area, an event brought me in contact with the puzzling physics of granular media: the

science exhibit "Le sable" (Sab) held in Neuchatel's natural science museum. In particular, the experiment demonstrating Reynold's dilatancy principle, shown on the right-hand side of picture 1, made me feel as astonished as the children in the picture. A bag full of sand saturated with water. The water level is clearly visible in the capillary tube. When the bag is squeezed, contrary to intuition, the liquid in the tube drops! Isn't this an amazing "magic trick"?

The surprise and emotion even increased when I understood that the same phenomenon ruling this experiment was also explaining the apparent drying of the wet sand on the splash zone of the beach, upon stepping on it. There were definitely enough motivations and enough passion to justify venturing in a PhD!



Figure 1: Counter intuitive experiment on Reynold's dilatancy during the exposition "Sable" at Muséum d'histoire naturelle, Neuchatel, Switzerland.

Getting progressively more familiar with granular media physics did not reduce the room for astonishment. When I first touched with hand the size segregation upon vibration and the Brazil nut effect, I could not retain myself from spreading this last (and erudite) magic trick among colleagues and friends. And the best thing about these adult magic tricks is that there is no trick! Well... at least that was my first belief upon reading the first simple explanations based on convection rolls and void filling (RPSS86). Since then, I progressively discovered the richness of this phenomenon and I started wondering again about finding the trick.

Granular media are indeed complex and often counterintuitive. Both these characteristics come from some essential features of this class of materials. They are athermal, non ergodic, non-equilibrium dissipative systems. As a consequence, highly history dependent. In front of the complexity of the global puzzle of granular media physics, any couple of pieces that scientists manage to match still pushes me to express a big WOW. One example is certainly the work on Brazil Nut and Reverse Brazil Nut effect, by Hong (Hon99), (HQL01) and all the scientists who followed (BEKR03). This topic will be described more in detail in paragraph 2.2. Another work that amazed me is the quest toward a granular rheology, coming from the consolidation work of O.Pouliquen and the french GdR MIDI (MiD04). Of course I will never forget either the emotion arising the first time I attended a class given by J.J.Moreau on the memory of MD

simulation with respect to NSCD techniques in Paris, nor H.Hermann presentation on dune motion and their coalescence in Stuttgart. And the list could be much longer.

What is source of fun about granular media on a beach, like the arching that allows to build fancy tunnels, does not make anybody laugh when it blocks industrial process and causes important economic losses. As a result, we are witnessing some diffusion of DEM within the process industry with large scale applications, beside the classical silo applications, like (CS02), (Cle04), (CSM06), (RGLB06), (SCM06) or with a development of the models to be applied for simulating fruit mechanics as in (TRDB03),(vZTD⁺06b), (vZTD⁺06a).

Outline of this work

This report starts by introducing in chapter 1 the DEM code developed by my predecessors at ROSO-EPFL and particularly the way it treats spherocylindrical grains.

The size segregation of cereals in a vertically vibrated cereal box is then studied in chapter 2. Three configurations are tested experimentally. A qualitative comparison with simulations is achieved for one of them. The importance of convection rolls and the role of particle and wall friction coefficients is illustrated.

We then extend the study in chapter 3 to the ordering behaviour of elongated grains under vertical vibrations. We show that this phenomenon is intrinsic to elongated grain and takes place also in the absence of help from sidewalls. We study the role of particle geometry and vibration acceleration and we provide an interpretation in terms of available kinetic energy and relevant potential energy barriers.

Building on these results, we then focus in chapter 4 on the shape segregation of rods from spheres. Experiments and simulations fit together nicely.

The flow and dosing from vending machine canisters is the second food application, treated in chapter 5. Dosing experiments using a vending machine canister are performed using a cohesive beverage powder and a mixture of glass beads. The effect of the dosing screw design on the flow in the canister is measured and a dosing coil improving the powder withdrawal across the canister is designed and successfully tested. An algorithm to detect the collisions between spherical grains and the helix auger is developed, which allows performing three-dimensional DEM simulations of the flow in the canister. A dosing experiment using glass beads is successfully compared with a simulation in terms of the evolution of both the shape of the surface and the dosed mass. Good agreement is reached. The flow in the canister simulation is studied, uncovering an unexpected explanation for the decreasing dose mass over time.

Conclusions and bibliography close this thesis.

Chapter 1

ROSO-EPFL non spherical DEM code

This section describes ROSO-EPFL DEM code and in particular its version capable of handling spherocylinders, developed by L.Pournin and M.Tsukahara and published in (PWT⁺05).

A pioneer article by Cundall introduced soft sphere distinct element simulation models (CS79). The main contribution of that model was how it handles contacts experienced by particles. It consists in considering pairs of spheres in contact as constituted of linear springs and dashpots generating forces both normal and tangential to the contact and similarly for the moments. In (M96) and later in (FL02) this model was implemented using power diagrams for particle contact detection, thereby yielding a particularly efficient code. The contact force models were discussed in (PLM02), where the authors point at problems with the dissipative behavior of the modeled media and propose a way to alleviate them. ROSO DEM code contains an extension of the distinct element method able to handle spherocylinder assemblies. A spherocylinder is defined as follows. Let σ be a line segment in \mathbb{R}^3 and δ a positive real. The spherocylinder of shaft σ and diameter δ is the set of points whose distance to σ is smaller or equal to $\delta/2$ (Figure 1.1). The length of σ is called λ as on figure 1.1. In other words a spherocylinder is the Minkowski sum of the line segment σ with a ball of diameter δ .

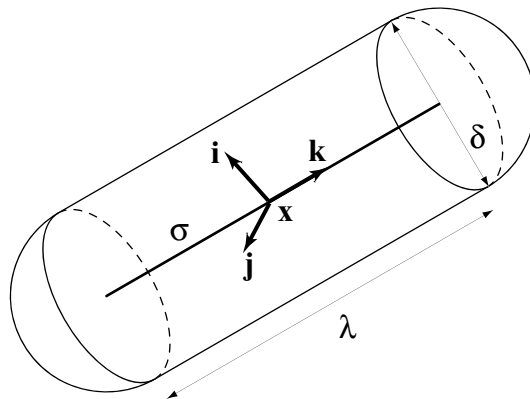


Figure 1.1: A spherocylinder of characteristic diameter δ and length λ and the referential.

The distinct element method iteratively updates the state of the medium, whose geometrical constituents are grains and walls. At every time-step, the contacts between the elements are

detected and values for the resulting contact forces are calculated. The model assumes those forces remain constant for the duration Δt of the time-step. The evolution of the state of the medium is then computed by numerical integration of Newton's laws of motion for each individual grain. The process is repeated at the next step with this new configuration. A rough flow chart of the simulation process is given in Figure 1.2.

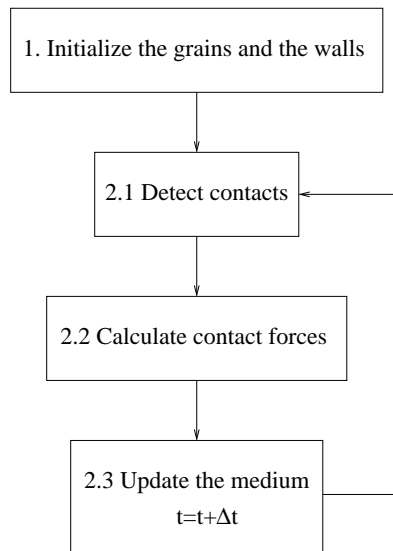


Figure 1.2: Simulation algorithm

A main issue encountered when simulating granular media is the choice of a suited physical contact model. In DEM, grains are assumed to be homogeneous, deformable solids. A grain which is in contact with others or with a wall experiences deformation. In general, precise determination of the contact deformation is not trivial. However, as stated in (CS79), the behavior of a granular medium as a whole is more conditioned by the motions of the particles than to their deformations which are comparatively small. Hence, precise knowledge of deformation is not necessary for a good approximation of mechanical behavior of the medium, for as long as the forces are realistic. In the model, a contact will occur whenever two objects (two grains or a grain and a wall) overlap. This overlap is taken as a measure of the deformation of the particles at the contact point (see figure 1.3). The contact force is then modeled by a force-overlap relation, taking into account the overlap and its time derivative. A motivation to model grains with spherocylinders is that an overlap can easily be defined with this particular shape. Two spheres overlap when the distance between the grain centers is smaller than the sum of their radii. Analogously, two spherocylinders will overlap when the distance between their shafts is smaller than the sum of their radii.

As shown in Figure 1.2, at every iteration of a simulation, one must detect all the contacts between pairs of grains. One first possibility is to check for contacts between each pair of grains. This leads to contact detection in $O(n^2)$ time where n is the number of grains. The complexity of detection can be reduced by considering subdivisions of the simulation space so that grains that are in contact may only be found in adjacent cells. However, one must track the grains that are in each cell. Quadtrees are successive subdivisions of the simulation space until there is no more than one grain per cell. A very efficient algorithm for detecting contacts uses dynamic triangulations so that grains which are in contact are connected by an edge (M96; FL02).

Implementation of the model was based on the program previously developed by the authors (FL02) for the simulation of spherical grains. Pournin developed a triangulation-based contact detection for spherocylinders and later an extension to more complex particle shapes (Pou05), (PL05). However, a spatial sorting algorithm was preferred to obtain the results reported in next chapters. This method consists in enclosing each spherocylinder in a ball and testing those pairs of spherocylinders for contacts whose enclosing balls intersect. In order to find the pairs of enclosing balls which intersect, we chose a naive method which has the virtue of being very simple. While not adequate for large grain populations, this method is quite suited for our purposes since it allows to treat cases with 1000 to 2000 grains without much overhead. Taking some direction d as the altitude, it consists in sorting the balls in decreasing order with respect to their highest point. They are then scanned in this order and a given ball b is only tested for contact with those balls whose highest point lies above the lowest point of b . As the balls are sorted, we obtain a mean complexity of $O(n^{\frac{5}{3}})$, which is nearly quadratic but reveals itself as helpful in practical cases.

1.1 Physical contact model

Consider two spherocylindrical grains G_i , $i = 1, 2$ (given by their characteristic diameter δ_i , half-shafts a_i , position x_i of the mass center, shaft σ_i , linear velocity v_i and spin vector ω_i) experiencing a contact (Figure 1.3).

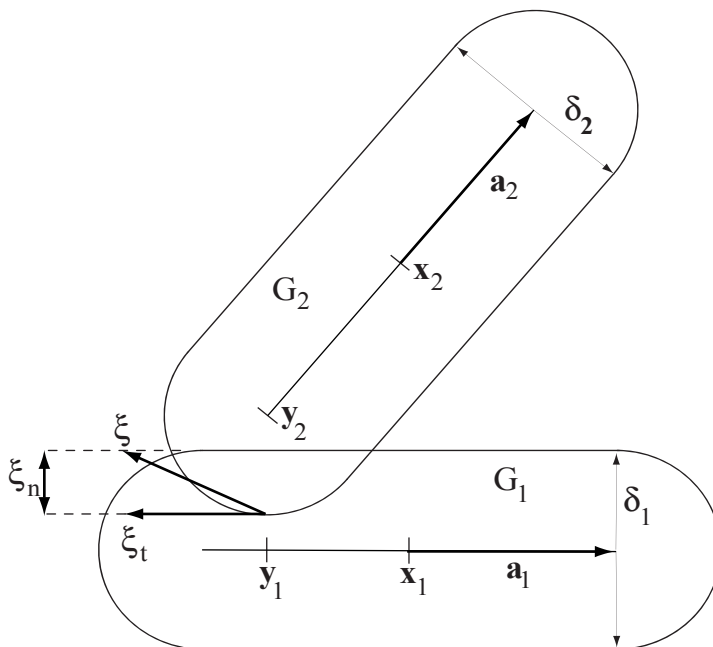


Figure 1.3: A contact between two spherocylinders

Let $f_{G_1 \rightarrow G_2}$ and $f_{G_2 \rightarrow G_1}$ be the forces applied by G_1 on G_2 and by G_2 on G_1 respectively. Newton's third law gives $f_{G_1 \rightarrow G_2} = -f_{G_2 \rightarrow G_1}$, and we denote $f = f_{G_1 \rightarrow G_2}$. In order to model those contact forces and give their application points on either grain, we need to define some parameters which will quantify the geometry of the contact area. In particular, we need to find two points $y_1 \in \sigma_1$ and $y_2 \in \sigma_2$ for which the shortest distance between σ_1 and σ_2 is attained, that is, $\|y_1 - y_2\| = d(\sigma_1, \sigma_2)$.

Let us first consider the case when the shafts σ_1 and σ_2 of G_1 and G_2 are in general position. In this case, the pair (y_1, y_2) is unique. Let $\psi_{\sigma_1} : s \mapsto x_1 + sa_1$ for $s \in [-1, 1]$ and $\psi_{\sigma_2} : t \mapsto x_2 + ta_2$ for $t \in [-1, 1]$ be parametrizations of σ_1 and σ_2 . We suppose that the shafts are non-degenerate, that is to say $a_1 \neq 0$ and $a_2 \neq 0$ otherwise the computation is either trivial or reduces to finding the point on a segment closest to another point. Finding y_1 and y_2 amounts to minimizing $\|\psi_{\sigma_1}(s) - \psi_{\sigma_2}(t)\|^2$ for $(s, t) \in [-1, 1]^2$. A solution to this optimization problem was previously derived (Lum85; VL94). Letting s^* and t^* be the optimal solution, y_1 and y_2 are given by : $y_1 = \psi_{\sigma_1}(s^*)$ and $y_2 = \psi_{\sigma_2}(t^*)$. Here is the procedure we use :

Input : x_1, a_1, x_2, a_2

Output: $(s^*, t^*) \in [-1, 1]^2$ so that $\|\sigma_1(s^*) - \sigma_2(t^*)\|$ is minimal.

1. Compute $a = a_1^2, b = -a_1 a_2, c = a_2^2, d = a_1(x_1 - x_2), e = -a_2(x_1 - x_2), \delta = ac - b^2$.
2. Compute $t = \alpha(\frac{bd - ae}{\delta}), s = \alpha(\frac{-bt - d}{a})$. If $\frac{-bt - d}{a} \notin [-1, 1]$, compute $t = \alpha(\frac{-bs - e}{c})$.
 $(s^*, t^*) = (s, t)$. Stop.

Where α is defined as :

$$\alpha(u) = \begin{cases} -1 & \text{if } u \leq -1 \\ u & \text{if } u \in]-1, 1[\\ 1 & \text{if } u \geq 1 \end{cases} \quad (1.1)$$

Now suppose σ_1 and σ_2 are parallel. In this case, we may have several choices for the pair (y_1, y_2) . Let $p : \sigma_1 \rightarrow \mathcal{D}$ be the projection of σ_1 on the line \mathcal{D} supporting segment σ_2 . If $p(\sigma_1) \cap \sigma_2 = \emptyset$ then the y_2 is the point on σ_2 closest to $p(\sigma_1)$ and y_1 is the point on σ_1 whose image under p is the point of $p(\sigma_1)$ closest to σ_2 . If $p(\sigma_1) \cap \sigma_2 \neq \emptyset$, we choose y_2 as the center of $p(\sigma_1) \cap \sigma_2$ and y_1 as the point on σ_1 which projects on y_2 .

Knowing y_1 and y_2 , we define the unit vector normal to the contact as :

$$u_n = \frac{y_2 - y_1}{\|y_2 - y_1\|} \quad (1.2)$$

For tangent spherocylinders, u_n is the normal vector to the tangent plane. We define the application points of forces $f_{G_1 \rightarrow G_2}$ and $f_{G_2 \rightarrow G_1}$ as the intersections of the segment $[y_1, y_2]$ with the boundaries of G_2 and G_1 , that is respectively $c_2 = y_2 - r_2 u_n$ and $c_1 = y_1 + r_1 u_n$. The relative velocity v_r at the contact is introduced as the velocity of c_2 with respect to c_1 ,

$$v_r = v_2 - v_1 - (y_2 - x_2 - r_2 u_n) \wedge \omega_2 + (y_1 - x_1 + r_1 u_n) \wedge \omega_1 \quad (1.3)$$

The overlap ξ is defined as the solution of the differential equation

$$\dot{\xi} = -v_r \quad (1.4)$$

for which $\xi = 0$ when the contact begins. The normal and tangential overlaps are the projections of ξ on u_n and on the plane perpendicular to u_n , $\xi_n = \xi \cdot u_n$ and $\xi_t = \xi - (\xi \cdot u_n)u_n$. We assume that u_n is constant during a contact. Then the time derivatives of the normal and tangential overlaps are

$$\dot{\xi}_n = -v_r \cdot u_n \quad (1.5)$$

$$\dot{\xi}_t = -v_r + (v_r \cdot u_n)u_n. \quad (1.6)$$

Equations (1.2), (1.3) and (1.5) yield

$$\xi_n = r_1 + r_2 - \|y_2 - y_1\| \quad (1.7)$$

which expresses the normal overlap as the length of the segment joining c_1 and c_2 . Practically, throughout a contact, the time derivatives of both overlaps and the normal overlap are calculated by direct application of equations (1.5), (1.6) and (1.7). On the other hand, the tangential overlap is computed by numerical integration of (1.6).

The components of f parallel and perpendicular to u_n , the normal force f_n and the tangential force f_t , are calculated by a force-overlap relation. In the program, the force-overlap relation used is the linear viscoelastic model first proposed in (CS79), $f_n = (k_n \xi_n + c_n \dot{\xi}_n)u_n$ and $f_t = k_t \xi_t + c_t \dot{\xi}_t$. We take friction into account by replacing f_t by $f_t = \mu \frac{\|f_n\|}{\|f_t\|} f_t$ whenever $\|f_t\| > \mu \|f_n\|$, where μ is the Coulomb coefficient. More details on that kind of force models, and especially about the way k_n and c_n may be chosen is available in (PLM02). For the sake of simplicity, this model takes no account of the relative orientation of the contacting grains. While the validity of this approximation should certainly be further analysed, the simulation results we obtain speak in its favour.

1.2 Contact between a grain and a wall

Two types of walls are simulated with spherocylinders: planar and cylindrical walls. In the simulations performed, the shafts of the grains stay in one half-space defined by each plane and in the cylindrical space defined by each cylindrical wall. Under these conditions, a grain G is in contact with a wall if and only if the distance from one or both ends of its shaft to the wall is smaller or equal to the radius of the grain. Suppose this takes place for an end e . Let d be the normal to the wall and passing through e . We define the application points of the forces acting on the grain and the wall as the intersections of d with the boundary of the grain and with the wall. The contact force is calculated similarly to the contact between two grains. When overlaps exist at both ends, for example if the grain is parallel to the wall, the contact is modeled by two forces.

A much broader variety of walls can be simulated in the ROSO-EPFL DEM code using spherical grains. Many of these walls are used in chapter 5, where a novel algorithm is introduced to detect contacts between spheres and a helix coil.

1.3 Updating the state of the medium

For each contact, applying the physical contact model yields expressions for the forces that act on the grains and the walls and their application points. Let G be a grain as that of figure 1.1, with mass m , inertia tensor I and subject to a set of forces f_1, \dots, f_n . Suppose that force f_i has application point c_i . The laws of motion for G are

$$m\ddot{x} = mg + f_1 + \dots + f_n \quad (1.8)$$

$$I\dot{\omega} = (c_1 - x) \wedge f_1 + \dots + (c_n - x) \wedge f_n \quad (1.9)$$

In the model, the motion of the particles is updated individually by numerical integration of equations (1.8) and (1.9). In the program, the forward Euler method is used for these integrations. The orientation of the particles is represented using quaternions.

For spherocylindrical grains, the inertia tensor expressed in the referential (x, i, j, k) of figure 1.1 is a diagonal matrix, whose diagonal elements I_{ii} , I_{jj} and I_{kk} are given by

$$\begin{cases} I_{ii} &= \frac{1}{48}\pi\rho\delta^2\lambda^3 + \frac{3}{64}\pi\rho\delta^4\lambda + \frac{1}{60}\pi\rho\delta^5 + \frac{1}{24}\pi\rho\delta^3\lambda^2 \\ I_{jj} &= I_{ii} \\ I_{kk} &= \frac{1}{32}\pi\rho\delta^4\lambda + \frac{1}{60}\pi\rho\delta^5 \end{cases} \quad (1.10)$$

Chapter 2

Spherical cereals shaken in a cereal box

2.1 Summary

The behaviour of (almost) spherical breakfast cereals in a vertically shaken cereal box geometry is studied both experimentally and numerically. Size segregation experiments on a binary mixture are run at 12.5 Hz frequency and 2g peak acceleration, varying the box configuration. In all three configurations the bigger particles segregate to the surface, following the classical Brazil nut's effect. Qualitatively the fraction of smaller particles increases monotonically from top to bottom in the plexiglass box, while it shows a maximum for the "bag in box" configuration. Quantitatively, the segregation is very low at the bottom of the box for the "bag in box" configuration. A third configuration is tested to gain more insight on whether wall friction is the only cause of difference between the other two configurations. It is argued that beside the different friction, the bag has also a damping effect that dissipates part of the vibration energy.

Under same vibration conditions, experiments with a single particle size show the development of convection rolls within the box. In the "bag in box" configuration, convection does not involve the bottom of the box which can justify the lower segregation observed for the same configuration using the binary mixture. The particle restitution coefficient is evaluated experimentally, while the particle(-particle) and wall(-particle) friction coefficients are used as DEM degrees of freedom to try to match simulations and experiments. The experimental trends can be qualitatively reproduced, but quantitatively both segregation and convection are stronger in the simulations than in the experiments. Two sets of parameter that give qualitative agreement are identified for both the plexiglass box and the "bag in box" configuration. The convection observed is always directed downwards along the smallest sidewalls. The interplay between wall and particle friction conditions the convection flow field within the box. At high particle friction and low wall friction, the convection pattern tends to become two dimensional, with little variation across the smallest dimension of the box. Using same frictions or higher wall friction, the convective flux is downwards also at the largest wall, with an upward stream at the centre of the box.

2.2 Introduction

As an appetizer for the rest of this work, what better than revisiting a classical, but evergreen area of investigation such as the behaviour of vibrated spherical media? Despite the fact that compaction, convection and size segregation in vibrated granular media have been widely studied using different materials as seeds, metal or glass beads and through modelling, still only few well established universal conclusions are able to unify some of the available data. In front of the enormous amount of research published in this domain, proposing a comprehensive literature review becomes a gigantic endeavour. Without such an ambition, the author would like to present in this section a selection of articles relevant for this application, ordered as to cover respectively fluidisation, compaction, convection and finally size and density segregation.

Early studies on fluidisation by vibration from (ESD90) identified a threshold acceleration of 1.2g above which a medium is fluidised. Luding (LHB94) identified the way the increase in height of the centre of mass of a vibrated medium depends on the restitution coefficient, number of particles and maximum velocity of the exciting plate. Van Door (vB97) used the simple inelastic ball bouncing model (IBBM) to interpret many features of a fluidised vibrated medium.

Many review papers on compaction and size segregation compiled the continuously evolving state of the art (JN96), (RBZL02), (Kud04). In a milestone paper on compaction, Nowak et al. (NKBN⁺98) (NKP⁺97) showed that compaction is logarithmically slow in time and can lead to irreversible or reversible density variation depending on the acceleration of the system. Richard et al. (RND⁺05a) recently published a review on granular compaction. Ribière (RRP⁺07) recently continued Nowak's work exploring different vibration patterns. Among many different studies coupling DEM and experiments on compaction, Matchett (MYOK00) compared experimental and DEM energy dissipation in vibrated granular media and Zhang (ZRV04) investigated the spatial evolution of the kinetic energy of vibrated grains.

The onset and characteristics of convection roll in vibrated granular media has also been studied extensively. The threshold acceleration to generate convection was studied both experimentally and numerically (Tag92) and found to be close to the fluidisation threshold. Care has to be taken when predicting numerically the onset of convection while decreasing artificially the collision time to accelerate the calculations (LCB⁺94). Convection roll direction is influenced by the relative value of wall and particle friction coefficients (LR97). High particle friction and low wall friction leading to downward motion at the centre, while the opposite and most common pattern is observed for same frictions or particle friction lower than wall friction. The same authors find a dependence of the onset of convection not only on the acceleration but also on the ratio between the amplitude and the particle diameter. Several papers (Lee94) (GHS92) (Tag92) explain the convection roll direction in terms of a difference in the medium density during its downward and upward motion relatively to sidewalls. Aoki (AAMW96) studied the transitions between downward and upward convection by increasing acceleration at constant frequency in rectangular boxes as well as the transitions to multiple convection rolls. A significant recent progress was triggered by Rodríguez-Liñán et Nahmad-Molinari (RLNM06). They analysed the relative motion of a vibrated medium with respect to the vibrated container and introduced as control parameter the excess amplitude as the difference between the vibration amplitude and the critical amplitude at the onset of convection. The average bed-plate distancing velocity scales with the square of the excess amplitude. Measurements showed that the convection speed

close to the wall follows the same scaling too. Convection would therefore be directly related to the shear stress exerted by the walls on the bed during the distancing part of the vibration cycle. This shear stress cannot be compensated in the approaching part of the cycle due to the lower density of the medium in this phase.

Knight characterised the convective flow field in a cylinder and showed experimentally (Kni97) that more generally the convection roll direction can be influenced by varying the orientation of sidewalls. Grossman (Gro97) reproduced these findings via simulation.

Air pressure can also influence granular convection, particularly for particles below 1mm diameter, deep bed and large vibration amplitude (PVB95).

Besides convection induced by shearing due to friction and boundaries, another form of convection can exist in strongly agitated granular media, which is analogous to the "natural" (using a chemical engineering term) or Rayleigh-Bernard (using a physical term) convection in fluids (RRCV00). The temperature profile within a vibrated medium and thus the resulting convection, were shown to be controlled by the average energy loss per collision, rather than friction or restitution coefficient alone (RSG⁺05).

Generally two regimes, which influence segregation, are identified in vibrated media. In the "vibro-fluidised" regime, particles mainly undergo binary collisions, their energy is sufficient to widely explore the configuration space and buoyancy is proposed to explain segregation. In the "dense" or "jammed" regime, enduring contacts occur and different local mechanisms such as void-filling, convection trap, and inertia are proposed to explain segregation. The link between convection and segregation is discussed among others by Herrmann and Luding (HL98). Big particles tend generally to emerge to the surface when a mixture of small and big particles is shaken vertically. The first qualitative interpretation of this phenomenon, the so-called Brazil-Nut effect (BN), was given by Rosato et al. (RSPS87) (RPSS86) using MC simulations. Experiments and modelling have shown that this phenomenon can be explained in terms of a geometrical void-filling mechanism (Ris00a) and follows different patterns and dynamics depending on the presence or absence of convective streams. When vibration is sufficiently energetic to induce convection rolls, upward and downward streams form in the system. The upward stream can be located at the wall or at the centre of the system depending on wall friction and inclination. If walls are vertical and wall friction sufficiently strong, the upward stream is located at the centre. In this case small and big particles are conveyed to the surface where segregation occurs because big particles are trapped, whereas small particles are entrained back in the bulk by downward streams. When convection does not take place, big particles ascend because small particles can more easily fill the voids left by big particles than the opposite. Acceleration conditions the size of the voids appearing in the medium and thus segregation (HY97). The interplay of density and size in the segregation in vibrated systems has been studied recently by a number of authors and showed a very rich behaviour. When the constituents of a mixture vary by both density and size, segregation can give rise to either the usual Brazil-nut effect (BN) or the opposite Reverse Brazil-nut effect (RBN), with big particles sinking to the bottom of the mixture. Shinbrot and Muzzio (SM98) first observed RBN and reported the counterintuitive phenomenon that a large heavy intruder can raise and a large light intruder can sink in a mixture. Using statistical mechanics Hong et al. (Hon99) and Quinn et al. (QH00), predicted the critical temperature (T_C) for the onset of condensation for rigid spheres.

Whenever a mixture is given sufficient energy to fluidize only the smallest particles:

$$T_C^{Small} < T_{Gran} < T_C^{Big} \quad (2.1)$$

where:

$$T_{Gran} \propto \frac{1}{N} \sum_i \left(\frac{m_i}{2} (v_i - \bar{v})^2 \right) \quad (2.2)$$

$$\bar{v} = \frac{1}{N} \sum_i (v_i) \quad (2.3)$$

and the condensation of biggest particles prevails on the percolation of the smallest particles in the voids of the biggest:

$$\frac{d_{Big}}{d_{Small}} > \frac{\rho_{Small}}{\rho_{Big}} \quad (2.4)$$

RBN occurs, i.e. big particles tend to sink below smaller particles instead of raising. MD simulation of mixtures vibrated with uniform granular temperature and white noise drive by Hong et al. (HQL01) confirmed the previous frontier between BN and RBN as also summarised in (MLNJ01). Breu (BEKR03) experimentally confirmed the previous prediction for a great number of mixtures. Mixtures for which this prediction were not confirmed were thought not to satisfy the hypothesis of rigid spheres.

Fine particles of same size and different densities were found to segregate in a vibrated mixture due to the air entrainment (BKS02). Biswas (BSSK03) reproduced the main features of these experiments using MD simulation. Yan (YSH⁺03) considers specifically RBN. Huerta (HRS04) observed a marked influence of frequency on occurrence of BN or RBN at same sinusoidal peak acceleration. At higher frequency (50 Hz) ordinary buoyancy prevails with large heavy intruders sinking and large light intruders raising. At lower frequency (5 Hz) BN or RBN take place depending on intruder size and density, driven by inertia (NMCCRS03) or convection.

The overall puzzle is very complex. Still recently a review in Nature (Shi04) by Shinbrot, who first reported RBN, emphasized the state-of-the-art saying: "We find ourselves facing the situation anticipated by Mark Twain: The researches of many commentators have already thrown so much darkness on this subject, and it is probable that, if they continue, we shall soon know nothing about it".

A recent paper by Pica Ciamarra (CVF⁺06) draws precise boundaries between conditions leading to BN segregation, mixing or to RBN segregation. Another recent study by Schröter (SUK⁺06) analyses the relevance of the mechanisms proposed to explain the occurrence of either BN or RBN at different driving frequencies and amplitudes. Few weeks before completion of this thesis manuscript an intriguing spontaneous transition from a RBN to a BN due to the ageing of the particles being vibrated was reported by Ulrich et al. (USS07).

Many studies consider also segregation of a monolayer of grains under either the swirling gold-seeker-like motion (AKR01) or horizontal motion (SBKR05).

Table 2.1: Property of the mixture used for the size segregation tests.

	Big	Mini
Diameter [mm]	11.8	7.2
Density [kg/l]	0.311	0.345
Weight Fraction [%]	50	50

2.3 A food application: size segregation of spherical cereals in a vibrated box

Breakfast cereals are often cited as a classical "in-home" system where one can experience segregation induced by vibration. Some authors (MK02) suggest even ironically to shake Muesli before serving oneself to get the best bits!

The phenomenon unfortunately occurs also excluding such deliberate practices and indeed vibrations during manufacturing and transport of breakfast cereals can cause undesired segregation. The goal of these tests is to study a reference binary mixture of cereals to:

1. Observe segregation, better understand its mechanism and quantify the effect of most significant parameters.
2. Compare experiments and DEM simulations quantitatively.

2.4 Experiments

2.4.1 Methodology

The properties of the mixture used for the size segregation tests presented in this chapter are summarised in table 2.1.

Testing followed this methodology:

1. Four separate layers are prepared by weighing the two constituents;
2. Each layer is mixed separately and then introduced into the cereal box;
3. The box is vibrated sinusoidally at 12.5 Hz frequency and 2g peak acceleration for the desired duration;
4. The top of the mixture is blocked with a lid to avoid product spilling. The box is then turned and one lateral wall is pulled out.
5. The mixture is separated into four vertical layers, from the bottom to the top of the medium. Each layer is then sieved into the two constituents which are weighed.

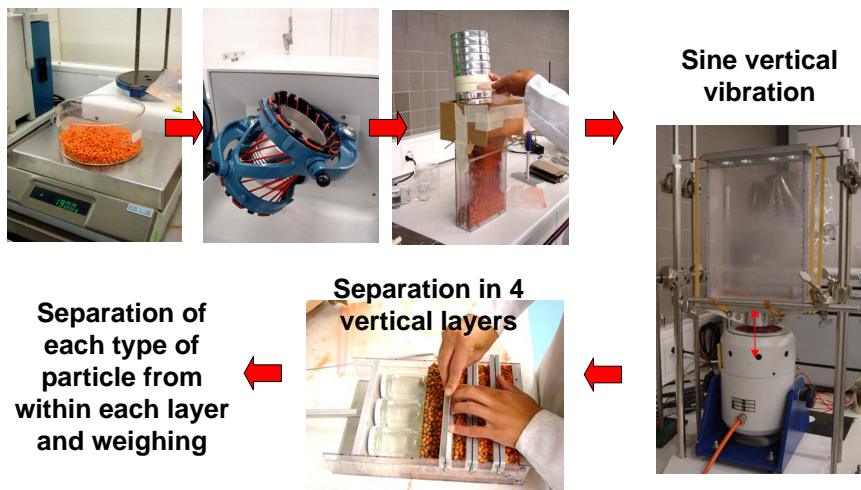


Figure 2.1: Procedure followed during the size segregation tests.

Table 2.2: Size segregation experiments varying the cereal box configuration.

Exp.	Configuration	Time [min]	Repetitions
1	Plexiglass walls	0, 5, 10, 20.	3
2	Bag in box	0, 5, 10, 20.	3
3	Bag liner on walls	5, 20.	1

Preparation in four layer turned out to be necessary because of the significant tendency to demix. This makes the preparation in one go too irregular, as shown by the size of the dashed error bars of figure 2.1 compared to the narrower solid error bars of the four layer preparation. All experiments were run using 0.38 kg of cereals.

Three different box configurations were tested, as described in table 2.2. In the first one, the particles are filled in a plexiglass box having same size as a cereal box: 0.193m x 0.057m, 0.27 m high. The second experiments is closer to the real cereal box setup: cereals are filled in a bag that is put inside the plexiglass box and left free to move with respect to the box itself. The bag volume is close to the box volume, only corners are somewhat rounder. Finally, for the third experiment the plexiglass walls were covered with the same materials, the plastic liner, which the bags are made of. In this configuration the liner moves together with the box and follows exactly the box dimensions. Several experiments varying the vibration duration are made with each configuration (column 3 of table 2.2) as to obtain a time evolution of the segregation. Some repetitions of different durations and conditions were performed, these are summarised in the last column of table 2.2.

2.4.2 Size segregation results

Segregation can be observed visually from the sides of the box as reported in figure 2.3. Quantitative data are reported in figure 2.4 where it can be appreciated how the composition of each layer of the box varies with time. Segregation always drives big particles to the top of the mixture, lowering top composition in Mini particles below 50%. These systems are thus all

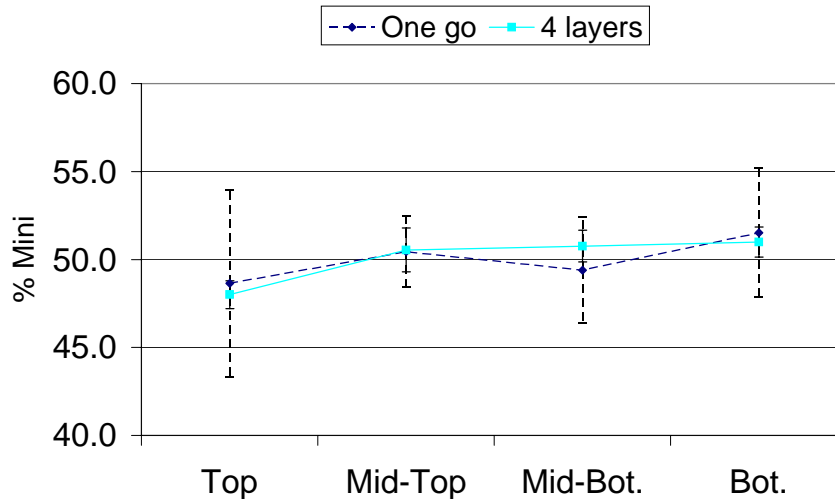


Figure 2.2: Uniformity of the initial mixture obtained when preparing the medium in four layers (solid line) and in one go (dashed line). Standard deviation is reported as error bars.

following the classical Brazil nut effect. Experiment 1 shows a non-monotonous increase in segregation along time with stronger segregation at 5min than at 10min. The differences are however close to the limit of reproducibility of the data. The experiment configuration has a clear effect on the segregation at the bottom of the box. Figure 2.5 compares the segregation obtained after 20 min of vibrations. Experiments 1 using the plexiglass box, and experiment 3 using the bag liner on the box walls, show significant segregation at the bottom of the mix, where Mini particles reach 65% of the weight. On the contrary during experiment 2, with the "bag in box", no significant segregation occurs at the bottom of the box. Segregation takes place only in the topmost three quarters of the box with the topmost quarter becoming richer in big particles and the two layers below richer in small particles.

During the vibration the mixture also settles, increasing its density. Beside observing qualitatively settling from the images reported in figure 2.3, this can be quantified through the decrease in height of the medium. Figure 2.6 reports the evolution with time of the position of the surface of the bed expressed as a percentage of the initial position. The test using the bag gives rise to higher settling. This could be caused by a progressive deformation of the bottom of the bag, which becomes progressively more able to fill corners of the box hosting the bag.

2.4.3 Some observations on convection in mono-sized cereals.

To shed some light on the segregation patterns observed in the previous paragraph, it is useful to consider the behaviour of vibrated mono-sized cereals. Mini particles were vibrated following the same conditions as for size segregation tests, to observe more easily the overall movement of the particles without the influence of segregation. A layer of particles was coloured to provide a visual benchmark. Figure 2.7 shows lateral snapshots taken during the vibrations in the same configuration as the experiment 1, reported in the previous paragraph. A convective movement can be observed, which brings particles downwards at the corners. The time needed for the

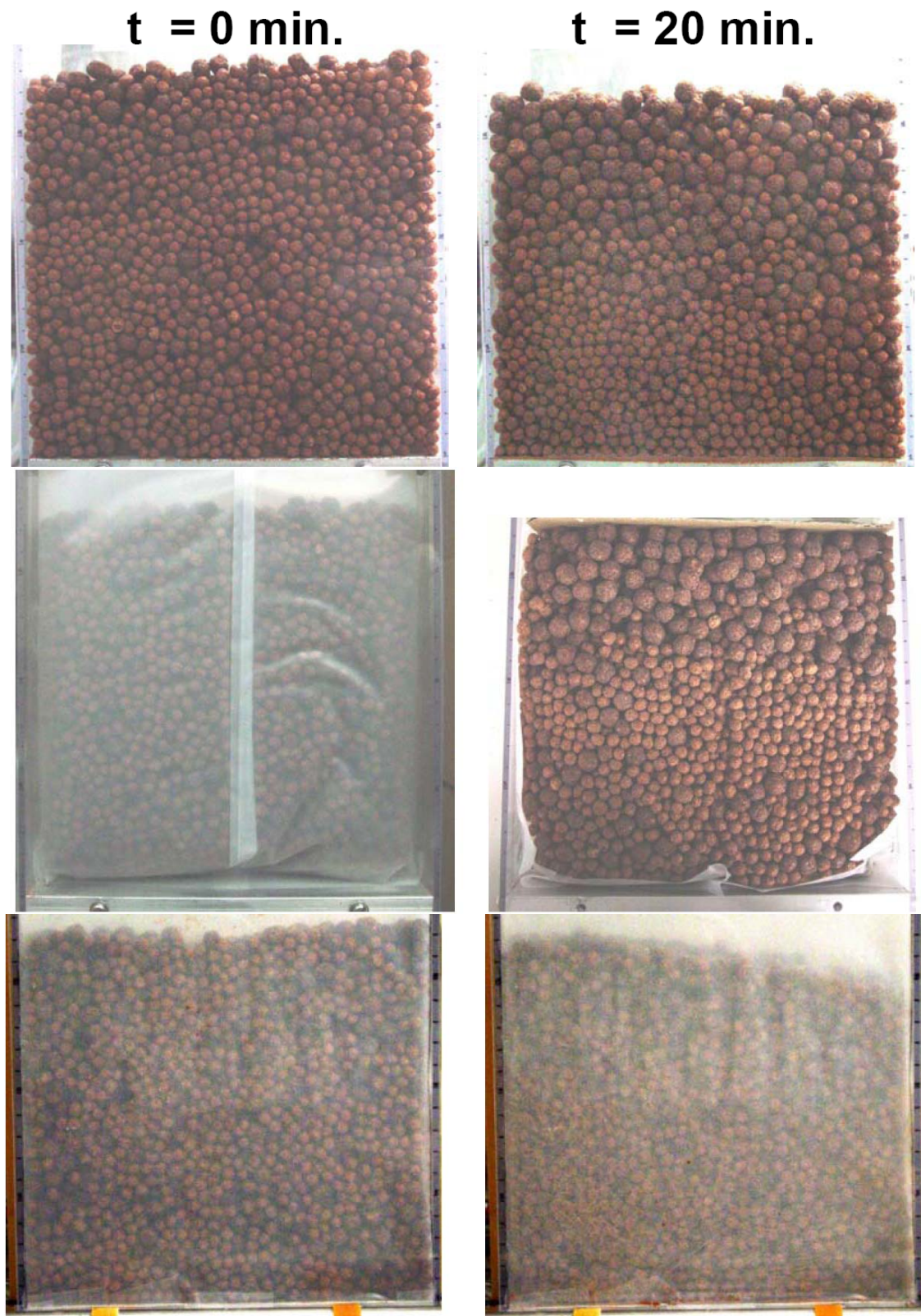


Figure 2.3: Pictures showing segregation observed after 20min vibration: Exp.1 - Top / Exp.2 - Centre (bag is cut for better picture quality) / Exp.3 - Bottom.

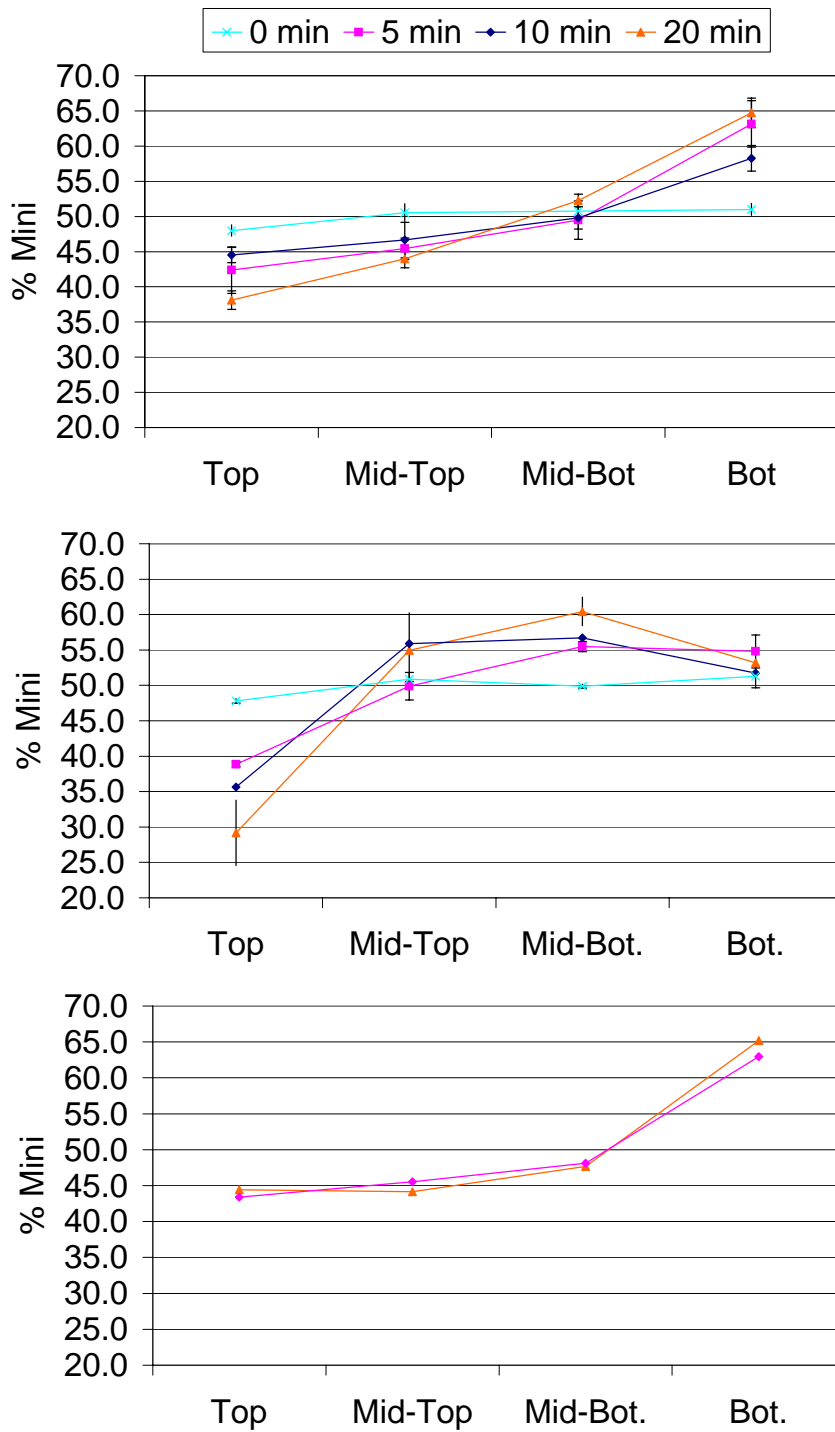


Figure 2.4: Evolution with time of the size segregation: Exp.1 - Top / Exp.2 - Centre / Exp.3 - Bottom. Below 50% corresponds to fractions rich in big particles.

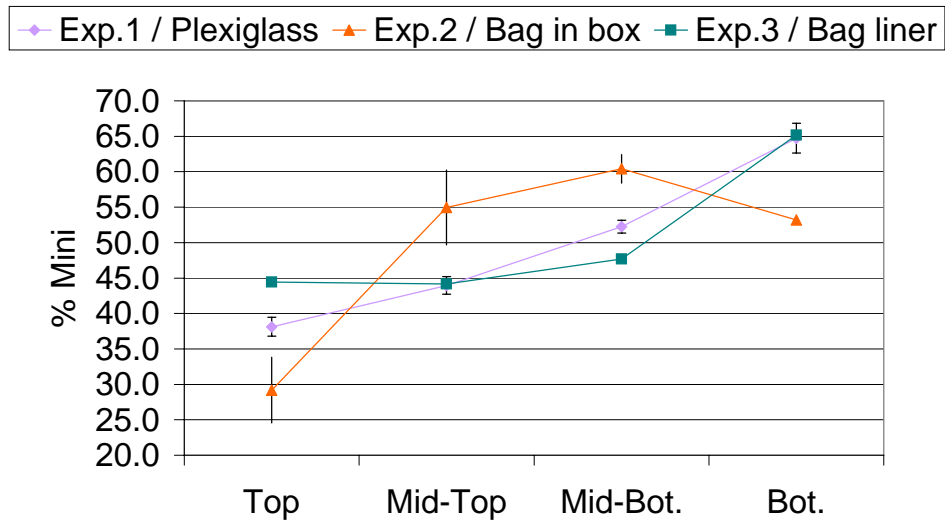


Figure 2.5: Effect of the box configuration on the segregation after 20 min of vibrations.

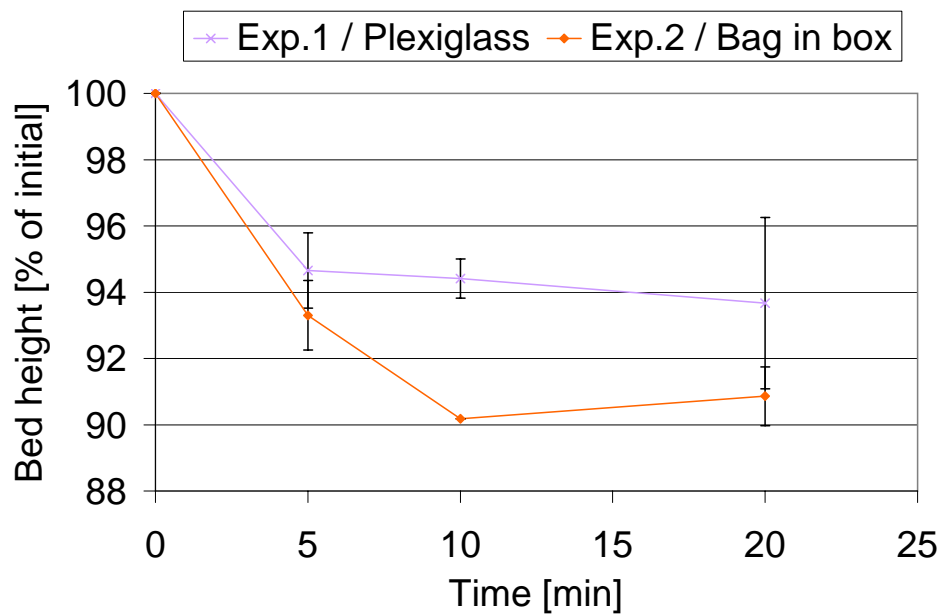


Figure 2.6: Evolution with time of the settling of the particles for different box configurations.

particles at the corners to reach the bottom of the box is about 75s. Particles at the walls and far from the corners move only slightly, but their movement is hard to follow because they can be hidden by other particles. Simoultaneously an upward movement takes place at the centre of the box. The time-to-surface for the first white particles to appear at the top is about 160s. This convection pattern is similar to what observed in (LR97) for wall friction higher or equal to particle friction. A similar experiment was performed using the bag in box configuration of the experiment 2 of previous paragraph. Lateral snapshots are reported in figure 2.8. Again some downward movement appears at the corners and upward movement arises at the centre of the box and in this case also at the sidewalls, far from the corners. The time-to-surface is in this configuration about 125s. Convection does not involve the bottom of the box as in the previous configuration. This can be qualitatively appreciated from the few coloured particles present within the bottom-most layer of the box at the end of the experiment. The fact that convection does not reach the bottom of the box can explain why, in the bag in box configuration, segregation is not taking place at the bottom of the box as reported in the central plot of figure 2.4. At each rebound the bag detaches from the box. An explanation for the different convection pattern, suggested by the visual observation of the experiment, is that the bag dissipates part of the energy of the system at each landing, thus leaving only a lower amount of energy for the fluidisation of the particles. Following Quinn et al. (QH00) this would in turn reduce the height of the fluidised top layer. Further investigations would be necessary to confirm this hypothesis.

2.4.4 Impact tests to assess cereal restitution coefficient.

This paragraph reports the results of some single particle impact tests performed to estimate the restitution coefficient of the cereals used in these segregation tests. The particles were released with zero velocity from an initial height varying from 150 to 300mm over a flat glass surface. A sketch of the impact test setup is shown in figure 2.9.

Due to the irregular shape of the particles, their rebound is not perfectly vertical, which makes the assessment of their restitution coefficient a bit tricky. The impact was recorded with a fast camera. The following quantities were extracted from the images:

- $H_{max}(t_{max})$ is the maximum height of the particles after the rebound.
- $\Delta x(t_{max})$ is the lateral displacement of the particle with respect to the impact point, measured at the moment in time when the particle reaches the maximum height.
- $\Theta_y(t_{max})$ is the rotation angle in the direction orthogonal to the observation plane.

From these quantities the restitution coefficient can be computed as follows:

$$\varepsilon = \sqrt{\frac{r^2 \left(\frac{\Theta_y(t_{max})}{t_{max}}\right)^2 + H_{max}g + \frac{1}{2} \left(\frac{\Delta x(t_{max})}{t_{max}}\right)^2}{H_0g}} \quad (2.5)$$

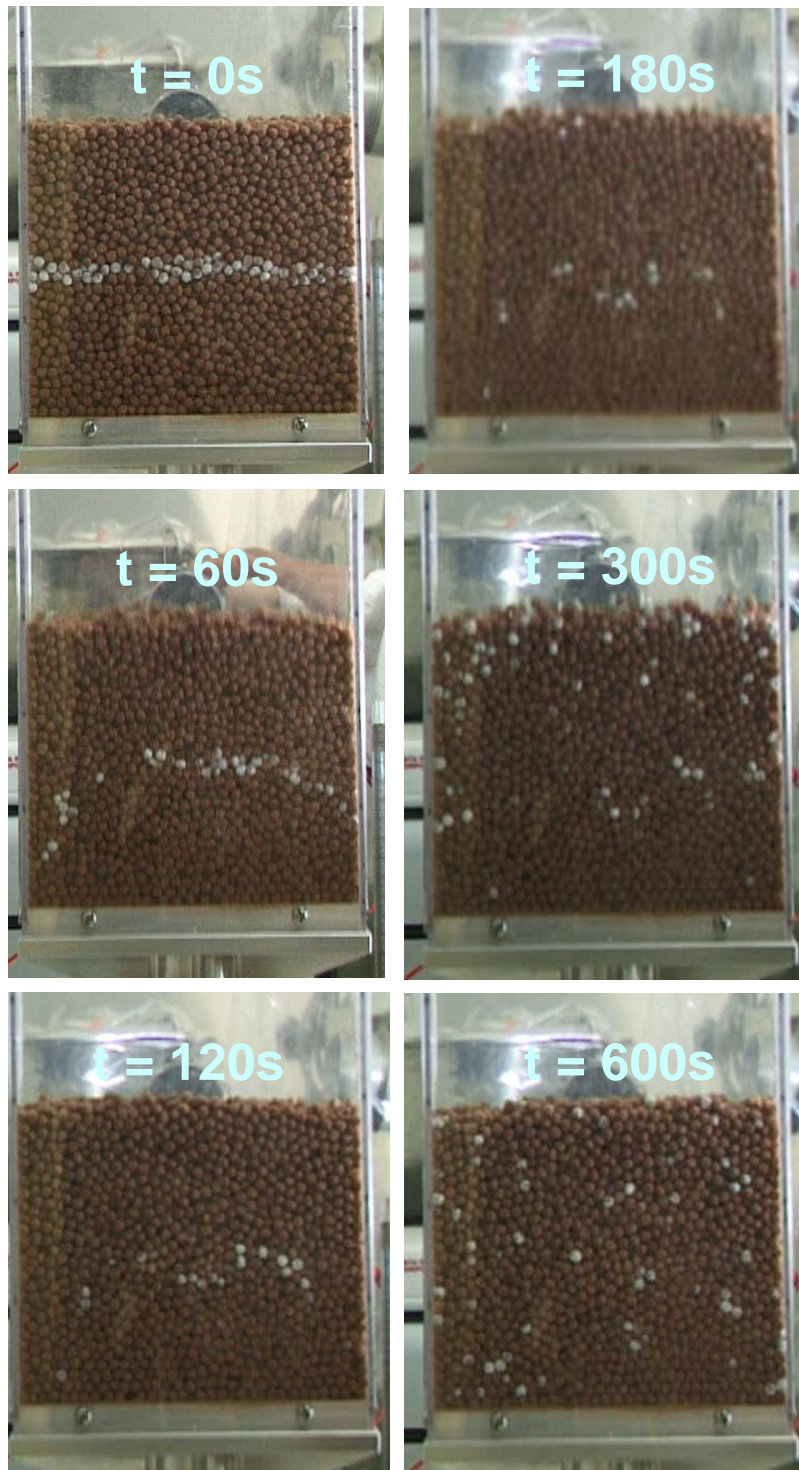


Figure 2.7: Convection generated on an uniform population of Mini particles in a plexiglass box.

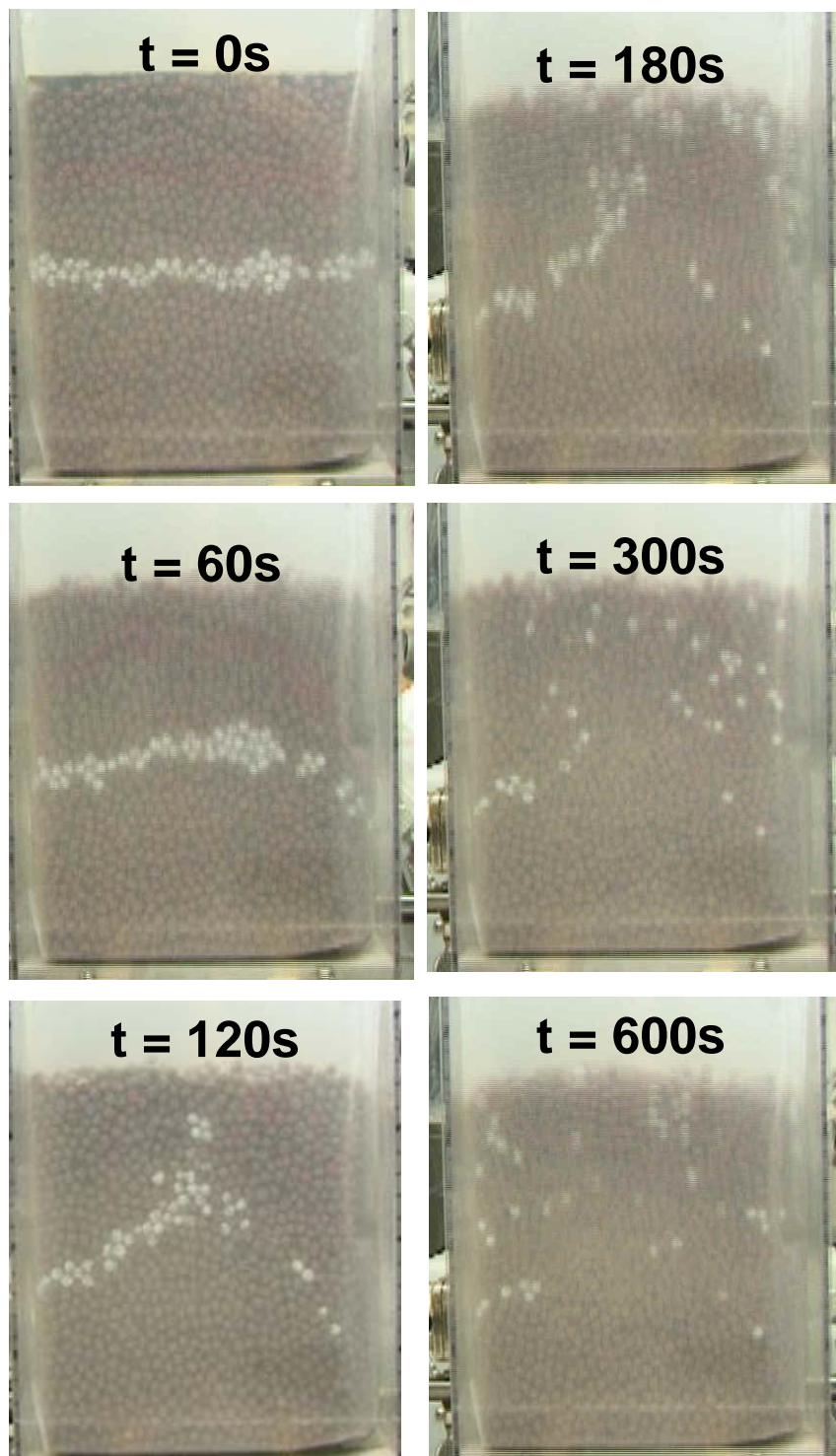


Figure 2.8: Convection generated on an uniform population of Mini particles in a bag inside a plexiglass box.

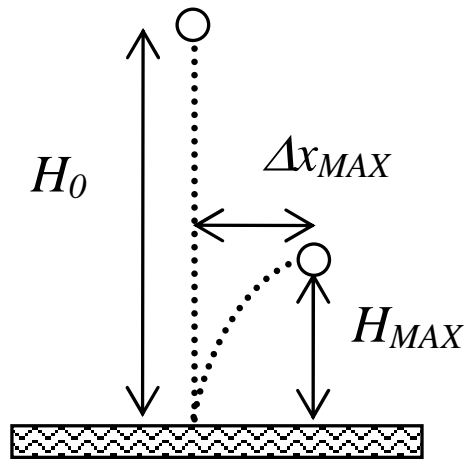


Figure 2.9: Sketch of the impact test setup to estimate the cereal restitution coefficient.

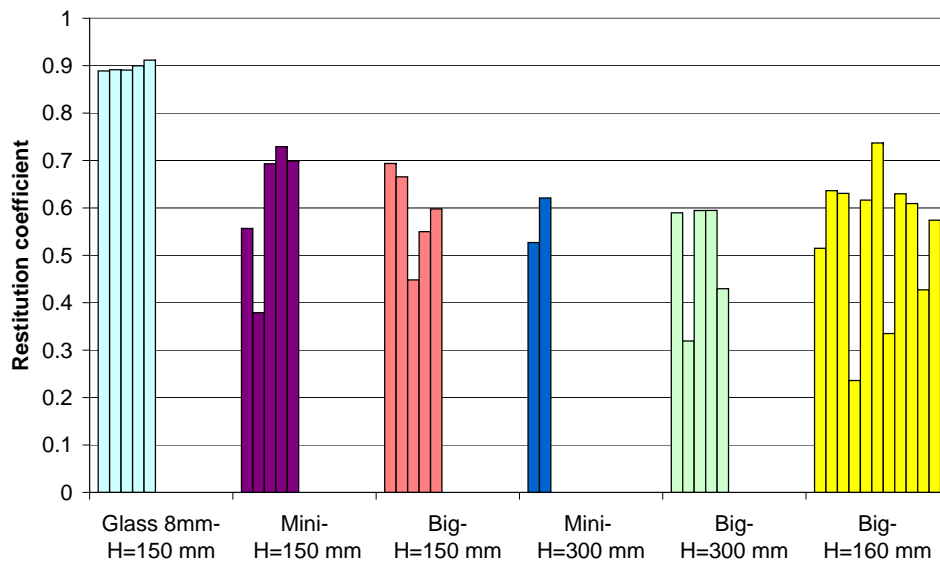


Figure 2.10: Restitution coefficient resulting from the impact tests.

Equation 2.5 considers the potential energy, the rotational energy in the observation plane and the translational energy in the observation plane, but neglects the rotational and translational energies along the direction orthogonal to the observation plane. The restitution coefficients measured for glass beads, Mini and Big cereals are summarized in figure 2.10. Glass beads' restitution coefficient of 0.9 is close to values that can be found in the literature (FLCA94). Cereal impact tests gave results with a higher degree of variability. Some impacts caused a visible breakage of the particles and were discarded. This limited in particular the number of results that could be obtained using a drop height of 300mm. Some local breakage of the particles can also explain the overall restitution coefficient variability. Considering all the limitations of these experiments, overall we estimate the cereal restitution coefficient to be about 0.6. Over all the impacts here considered, the average contribution to the restitution coefficient of the in-plane lateral and rotational motion summed together is only 3.6% of the total. We expect the omission of the out-of-plane components to cause a similar underestimation, which we consider acceptable, considering the much bigger influence of the erratic local breakage of the particles. It was decided therefore not to venture in a more complex three dimensional determination of the restitution coefficient.

2.4.5 Inferring friction properties.

Several possible ways to measure or infer particle friction were considered. As for the assessment of other particle properties that are aimed at being used for a DEM simulation, the first dilemma is whether measuring a true particle property or rather a bulk property related to the particle property that is unknown, but also related to the final simulation set-up. DEM particle friction plays in reality the role of a lumped coefficient, that is influenced by the other assumptions made while modelling. Assuming spherical particle geometry, or neglecting particle rolling friction are simplifications which might call for a compensation in the way the particle friction coefficient is chosen. Naturally the fact of assuming that such simplifications can be compensated in this way, is risky. This assumption can be verified only via a comparison with experiments. A recent paper (PSO⁺06) compares single particle tribologic measurements like scratch test, sliding particles acceleration measurement and the measurement of the critical angle initiating the sliding motion (the latter is used also in (USS07). Pohlman (PSO⁺06) also compares these single particle measurements with a bulk angle of repose test in a rotating drum. Other bulk tests like ring shear tests, angle of repose tests, particle "viscosimeters", Flowdex (PRFL07) can provide measurements more or less directly related to friction properties. They can be preferred to microscopic tests for applications where the flow field is close to the one occurring in the test. The use of an angle of repose test (figure 2.11) has been considered in the framework of this study, and some preliminary tests performed mainly using the cohesive powder described in chapter 5. Finally the pragmatic approach of using particle(-particle) and wall(-particle) friction coefficients as degrees of freedom to match experimental observations is retained, as described in the next paragraphs.



Figure 2.11: Image from an angle of repose test.

2.5 DEM simulations.

2.5.1 Size segregation.

The first experiment described in Table 2.2, i.e. using the plexiglass box, was chosen as target to be reproduced by DEM simulation. Different values of the three most important particle parameters, namely particle restitution coefficient, particle(-particle) friction, wall(-particle) friction were varied trying to achieve the best possible agreement with the experiment. To compare simulation with experiments the cereal bed is cut in the simulations in four horizontal layers, taking care that the weight of each layer is the same as in the experiments. It was verified that cutting the layers during vibration leads to computed mass fractions that are close to those that one obtains after having let the medium come to rest. Table 2.3 shows a subset of the simulation plan including only the simulations that resulted in some level of agreement with experiments. For each simulation, the parameters are reported together with the relative error between simulation and experiment, defined as follow:

$$Rel\ Err = \frac{1}{4} \sum_{layers} \frac{abs(W_{Mini}^{Exp} - W_{Mini}^{Sim})}{W_{Mini}^{Exp}} \quad (2.6)$$

Further simulations using other sets of parameters predict excessive segregation compared to the target and are omitted. The comparison of the measured and simulated Mini mass fraction at 5, 10, 20min. is reported respectively in Figure 2.12, 2.13, 2.14. To help the reader spotting the simulations that better approach the experiment, labels "ok" are added in table 2.3 close to the fraction whose relative error lays below 0.2. Generally speaking, the agreement with experiments is better at 5 min than for the following measurements and simulations tend to overestimate segregation, particularly at the top of the box. The 10 min measurement, which as already discussed shows lower segregation than at 5 min, is not captured satisfactorily by the simulations. Overall, the best set of parameters to reproduce segregation are highlighted in table

SIMULATION	Rel Err 5 min.	Rel Err 10 min.	Rel Err 20 min.	Mean Rel Error
SS12: FricP=0.15 / FricW=0.01/ e_rest=0.4	0.197 OK	0.228	0.218	0.215
SS14: FricP=0.05 /FricW=0.01/ e_rest=0.6	0.284	0.312		0.2981
SS15: FricP=0.25 /FricW=0.01/ e_rest=0.6	0.147 OK	0.216		0.1815 OK
SS16: FricP=0.50 /FricW=0.01/ e_rest=0.6	0.143 OK	0.313		0.2283
SS17: FricP=0.15 /FricW=0.15/ e_rest=0.1	0.130 OK	0.156 OK	0.15847 OK	0.1481 OK
SS18: FricP=0.15 /FricW=0.15/ e_rest=0.6	0.191 OK	0.192 OK	0.13713 OK	0.1734 OK
SS19: FricP=0.95 /FricW=0.01/ e_rest=0.6	0.184 OK	0.374	0.41319	0.3237
SS20: FricP=0.95 /FricW=0.01/ e_rest=0.1	0.489	0.642		0.5655
SS21: FricP=0.75 /FricW=0.01/ e_rest=0.6	0.149 OK	0.376	0.45205	0.3257
SS22: FricP=0.75 /FricW=0.01/ e_rest=0.1	0.430	0.603		0.5165
SS24: FricP=0.15 /FricW=0.15/ e_rest=0.01	0.118 OK	0.167 OK	0.11451 OK	0.1332 OK
SS25: FricP=0.25 /FricW=0.01/ e_rest=0.1	0.087 OK	0.274	<i>0.3573</i>	0.2393
SS26: FricP=0.15 /FricW=0.01/ e_rest=0.1	0.112 OK	0.236	<i>0.3279</i>	0.2254
SS27: FricP=0.15 /FricW=0.01/ e_rest=0.6	0.265	0.225	<i>0.2167</i>	0.2453

Table 2.3: Relative error between cereal size segregation measurements and simulations. Data in *italic* are simulated at 820s and compared with the experimental data at 1200s.

2.4. The sensitivity to the friction coefficients seems higher than to the restitution coefficient. A qualitatively different segregation pattern is obtained when a low coefficient of wall friction is used. The Mini fraction does not decrease monotonically with height but shows a maximum in the second layer from the bottom, with lower segregation occurring at the box bottom. This trend is similar to that obtained experimentally in the bag in box configuration. A comparison of the experimental and simulated results at 5 and 20 min, is reported in figure 2.15. Naturally there is some contradiction between the results of Experiment 3 and this last observation on the segregation pattern observed in simulations with low wall friction. Further investigations would be necessary to solve this contradiction, possibly starting by assessing the reproducibility of Experiment 3.

Table 2.4: Size segregation simulations reproducing more closely the experimental features.

Simulation	e_{rest}	μ_{part}	μ_{wall}	mean relative error
18	0.6	0.15	0.15	0.173
17	0.1	0.15	0.15	0.148
24	0.01	0.15	0.15	0.143

2.5.2 Convection in mono-sized cereals.

Convection in a box full of Mini cereals was simulated, to allow comparing with the convection experiments described in paragraph 2.4.3. Similarly to experiments a layer of particle at the centre of the box is coloured in white to visualize the convective patterns. A polydispersity is introduced in the simulations to avoid an excessive degree of crystallisation which would limit the relative movement of the particles. A uniform distribution of particle diameter is used in the interval $7.2\text{mm} \pm 7.5\%$. This polydispersity is close to the measured one for the Mini particles. The effect of particle properties, and especially friction coefficients, is studied as described in table 2.5. The same table also reports the resulting time-to-surface and direction of the convective flow at largest walls, far from corners.

All simulations show convection and in all simulations the flow is downwards along the shortest sidewalls and upwards at the centre of the box. Varying the friction coefficients affects quali-

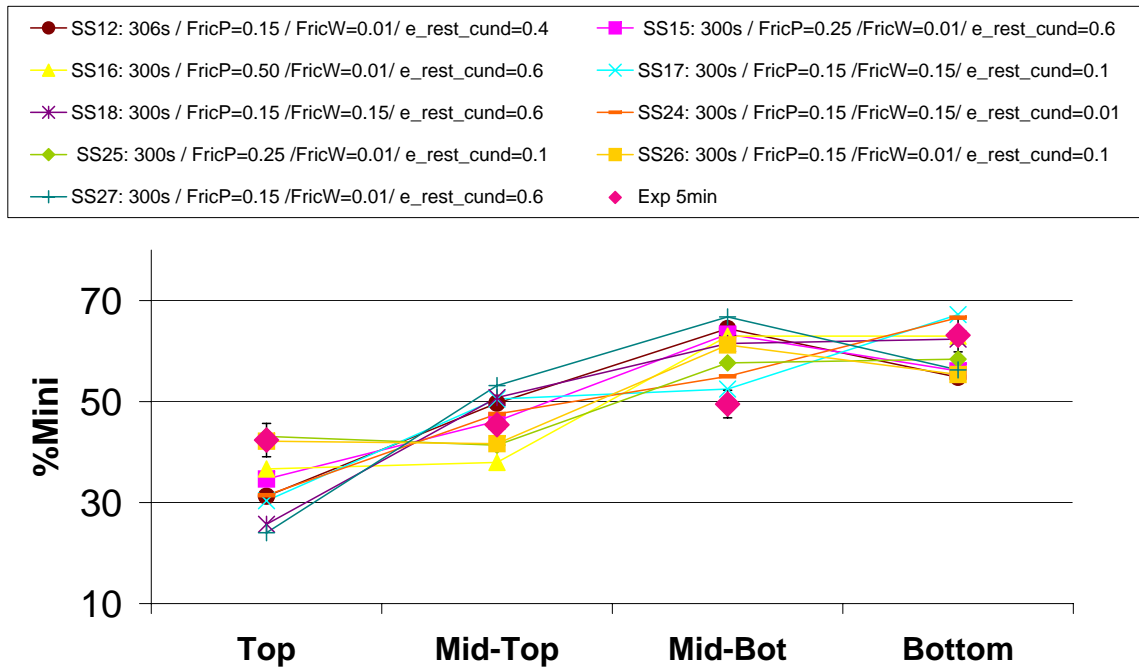


Figure 2.12: Comparison of experimental and simulated Mini fractions after 5 minutes of vibrations.

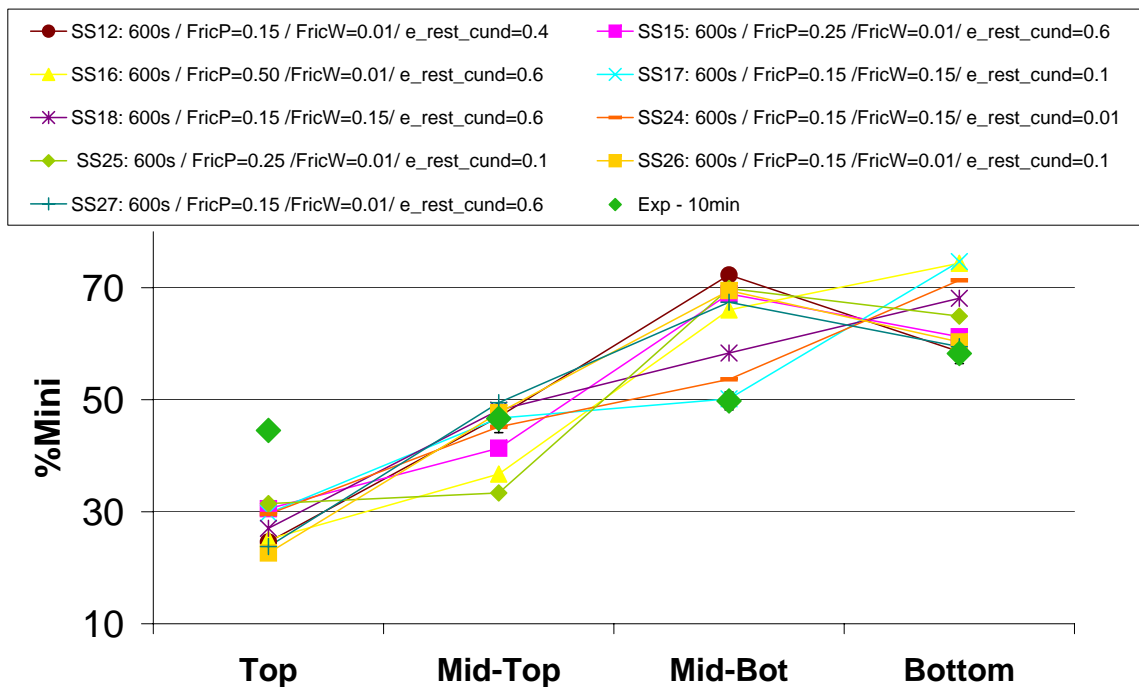


Figure 2.13: Comparison of experimental and simulated Mini fractions after 10 minutes of vibrations.

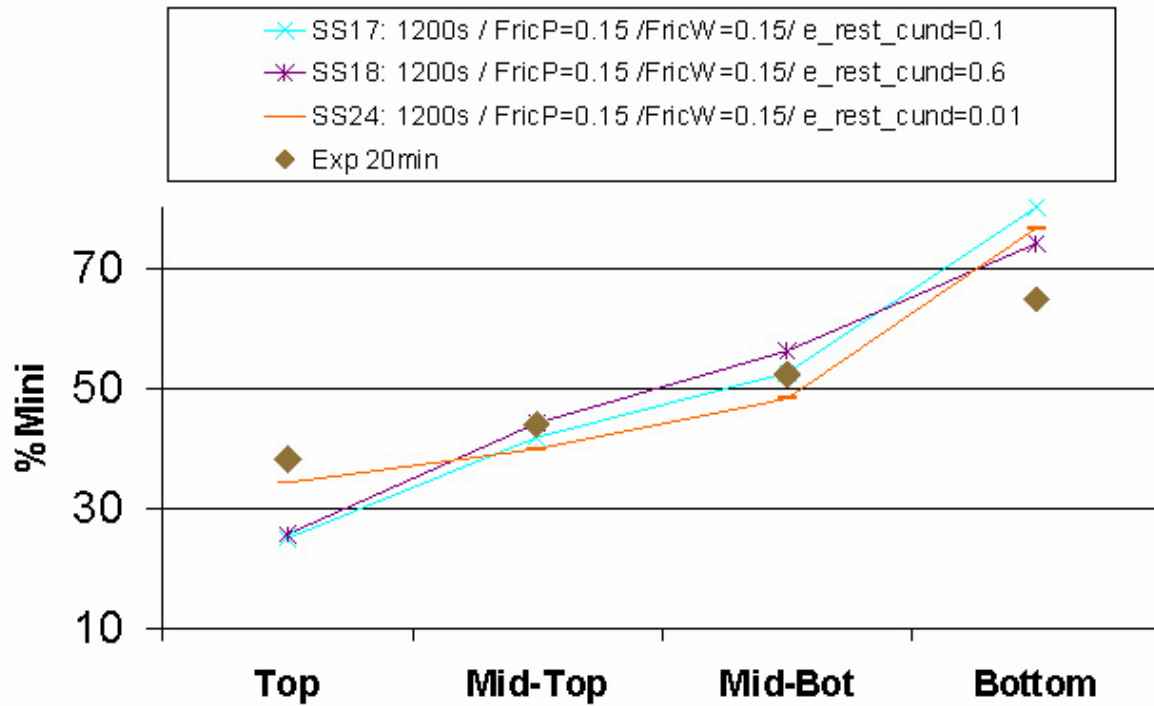


Figure 2.14: Comparison of experimental and simulated Mini fractions after 20 minutes of vibrations.

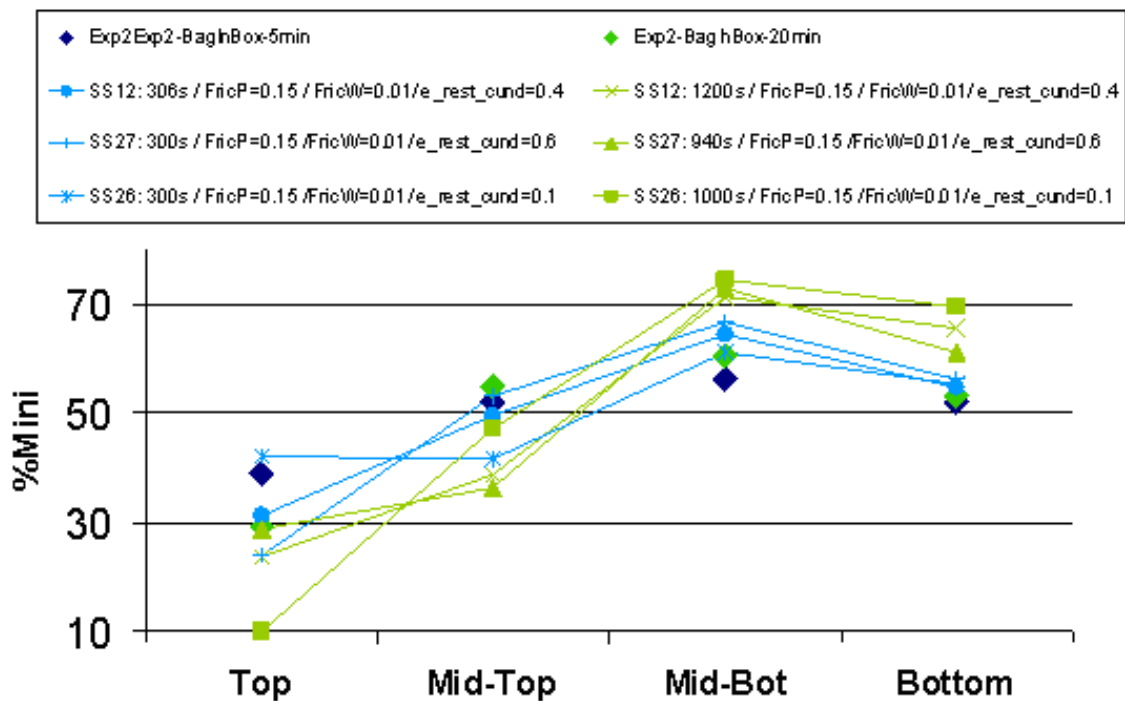


Figure 2.15: Comparison of experimental segregation in experiment 2 (bag in box configuration) and simulations using low wall friction.

Table 2.5: Mini convection simulation conditions. Resulting time-to-surface and flow direction at largest walls, far from corners.

Simulation	e_{rest}	μ_{part}	μ_{wall}	Time-to-surface (s)	Flow direction at largest wall.
Conv9	0.1	0.75	0.75	7.2	DW
Conv17	0.1	0.25	0.25	60	-
Conv13	0.1	0.15	0.15	72	-
Conv14	0.1	0.15	0.75	12	DW
Conv15	0.1	0.75	0.15	41	UW
Conv16	0.1	0.15	0.01	49	UW
Conv18	0.1	0.15	0.05	110s	mildly UW
Conv19	0.6	0.15	0.15	92s	-

tatively the flow patterns at the largest walls, far from the corners. It is worth spending some words to explain this interesting zone of the box. The left side of figure 2.16 shows the initial conditions that are the same for all convection simulations. Figure 2.16 centre and right show lateral snapshots of the convection patterns in simulations Conv13 and Conv18 respectively. With 0.1 restitution coefficient, equal particle and wall friction coefficient as for Conv13, or higher wall friction than particle friction, generate a very mild and downward convection at the centre of the large wall. The simulation Conv13 (centre of figure 2.16) generates convection similar to the experiment reported in figure 2.7. The convective field is truly three-dimensional in this case. On the contrary, using higher wall friction than particle friction, the convection at the large wall, far from the corners, is upwards. An example is the snapshot of simulation Conv18 shown on the right side of figure 2.16. This trend has been observed experimentally using the "bag in box" configuration (see figure 2.8). The more the particle friction is increased with respect to wall friction, the more the convection field becomes two dimensional in the plane parallel to the largest walls of the box. To the author's knowledge, the observation of such transition from two dimensional to three dimensional patterns had not been reported in the literature so far.

Next to last column of table 2.5 reports the simulated time-to-surface. A lower bound is reported whenever the exact value is not available. When the two friction coefficients are equal, increasing friction reduces the time-to-surface, because of the increased convection. A comparison of experimental and simulated time-to-surface shows that the dynamics of the convection is faster in the simulations than in experiments.

The same set of parameters $e_n=0.1/0.6$, $\mu_{part}=0.15$, $\mu_{wall}=0.15$ seems the best choice to get closer to both convection and size segregation simulations (as reported in table 2.4) for the plexiglass box. In both cases however the simulations overestimate the phenomena. Another interesting range of parameters is $e_n=0.1/0.6$, $\mu_{part}=0.15$, $\mu_{wall}=0.01/0.05$, that for both segregation and convection generate the same qualitative trends as experiment 2, in the "bag in box" configuration. Again, for both segregation and convection, the simulations dynamics is too fast with respect to experiments.

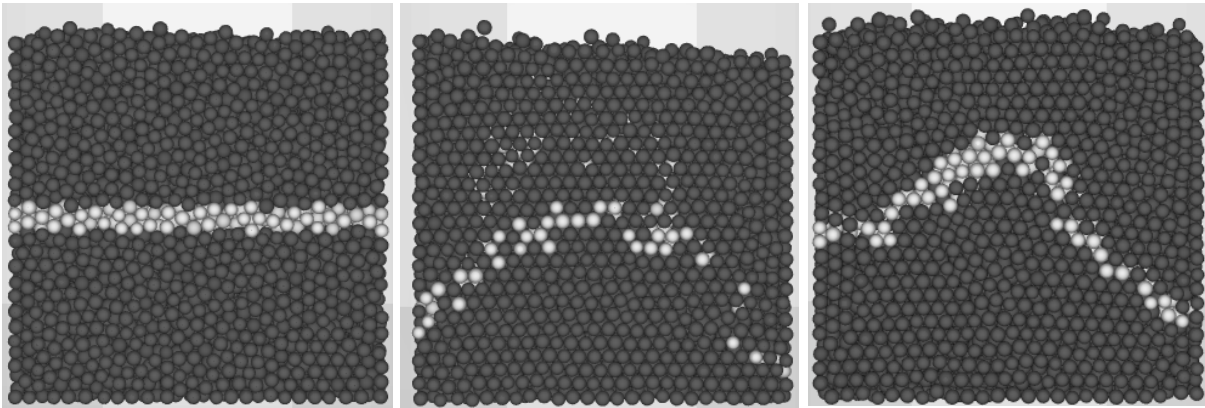


Figure 2.16: DEM simulation of the convection of vibrated Mini particles. Initial conditions are the same for all simulations and are shown on the right. At centre: simulation Conv13 after 60s vibrations. On the left: Conv18 after 38s vibrations.

2.6 Next steps

Some further investigations are still necessary to achieve a quantitative agreement between size segregation experiments and simulations. Some interesting directions:

- Quantify cereal friction coefficients.
- Estimate cereal contact time. Reduce the contact time, if necessary, to avoid any bias of the contact model on the convection pattern ((LCB⁺94)).
- Further investigate experimentally the third configuration with bag liner on the walls.
- Study via simulation the convection in boxes with different aspect ratios, consolidating robust statistics on average properties as the mean downward velocity at the smallest wall, etc. A thorough understanding of such convection patterns can be the base for a deeper comprehension of the effect of box geometry and vibration intensity and frequency on cereal segregation.
- Develop a stochastic impact model that mimics cereal asperities and microbreakages, leading to a variable restitution coefficient and non normal rebound even with a normal approach velocity. Since the system seems more sensitive to friction than it is to restitution coefficient, a lower priority should be given to this direction with respect to previous two.

2.7 Conclusions

Experiments show the occurrence of Brazil nut effect when vibrating a binary mixture of cereals in a cereal box. The segregation using a plexiglass box is quantitatively and qualitatively

different from the "bag in box" configuration. The latter shows an absence of segregation at the bottom of the box, which makes the composition not monotonous with the height in the box. Based on a third experiment, it is argued that the difference does not only stem from the different friction, but it is also due to some damping caused by the repeated landing of the "bag in the box".

Other experiments highlight the convection that takes place when vibrating particles of uniform size. The different segregation pattern can be qualitatively related to the absence of convection at the bottom of the box in the "bag in box" configuration. Simulations varying friction and restitution coefficients reproduce qualitatively both segregation and convection patterns, but overestimate their extent. The convection observed is always directed downwards along the smallest sidewalls. However, the interplay between wall and particle friction conditions the convection flow field within the box. At high particle friction and low wall friction, the convection pattern tends to become two dimensional, with little variation across the smallest dimension of the box. Using same friction coefficients or higher wall friction than particle friction, the convective flow is downwards also at the largest wall, with a narrower upward stream at the centre of the box. To the author's knowledge, the observation of such transition from two dimensional to three dimensional patterns had not been reported in the literature so far.

Two interesting sets of parameters are identified which allow reproducing the qualitative features of both plexiglass box and "bag in box" configuration for what concerns segregation and convection experiments. Some next steps are outlined to improve further the realism of simulation with respect to experiments.

Chapter 3

On the vertical ordering of rods vibrated vertically.

3.1 Summary

Granular media composed of elongated particles had been observed to rearrange and order vertically upon vertical vibration in a cylindrical container. A preliminary set of experiments and discrete element simulations is performed in a pseudo-two-dimensional box, which shows that vertical ordering is preferred with respect to horizontal ordering also in absence of curved walls and regardless of initial orientation. DEM simulations are found to agree with experiments.

We further study the influence of particle geometry and vibration acceleration on rod vertical ordering, simulating the rearrangement of particles of different lengths in a box with lateral periodic boundaries. Those boundaries show that no help from vertical walls is either needed to generate vertical ordering.

The sizes of voids forming during vibrations are analyzed and a void-filling mechanism is considered to explain the observed vertical ordering. Void filling can explain why short rods are less prone to align vertically than long ones. Void-filling alone cannot however explain the existence of an optimum acceleration to promote vertical ordering and its dependence on particle length.

We finally introduce a novel interpretation of the phenomenon, by considering the energetic barriers that particles have to overcome to exit a horizontal or a vertical lattice. By comparing these energetic thresholds with the peak mean particle fluctuant kinetic energy, we identify three different regimes. In the intermediate regime a vertical lattice is stable, while a horizontal is not. This interpretation succeeds in reconciling both dependencies on vibration acceleration and on particle length. This work was published partly in (RPL05) and then completely in (RPL07).

3.2 Introduction

Over the last half decade, the research for understanding the complex collective behavior of granular media has progressively been shifting its focus from spherical to the more relevant non spherical particles. Real-world grains are indeed far from being spherical and particle geometry is commonly thought to strongly influence the behavior of dense granular media. Getting better insight into the behavior of monodisperse anisotropic media subject to vibration is a key step towards explaining compaction mechanisms (RND⁺05b) in real granular media. Moreover, such insight is also needed to interpret the segregation of mixtures of anisotropic particles just as understanding the behavior of vibrated monodisperse spheres has been a key to interpret sphere size segregation over the last decade (VRD97),(CVF⁺06).

Stokely et al. (SDS03) studied grain orientation and voids in two-dimensional piles of prolate grains. A density dependent isotropic-nematic transition was reported by Galanis et al. (GHS⁺06) in a horizontal pseudo-two-dimensional box vibrated vertically, showing the important role of walls. The importance of particle shape in such a configuration was studied too (NMR06). Ribière et al. (RRDB05) showed the importance of convection and Abreu et al. (ATC03) used Monte Carlo methods (MC) to simulate compaction of spherocylinders and shape segregation from spheres. Experiments by Villaruel et al. (VLMJ00), Blair et al. (BNK03) and Lumay et al. (LV04) showed that rods can orient vertically when vibrated vertically in a cylindrical container. Blair invoked first void-filling to interpret qualitatively this phenomenon. Volfson et al. (VKT04) studied the dynamics of a set of bouncing rods and the spontaneous development of a horizontal velocity.

The modeling archetype for elongated grains is the spherocylindrical rod: a cylinder with a hemisphere at each end. It is fully characterized by two geometric parameters: its total length L and the diameter D , identical for the cylinder and the hemispheres. Pournin et al. (PWT⁺05) proposed a DEM capable of handling spherocylinders, used to reproduce experiments by Villaruel et al. and later extended DEM to three-dimensional particles with more complex shapes (PL05). The vertical ordering of spherocylinders in a cylindrical container (see figure 3.1) was explained by the reaction torque occurring when a rod touches the curved sidewall with both tips in a non-horizontal position (PWT⁺05).

3.3 Some preliminary experiments

As already introduced in the previous paragraph and described in (PWT⁺05), the vertical ordering of spherocylinders in a cylindrical container (see figure 3.1) can be explained considering the torque generated upon contact with the curved sidewall of a rod with a non-horizontal orientation. This paragraph deals with some preliminary experiments and simulation to address three questions:

1. Is there another mechanism causing vertical ordering of spherocylinders in absence of curved walls?
2. Under vertical vibrations, is vertical alignment preferred with respect to ordering in any other, including the horizontal direction?

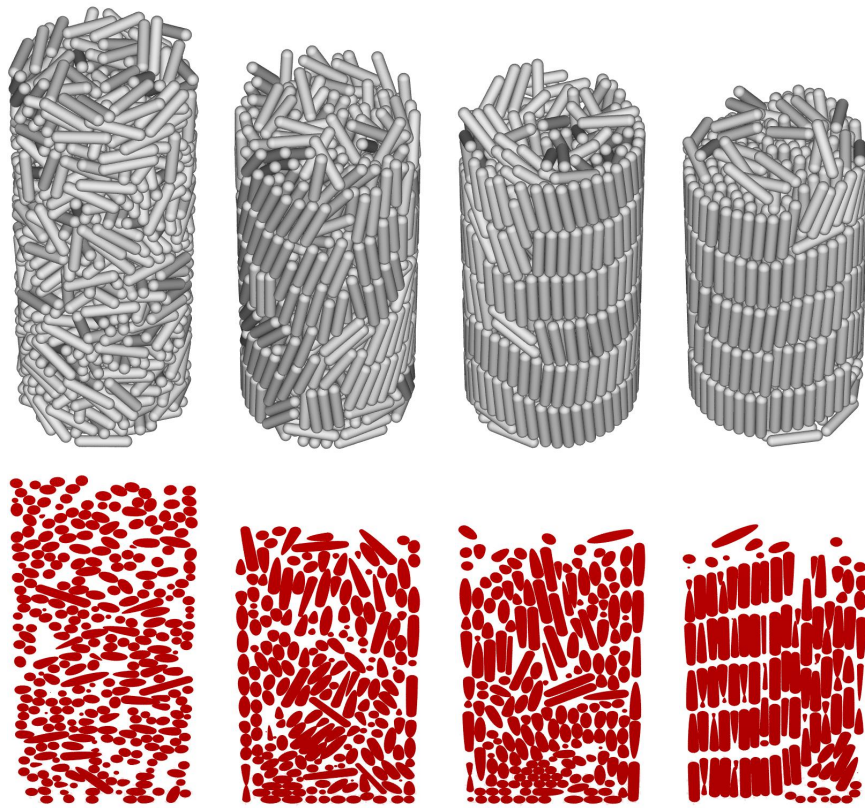


Figure 3.1: Vertical ordering of spherocylinders in a vibrated cylinder (PWT⁺05).



Figure 3.2: Simulation 1 - Starting configuration (left); positions of the particles during vibrations after 1200 s (right); the walls of the pseudo-two-dimensional box are omitted.

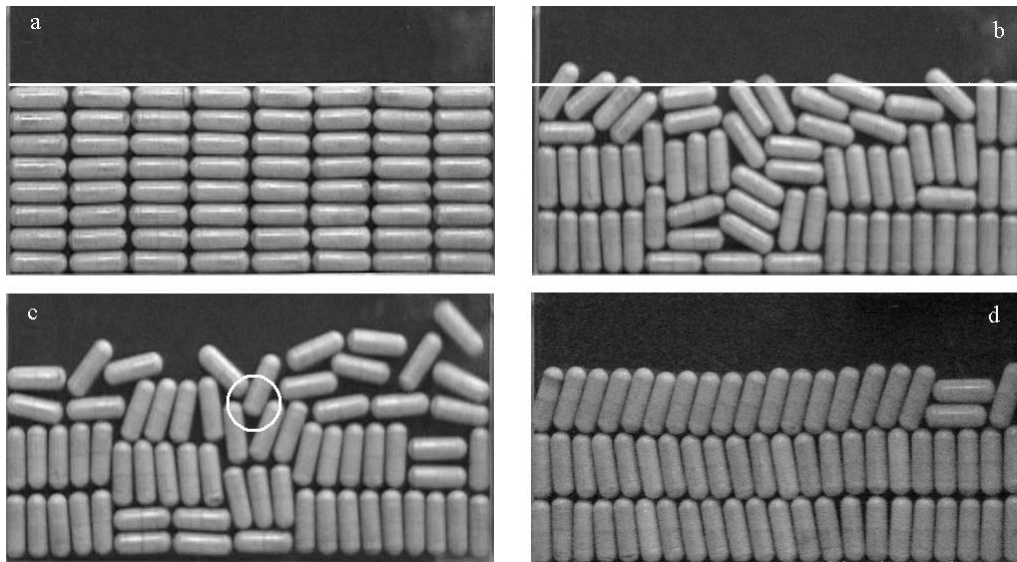


Figure 3.3: 2a. Exp.1 - Starting configuration; 2b. Exp.1 - Configuration at rest after vibrating 1200s; 2c. Exp.1 - Positions during vibration after 1650s. 2d. Exp. 3 - Configuration at rest after vibrating 1200s, initially particles were vertical.

3. Ordered configurations present high density, which could make it seem plausible that the main driving forces for rearrangement are the increase in density and decrease in potential energy. Is this true?

Table 3.1: Ordering experiments (Exp.) and simulations (Sim.) in a pseudo-two-dimensional box.

	Vibr.Freq.(Hz)	Vibr.Acc.(g)	Init.Orient.	Fric.
Sim. 1	12.5	3	Random	0.25
Sim. 2	12.5	3	Horizontal	0.25
Sim. 3	12.5	3	Horizontal	0.75
Exp. 1	12.5	3	Horizontal	<i>N/A</i>
Exp. 2	12.5	2	Horizontal	<i>N/A</i>
Exp. 3	12.5	2	Vertical	<i>N/A</i>

Table 3.1 lists selected experiments and three-dimensional simulations performed using 64 spherocylinders in a flat pseudo-two-dimensional box. The box is 0.186m wide and 0.009m thick. Particle characteristics used for both experiments and simulations are: $D = 0.0081$ m; $L = 0.023$ m; density = 2450 kg/m^3 . Simulation 1 starts by generating randomly oriented particles and letting them fall into the container (Fig. 3.2.-left). On the right part of Fig. 3.2 we show that after vibrating for 1200s most rods are oriented vertically. Assuming that our DEM faithfully reproduces the physical behavior, which will be confirmed below, this result suggests that vertical reordering of elongated grains occurs even in absence of the torque generated by curved walls.

Container and particle geometry are chosen such that the horizontal cubic-like lattice shown in Fig. 3.3a. minimizes the total potential energy of the particles. Experiments 1 and 2 were per-

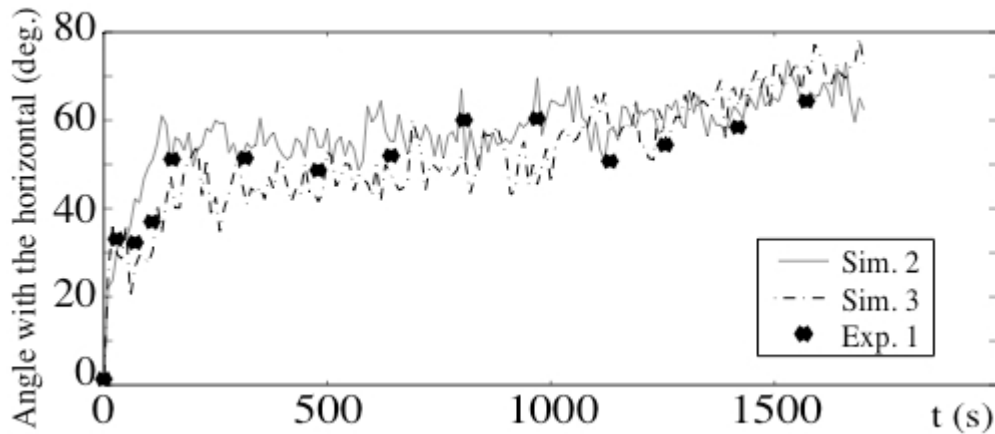


Figure 3.4: Experiment 1, simulations 2 and 3 - Evolution of the mean angle of the particles with the horizontal plane.

formed using this lattice as an initial configuration in order to check whether this arrangement is maintained upon vibration. Figs. 3.3b. and 3.3c. show the rearrangement observed during experiment 1, respectively after 1200s and 1650s. The initially perfect horizontal lattice is dismantled. Spherocylinders clearly rearrange toward a predominantly vertical lattice, although the ordering is not complete by the end of the experiment, whose duration was limited by the fragility of the rods used. Since the potential energy of the starting configuration is minimal, it can only increase during the experiment. In Fig. 3.3a. we highlight, using a white line, the height of the bed at the beginning of the experiment. Fig. 3.3b. shows that after 1200s the position at rest of some of the topmost particles exceeds the initial height of the bed. Upon image analysis one can observe an increase in height of the center of mass by about 4%. Hence, density increase and minimization of the potential energy of the system do not favor vertical ordering. Indeed, during flow or vibration, granular media do not necessarily evolve toward a configuration that minimizes the overall potential energy of the system. Local mechanisms such as void-filling, for instance, can generate size segregation and simultaneously increase the overall potential energy of the system. Experiment 2 shows a similar trend, with a much slower dynamics due to the smaller vibration amplitude. Its detailed discussion is omitted.

We chose to quantify the rearrangement of the particles by monitoring the evolution with time of the mean particle angle with the horizontal plane. Dots in Fig. 3.4 show the instantaneous mean angle obtained by analysis of images taken during experiment 1. We reproduced experiment 1 numerically with simulations 2 and 3. The friction coefficient of the particles used in the experiments is not known. In order to check the agreement of simulations and experiments quantitatively, the results of experiment 1 are therefore compared with two simulations performed with different friction coefficients. DEM predictions follow the same trend as experimental data and their agreement is within the magnitude of the fluctuations of the medium.

Experiment 3 is run starting from a vertical cubic-like lattice and using again 64 rods, a quantity which does not allow to fill completely the third vertical layer. No rearrangement is observed after 1200s as shown in Fig. 3.3d. Above observations therefore suggest a clear tendency of rods to evolve toward a vertical arrangement regardless of initial orientation and even in the absence of cylindrical walls.

However, the small, flat, lateral walls of our container do promote vertical ordering, when inclined rods touch them. This is particularly evident when we compare Fig. 3.3b. and Fig. 3.3c. and observe that rearrangement takes place first at the sidewall. In order to completely eliminate wall effects and convection, a thorough study is reported in next paragraph where sidewalls are replaced by model periodic boundaries.

3.4 DEM simulation set-up

We use Molecular Dynamics DEM to simulate the rearrangement of 256 particles of different lengths in a flat pseudo-two-dimensional container vibrated vertically. Details about the DEM used in the present study can be found in (PWT⁺05), (PL05).

Simulation conditions can be found in table 3.2. All simulations start from a horizontal lattice and use particles whose diameter is $D = 0.0081$ m. The box is 0.009 m thick and has lateral periodic walls. Simulation 4 uses the same particle geometry used in (RPL05) and a periodic box whose width (0.768m) is four times the width of the real box considered there. The behavior of particles of different lengths is investigated through simulations 4 to 10, using periodic walls allowing to host initially 256 particles ordered in 8 horizontal layers. The lateral periodicity is therefore reduced proportionally to the reduction in particle length. Besides varying particle length, we also modulated the vibration amplitude as to achieve different peak accelerations as summarized in table 3.2. Vibration frequency is kept constant at 12.5 Hz.

We varied the lateral periodicity using the longest particles, observing some effect on the ordering kinetics, but no effect on the steady-state ordering. The smallest periodicity tested (64 particles) showed strong fluctuations of the mean angle around the steady state value, due to the strong sensitivity to local lattice defects that are created by the vibrations. A population of 256 particles (and the corresponding periodicity), turned out to be a good compromise to observe steady state ordering in a reasonable computational time.

Table 3.2: Ordering simulations of particles of different elongations.

	Part. L(mm)	Accel.(g)
Sim. 4	23.0	1, 1.2, 1.5, 2, 3, 4, 6
Sim. 5	17.5	3
Sim. 6	16.0	1.5, 3, 4
Sim. 7	14.4	3
Sim. 8	12.9	3
Sim. 9	12.2	3
Sim.10	11.9	3
Sim.11	11.5	2, 3, 4, 6

3.5 DEM simulation results

Fig. 3.5 shows the rearrangement occurred in Simulation 4 after 1200 s: rods have rearranged away from the initial horizontal order, toward a predominantly vertical lattice. Our box does



Figure 3.5: Simulations 4 - Rearrangement after 1200s of vibrations. Initially the particles were ordered horizontally. Lateral walls are periodic.

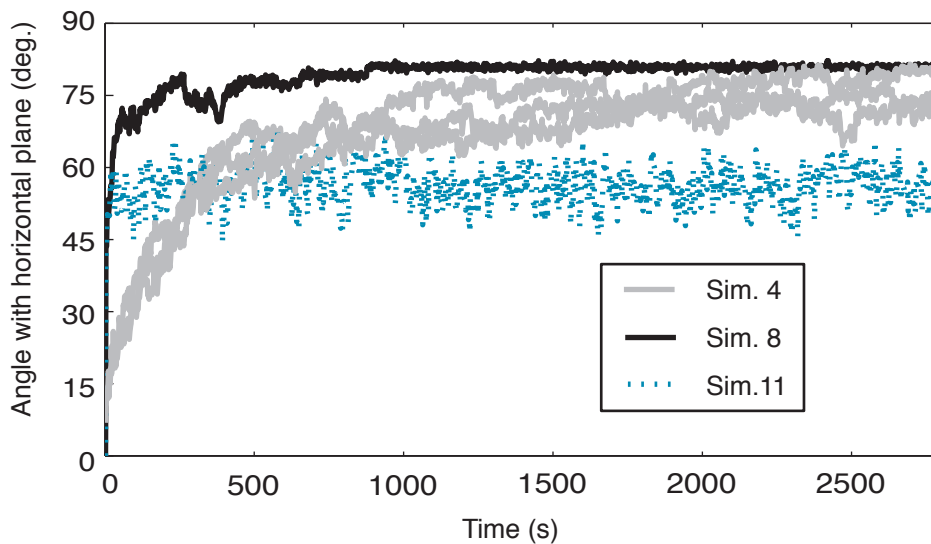


Figure 3.6: (color online) Sim. 4, 8 and 11 - Influence of particle length on vertical ordering induced by 3g acceleration. Plot against time of the mean angle with the horizontal plane of the bottom-most two layers of the medium.

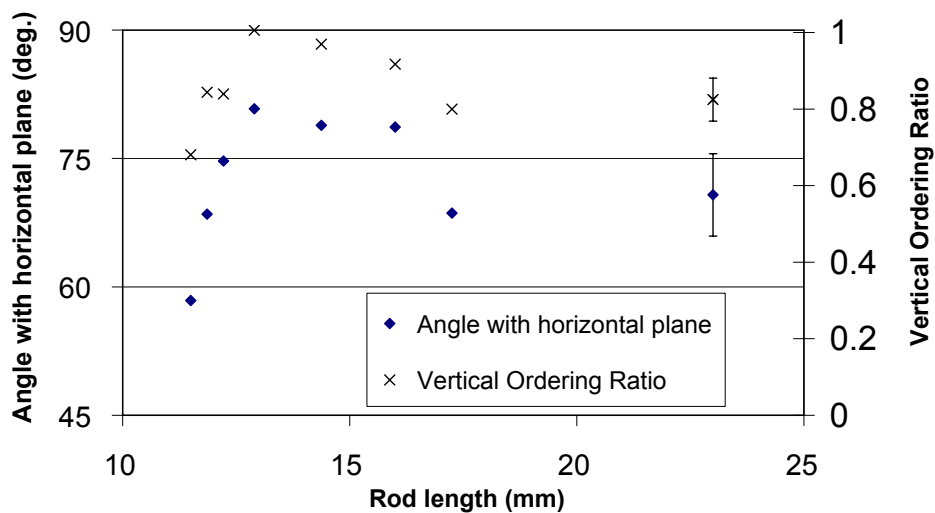


Figure 3.7: (color online) Effect of rod length on the vertical ordering achieved after 1400s vibration at 3g: mean angle with the horizontal plane of the bottom-most two layers of the medium (left axis) and Vertical Ordering Ratio (right axis).

not have vertical sidewalls that can promote vertical ordering when inclined rods touch them as observed macroscopically in (RPL05) or microscopically with the depletion-induced torque (RvRA⁺02) in colloids. Observing vertical ordering in such a periodic set-up confirms that this phenomenon takes place also in the absence of help from the walls. During rearrangement all the particles translate horizontally, similarly to what observed in experiments (VKT04).

To quantify the rod rearrangement, Fig. 3.6 shows the time evolution induced by 3g vibrations of the mean angle with the horizontal plane of the bottom-most two layers of the medium. The longest particles of Sim. 4, order vertically as observed in Fig. 3.5, till reaching a fairly vertical steady state. To appreciate the degree of robustness of the results we report three repetitions of simulation 4, obtained varying the initial arrangement. These three different initial states are obtained by perturbing the initial horizontal lattice with a very short inclined vibration. The ordering dynamics follows reasonably well the three regimes proposed by the adsorption-desorption model (TTV00a): the mean angle of the bottom-most two layers varies initially as $1/t$, then as $1/\ln(t)$, finally it follows an exponential decay. Fig. 3.6 shows also that the shortest rods (Sim.11) do not achieve ordering but an angle only slightly above the random angle of 45° , while the intermediate rods of Sim.8 achieve a very good ordering. It can also be observed that the shorter the particles, the more readily the initial horizontal lattice is broken up. This suggests that under same vibrations very long rods might stay trapped in a horizontal lattice.

A more detailed insight into the effect of particle length on steady state vertical ordering can be gained from Fig. 3.7. Here we consider the effect of particle length on the ordering achieved after 1400s of vibration at 3g. On the left axis we plot the mean angle with the horizontal plane of the bottom-most two layers of the medium, which shows a maximum for 12.9mm rod length (Sim.8). On the right axis we consider the Vertical Ordering Ratio defined as the ratio between the mean angle of the bottom-most two layers of the medium and the maximum angle achievable within each layer. Indeed 12.9mm rods used in simulation 8 reach the maximum angle they can achieve, considering the lateral periodicity of the box.

Fig.3.8 shows the effect of varying acceleration on the Vertical Ordering Ratio of the shortest particles used in simulation 11 (triangles), intermediate used in simulation 6 (squares) and longest particles used in simulation 4 (circles). The shortest particles, which do not order vertically at 3g as described previously, do so at 2g acceleration. At 3, 4 and 6g acceleration, they reach an angle approaching the random angle of 45° , while below 1.5g they stay rather horizontal. The intermediate (Sim.6) particles stay in the initial horizontal lattice at 1.5g, while they order vertically at 3g. They do not achieve a complete ordering at 4g, similarly to what is observed with shorter particles in Sim.8 at 3g. The longest particles (Sim.4) stay horizontal at 2g, they order vertically at 3g, as discussed above, and even better at 4g. At 6g the initial horizontal lattice is broken very quickly but the medium stays in a random configuration. We observe therefore the existence of an optimum acceleration to promote vertical ordering. This acceleration is around 4g for the longest particles used in simulation 4, closer to 3g for the intermediate particles used in simulation 6 and to 2g for the shortest particles used in simulation 10.

When vibrated at 12.5 Hz and 6g acceleration, all types of particles show occasionally a non homogeneous vibration pattern in which two vertical and neighbouring portions of the medium vibrate in opposition of phase. This can be easily explained by considering a simple inelastic ball bouncing model (IBBM) as per (vB97). The results of this model relevant for our system

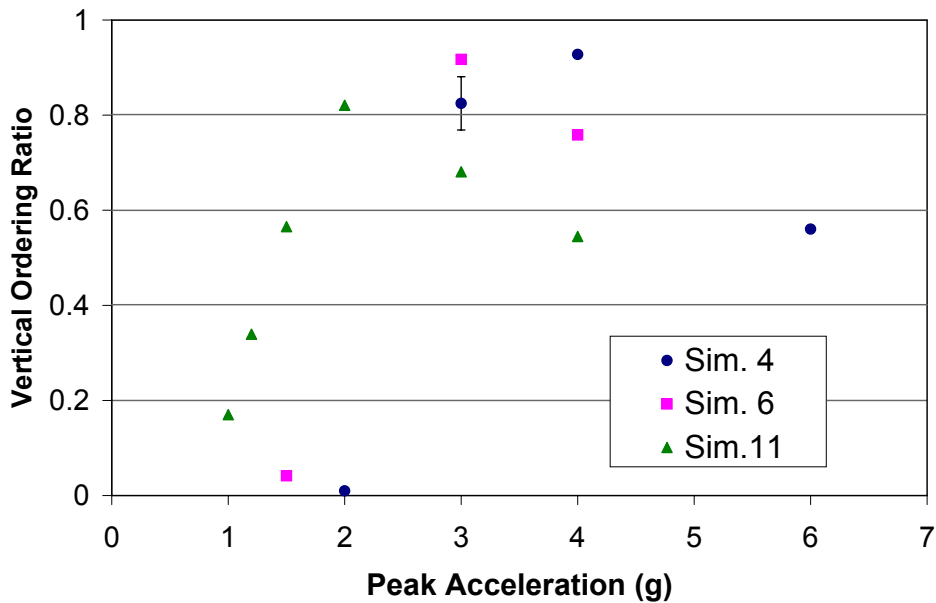


Figure 3.8: (color online) Influence of the acceleration on the Vertical Ordering Ratio achieved after 1400s of short (Sim.11), intermediate (Sim.6) and long rods (Sim.4).

are shown in figure 3.9. With increasing acceleration, the take off velocity of the ball increases and so do flight duration and distance. As reported long ago by Douady et al (DFL89) the spatially homogeneous temporal oscillation becomes unstable above a threshold acceleration and a period doubling occurs. At 4g the trajectory is not anymore the same for all flights and the ball undergoes an alternate series of short and long flights with a total periodicity that is twice the excitation period. At 6g the subsequent flights of a ball are the same but their period is still twice the excitation period. In both such cases two neighbouring portions of the medium can vibrate in opposition of phase.

3.6 Is vertical ordering linked to void sizes?

How can the rods' intrinsic tendency to form a vertical lattice and the behavior of particles of different lengths be explained?

When a granular medium is vibrated, gravity drives particles from upper layers to fill voids that may appear in the lower layers. We showed that spherocylinders orient vertically, regardless of boundary or initial conditions. During the rearrangement through vibrations, a frequent emergence of holes of the size of the particle diameter can be observed. An example of such a hole is highlighted with a white circle in Fig. 3.3. Such holes can host only particles that are rather vertical. The void-filling mechanism, usually explaining size-segregation of spheres (SUK⁺06), may therefore also be at the origin of the vertical ordering of spherocylinders, as already conjectured by Blair et al. (BNK03).

To test this interpretation, we analyzed the size distribution of the holes within the medium using the *Intersect Length Distribution (ILD)* approach. We considered several thousand lateral

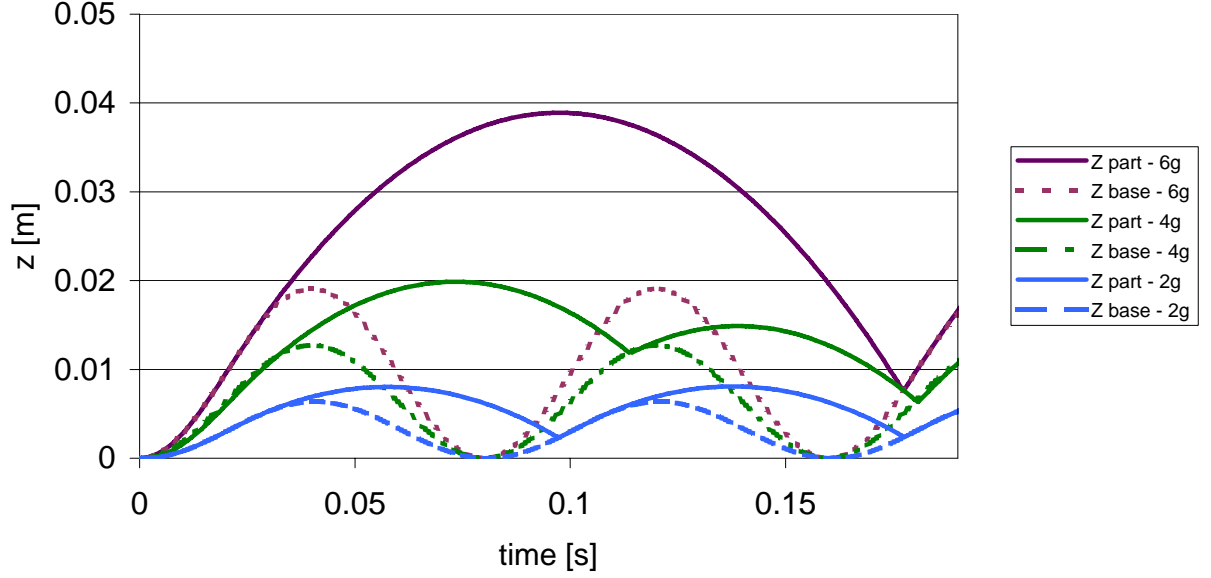


Figure 3.9: Trajectory of a point mass taking off from a base excited sinusoidally.

snapshots of the medium configuration at different moments in time during simulation 4 and filled the holes between the particles with horizontal segments, whose length was taken as a measure of the void size. The symmetry breaking introduced by the vertical orientation of the vibration conditioned our choice of considering horizontal segments.

We focused on two classes of holes: short holes, whose length falls in-between the diameter and the length of the rods and elongated holes, whose length is greater than rod length. Short holes cannot host a horizontal particle: they clearly drive the particles in the medium to orient vertically, if particle neighbors allow this rearrangement. Elongated holes can host a particle at a generic orientation. If a horizontal particle lands in such a hole, its orientation is not modified. If several vertically aligned particles fall into an elongated hole, their orientation is not modified either. However, a long hole can induce a particle of generic orientation falling into it to orient horizontally, thus acting as a horizontal wall, if particle neighbors do not prevent this.

We define λ_s and λ_l as the total length of respectively the short and long voids and λ_t the total void length. For instance the probability of a void to belong to the class λ_s is:

$$P_s = \frac{\lambda_s}{\lambda_t} \quad (3.1)$$

Similarly, indicating the medium porosity as ε , we can express the porosity due to small holes as:

$$\varepsilon_s = \varepsilon P_s \quad (3.2)$$

To judge on the validity of the void-filling interpretation, it is important to look at the void distribution in the portion of the vibration cycle when the medium is bouncing and the particles are forced to fill the available holes below their previous positions. The top-left curve in Fig. 3.10 shows the time evolution of the height of the medium H (left vertical axis) along few vibration cycles, the bottom-left curves that of the probability P_s , P_l of the short and long void

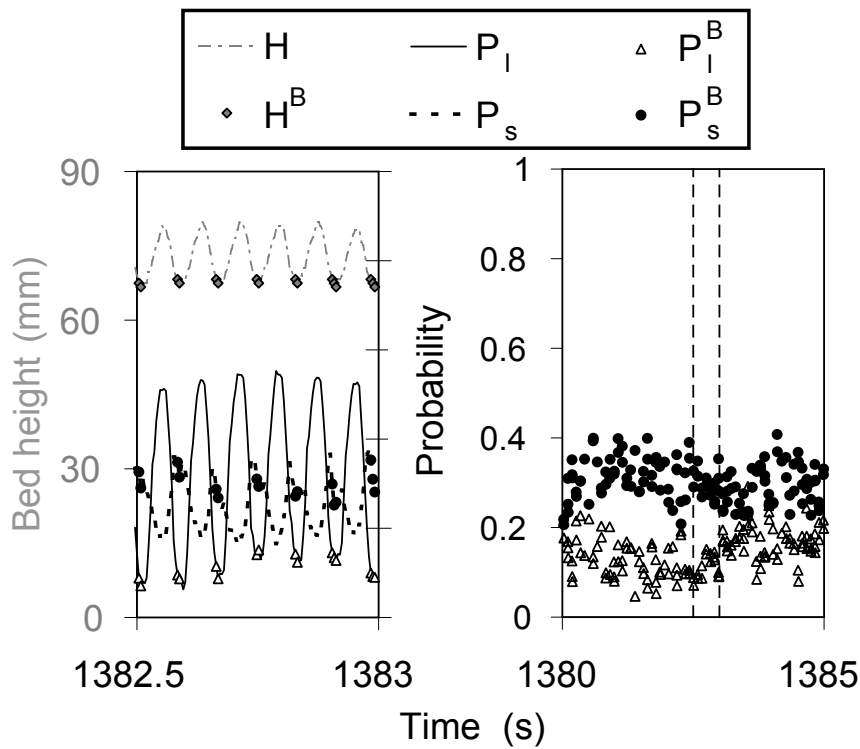


Figure 3.10: Simulation 4 - Left: detail of the time evolution of the medium height (H , top curve, left axis), and of the probability P_s , P_l of occurrence of short and long voids (bottom curves, central axis). Dots on each curve (H^B , P_s^B , P_l^B) identify the rebounds. Right: P_s^B , P_l^B along several vibration cycles. The dashed area corresponds to the time window magnified on the left side of the figure.

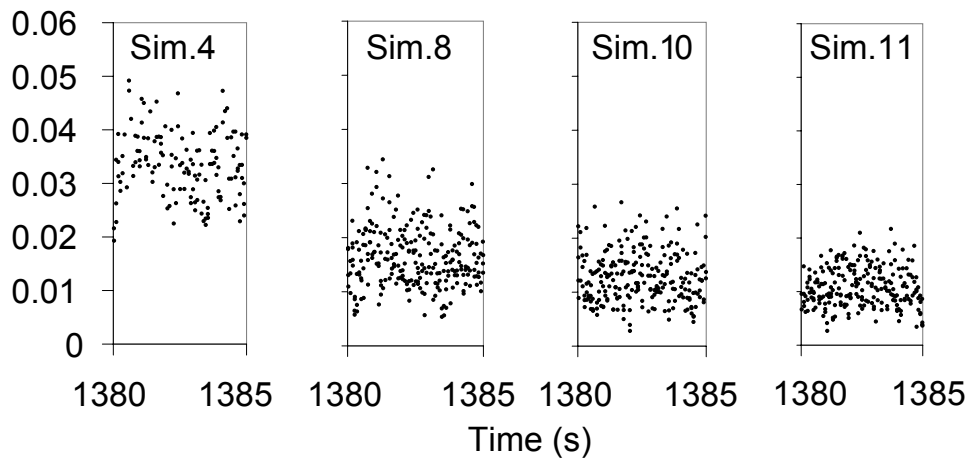


Figure 3.11: Influence of particle length on the porosity ϵ_s^B inducing rods to verticalize. From left to right: simulations 4, 8, 10, 11. The porosity due to long holes ϵ_l^B is similar for these four simulations and is omitted.

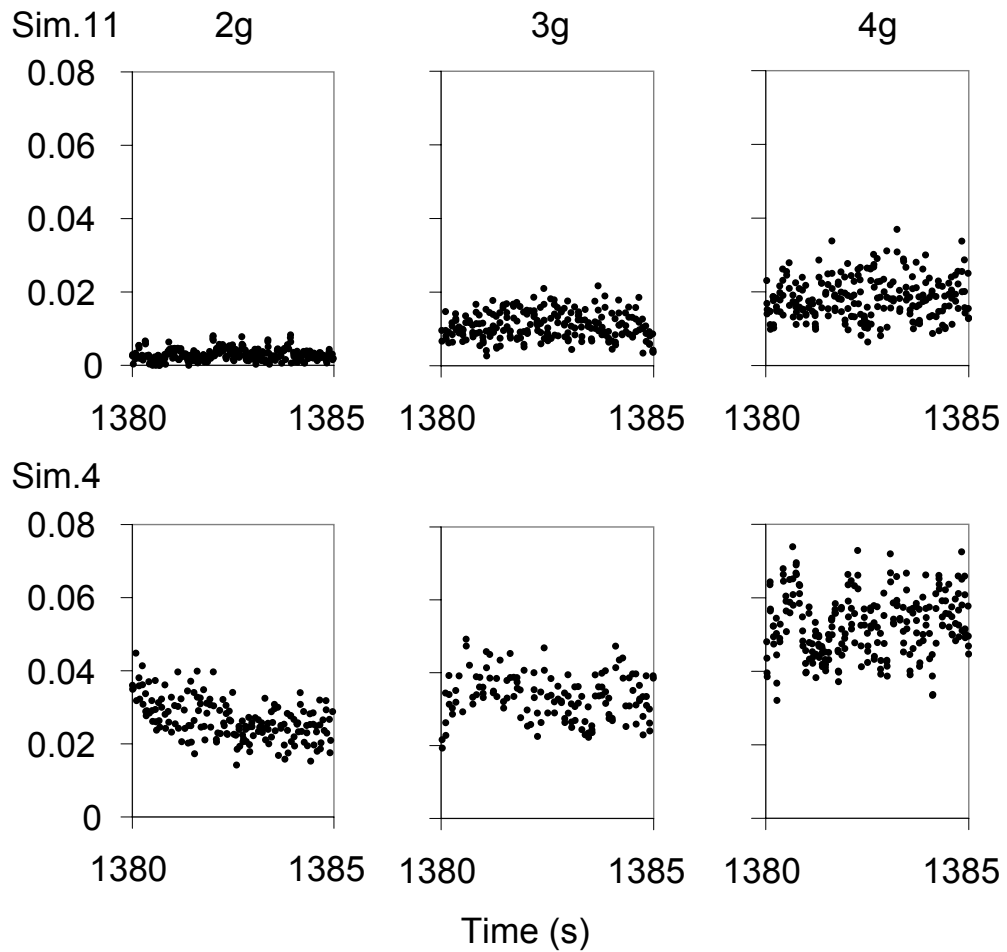


Figure 3.12: Effect of acceleration on the porosity ε_s^B inducing rods to verticalize. Acceleration changes from 2 to 3 to 4 times gravity moving from left to right. Simulations 11 with short particles are at top; simulations 4 with long particles are at bottom.

classes (right vertical axis). We carefully analyzed the height of the medium to identify instants within the vibration cycles where the medium bounces. These were characterized by a double condition: the medium height is below the threshold of 70 mm (about three particle lengths) and it is decreasing. The diamond-like gray points on the top-left curve of Fig. 3.10 highlight the value of the medium height when the medium bounces H^B . At those rebounds, the probabilities of the two void classes P_s^B, P_l^B are indicated respectively with black circles and white triangles in the bottom-left quadrant. One can see that short holes (of length in between the rod diameter and length) are more probable than long holes. The right side of Fig. 3.10 shows the probability of the void classes at rebounds P_s^B, P_l^B over a longer time-span and confirm this characteristic pattern: on average about 33 % of the void volume within the medium belongs to short holes that promote vertical ordering. This supports void-filling as an interpretation for vertical ordering. A lower percentage of the void volume, about 15 %, belongs to holes longer than particle length. The gap between the two probabilities is even bigger at an earlier stage, before reordering.

To appreciate the influence of particle length, Fig. 3.11 compares the porosity at bouncing due to short holes for simulations 4, 8, 10, 11. Shorter particles (Sim.11) show a lower porosity due to short voids, which promote vertical ordering. This observation is in agreement with the lower tendency of short particles to align vertically, shown in Fig. 3.6. It thus supports the void-filling interpretation, suggesting that a minimum availability of small voids is needed for vertical ordering to occur. ϵ_l^B is similar for these four simulations and is omitted.

In section III we discussed the effect of acceleration on ordering (Fig. 3.8). An optimum acceleration exists to promote vertical ordering, higher for the longest particles (Sim.4) than for the shortest particles (Sim.11). Applying the same *ILD* approach to these simulations, we obtain the void distributions shown in Fig. 3.12. For all accelerations, ϵ_s^B is higher for long particles (Sim.4) than for short particles (Sim.11) as already observed for an acceleration of 3g. The height of the medium as well as the porosity contributed by the long and short voids also increase monotonically with acceleration. As already commented, Fig. 3.8 shows that significant vertical ordering occurs in Sim.11 at 2g, while a random arrangement is obtained for higher accelerations. Therefore, the monotonic dependence of ϵ_s^B on acceleration does not, by itself, allow a clear and thorough interpretation of the dependence of vertical ordering on acceleration reported in Fig. 3.8. This led us to an alternate explanation to vertical ordering, which we describe next.

3.7 Potential energy barriers

Holes are needed to allow any reordering in the medium. Their sizes can influence the reordering, but cannot clearly explain its dependence on acceleration. The evolution of a horizontal or vertical lattice is affected on one side by the rate of creation of the lattice, which is conditioned by the appearance of holes, but also by the rate of its break-up. A lattice can be broken up because particles are either expelled from it or rotating into a different orientation. Such a particle has to overcome different energetic barriers. A rod of mass m jumping out of a horizontal resp. vertical lattice has to overcome an energetic barrier of:

$$U_H = mgD, \quad \text{resp.} \quad U_V = mgL. \quad (3.3)$$

A rod rotating from a horizontal into a vertical position has to overcome an energetic barrier of:

$$U_R = mg(L/2 - D/2). \quad (3.4)$$

For the range of particle lengths and the diameter considered in this study, the following inequalities hold:

$$U_R < U_H < U_V. \quad (3.5)$$

Shaking a horizontal lattice of rods with a low energy input is insufficient to break the horizontal lattice. Increasing the energy input allows the medium to reach the rotational threshold. In this intermediate range of accelerations, the rods have enough energy to break away from a horizontal lattice through rotation, but not to jump out of a vertical lattice. If energy input is close to the energy barrier that a rod needs to overcome to jump out of a vertical lattice, the latter becomes unstable too and the medium tends to orient at a random angle.

These energetic barriers must be compared with an appropriate measure of the energy available to the vibrated rods. The motion of each particle can be separated into a bulk motion due to sinusoidal vibration and a fluctuation due to collisions. Only the fluctuant part can generate a relative motion of a particle with respect to their neighbors. We therefore define the mean fluctuant kinetic energy of the rods as:

$$\widetilde{E}_K = \frac{m \sum_{i=1}^N (v_i - \bar{v})^2}{N} \quad (3.6)$$

We will not venture here into the still open question of defining a granular temperature, but simply call this quantity an energy. This quantity is found to follow periodic variations insensitive to any rearrangement of the rods. We normalize the mean fluctuant kinetic energy of the rods by the rotational and vertical potential energy barriers. Of particular interest are the peaks of these ratios, which give an insight into the ability of the system to break an existing arrangement.

In figure 3.13 we use the peaks of these two ratios to interpret all the results in the form of a phase diagram. A point corresponds to one simulation with given particle elongation and acceleration. Simulations with same rod geometry and increasing acceleration describe a ray moving away from the origin. Contours represent an interpolation of the Vertical Ordering Ratio (VOR): zero corresponds to a horizontal orientation, one to the most vertical orientation that rods can achieve. At low energy input, when not enough energy is available to overcome the rotational barrier ($E_K/U_R < 1$), the initial horizontal lattice is stable and no rearrangement occurs. At intermediate energy input, when rotation is enabled, rearrangement occur leading to a vertical lattice. When an excess of energy is available and rods can overcome the energy barrier to jump out of a vertical lattice ($E_K/U_V > 1$), the system breaks the initial lattice, but evolves toward a random orientation. The transitions between the three regimes are smooth and steady state orientation with intermediate angles are reached across transitions.

3.8 Conclusions

Vertical ordering of a vertically vibrated medium of rods initially in a horizontal lattice seems intrinsic to particle anisotropy, occurs regardless of initial conditions, and also with no help

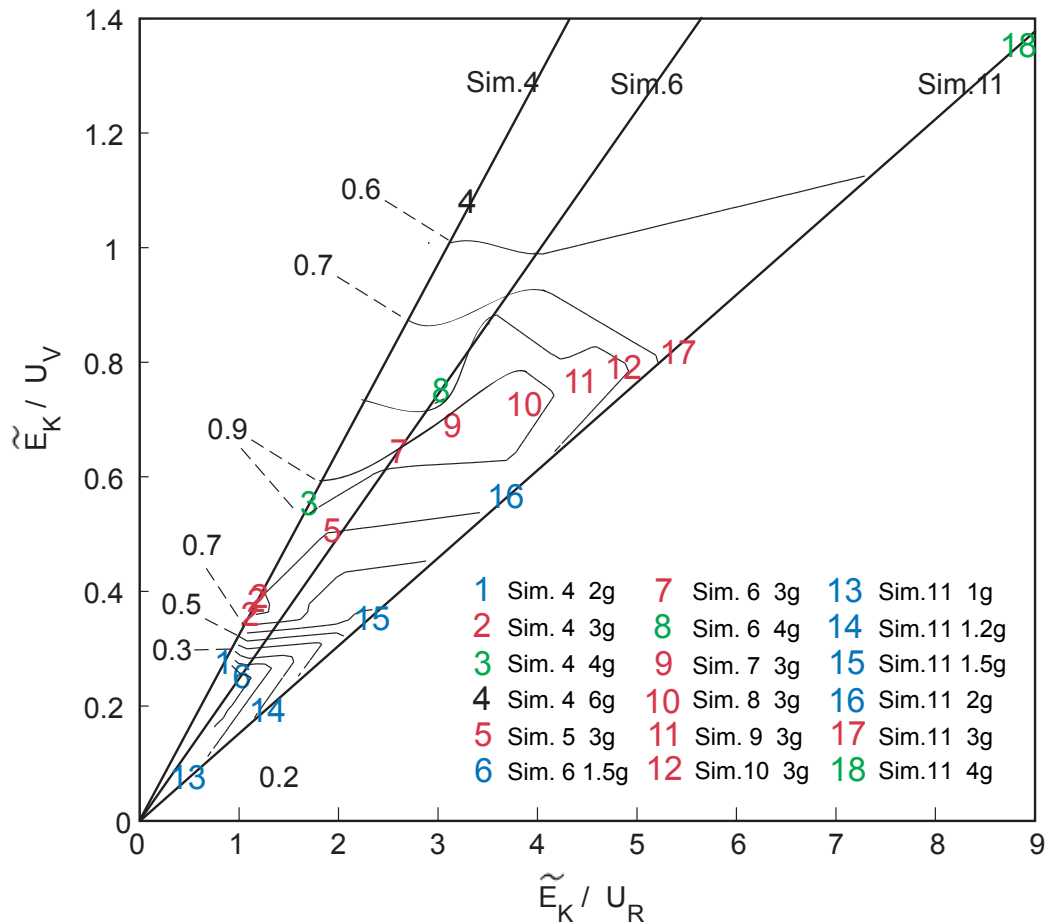


Figure 3.13: (color online) Phase diagram summarizing the peak values of fluctuant kinetic energy normalized by the rotational potential barrier on x-axis and by the vertical potential barrier on y-axis. Simulations with same rod geometry and increasing acceleration describe a ray moving away from the origin. Contours represent an interpolation of the VOR: zero corresponds to a horizontal orientation, one to the most vertical orientation that rods can achieve. Colors help grouping simulations based on their acceleration: blue identify acceleration lower than 2g, red 3g acceleration, green 4g and black 6g.

from side-walls. While short particles break away rapidly from the initial lattice but evolve toward a random orientation, longer ones have more difficulties leaving the initial horizontal lattice and they evolve toward a vertical lattice. Too mild a vibration can prevent breakage of the horizontal arrangement, whereas a too vigorous one can prevent the vertical ordering, leading to a random orientation. Thus an optimal acceleration promoting vertical ordering exists, which increases with rod length. We can explain through void-filling why long rods tend to orient vertically as opposed to short rods, by assuming that a minimum availability of short voids is needed. However, invoking just void-filling, no clear explanation of the dependence on vibration intensity can be found. We therefore consider the energetic barriers that particles need to overcome to exit a horizontal or a vertical lattice. Comparing the maximum available fluctuant kinetic energy with these energetic thresholds, we can identify three regimes. At low energy input, the initial horizontal lattice is stable. At intermediate energy the particles cannot escape from a vertical lattice, which is thus stable. At too high energy input, even the vertical lattice becomes unstable. The notion of low and high energy input depends on rod length, thus reconciling both the effects of the particle length and vibration acceleration on vertical ordering. This work was published partly in (RPL05) and then completely in (RPL07).

Chapter 4

Shape segregation of mixtures of rods and spheres vibrated vertically.

4.1 Summary

In this chapter, we study both experimentally and numerically the segregation of a binary mixture of spherocylindrical rods of same volume and different elongations (down to the limit of spheres, where elongation is zero), which is vibrated in a cylinder. It is to our knowledge the first experimental study of this phenomenon. In the conditions considered, we observed that short spherocylinders tend to migrate to the top, above the spheres, while long spherocylinders tend to migrate to the bottom. More generally short spherocylinders tend to migrate to the top of long spherocylinders. Moreover, the particles migrating to the bottom tend to arrange in an ordered state. Our discrete element model (DEM) faithfully captures the physical behavior. We extended the study to binary mixtures of spheres and spherocylinders that have different volumes, building a phase diagram characterizing the existence and direction of segregation as function of the geometry of the particles. Friction is shown numerically to have a strong impact on segregation. We link these observations to the tendency of rods to orient vertically studied in chapter 3. Part of this work was published in (RPL06).

4.2 Introduction

The introduction of chapter 2 gave an overview of the literature related to the segregation of vibrated spherical media. Albeit most studies on segregation induced by vibration concerned so far spherical particles, in most cases real-world products are far from spherical. Williams (WP03) simulated random packings of spheres and spherocylinders by mechanical contraction. Abreu (ATC03) used Monte Carlo methods to simulate compaction of spherocylindrical rods and shape segregation from spheres. Elongated grains are shown to have peculiar behaviors that differ substantially from that of spheres. Chapter 3 dealt with the vertical ordering arising in

elongated particles when vibrated vertically. The understanding of such vertical ordering will be exploited in this chapter to understand how a difference in particle elongation can drive a mixture toward segregation.









		Rod geometry	
		Diameter ϕ	
		($\times 1e-3$ m)	
Sim. 4		4	2.194
Sim. 5		4.25	1.718
Sim. 6		4.45	1.414
Sim. 7		4.75	1.042
Sim. 8		4.94	0.850
Sim. 9		5.5	0.434
Sim. 10		6	0.181
		6.5	0

Table 4.1: Geometry of the iso-volume particles used for shape segregation simulations. Each simulation considers a 50/percent mixture of rods of one type with the 6.5mm iso-volume spheres.

4.3 Simulating shape segregation of iso-volume particles.

This paragraph reports DEM simulations to quantify the segregation of seven binary mixtures of iso-volume particles vibrated in a cylindrical container. Particle geometries are reported in table 4.1. Each mixture is composed of spheres of diameter 0.0065 m and spherocylindrical rods of same volume but different elongations. Simulations start by filling a cylinder (diameter 0.05 m) with a homogeneous mixture of 135 spheres and 135 spherocylinders of density 450 Kg/m. The bottom wall is vibrated sinusoidally at 50 Hz with 5g peak acceleration. Friction coefficient is 0.75. Figure 4.1 shows typical lateral snapshots of the segregation observed after 600s. Images from from left to right correspond to mixture with increasing rod elongation. When short rods are mixed with sphere they are observed to segregate to the top of iso-volume spheres. Long rods on the contrary tend to segregate to the bottom. The bottom layers of the medium tend to crystallize, regardless of whether rods or spheres are at the bottom. Vertical ordering comes with crystallization when spherocylinders segregate to the bottom, as on the right of figure 4.1.

To quantify this segregation one can define the Vertical Segregation Ratio, $VSR(t)$ as the ratio of the height of the center of mass of the two species composing the mixtures.

$$VSR(t) = \frac{h_{CM,SCyl}(t)}{h_{CM,Sph}(t)} \quad (4.1)$$

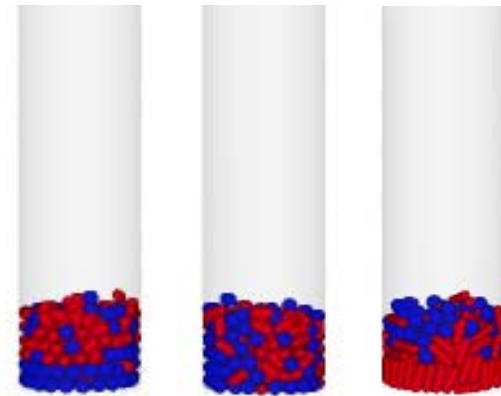


Figure 4.1: (color online) Lateral snapshots of the segregation obtained after vibrating 600s. Spheres are blue, rods red. Rod elongation increases from left to right.

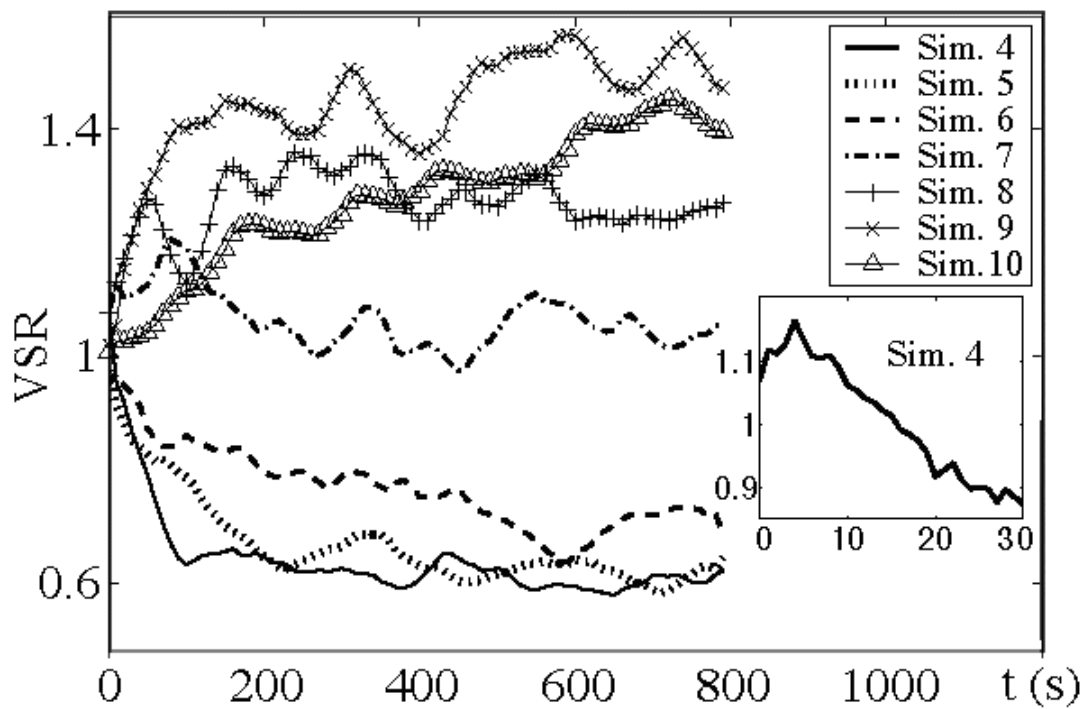


Figure 4.2: Dynamic evolution of $VSR(t)$ for simulations 4 to 10. A moving average on three samples was made to smooth the profile. Inset: detail of the non-smoothed $VSR(t)$ of Sim.4 at the beginning of the experience.

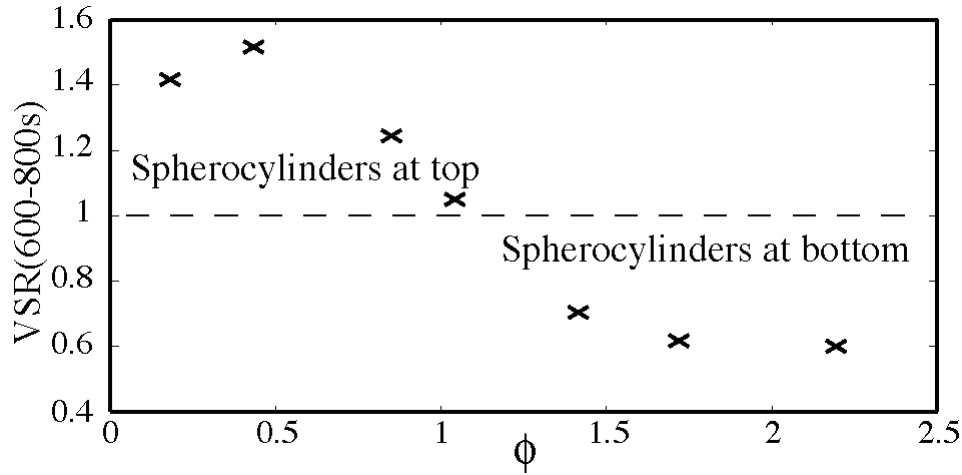


Figure 4.3: Influence of the elongation on the vertical segregation of spherocylinders from a binary mixture with iso-volume spheres.

To study the long term tendency of the mixture it is interesting also to define the time average of $VSR(t)$ from 600 to 800s:

$$\overline{VSR}(600 - 800s) = \frac{\int_{t=600s}^{t=800s} VSR(t) \cdot dt}{200} \quad (4.2)$$

The dependence of this latter quantity on the rod elongation ϕ is reported in Figure 4.3 for simulations 4 to 10. In accordance with the qualitative results shown in figure 4.1, short rods tend to migrate to the top of iso-volume spheres, while long to the bottom. No segregation occurs for the trivial limit of elongation going to zero, but also for rod elongation of about 1.1. In most cases the particles segregating to the bottom also orient vertically. Figure 4.2 shows the evolution of VSR over time. This ordering and segregation pattern can be interpreted thanks to the understanding of the vertical ordering of elongated grains gained in chapter 3. If the medium is driven with an amplitude and acceleration sufficient to orient vertically long rods, shorter rods will tend to a random orientation. Among iso-volume particles, short rods will therefore offer a characteristic size for segregation which is higher than spheres and long rods. As a result, short rods segregate to the top of a mixture with iso-volume spheres and long spherocylinders to the bottom. The link between vertical ordering and rod segregation can be confirmed analyzing the initial behavior of long rods used in Sim.4 (inset of figure 4.2). Upon pouring elongated spherocylinders have a low angle with the horizontal plane. When vibrated they initially tend to migrate toward the top of the bed, they then orient vertically and reverse their vertical migration, moving toward the bottom. This behavior is systematically observed with grains having sufficiently high elongation. The trend we observe in vertical segregation is opposed to what reported in (ATC03) based on MC simulations. The authors of that study never observed crystallization in a cylindrical container and observed long rods moving to the top of iso-volume spheres and short rods moving to the bottom. This discrepancy calls for an experimental check, which will be presented in paragraph 4.5.

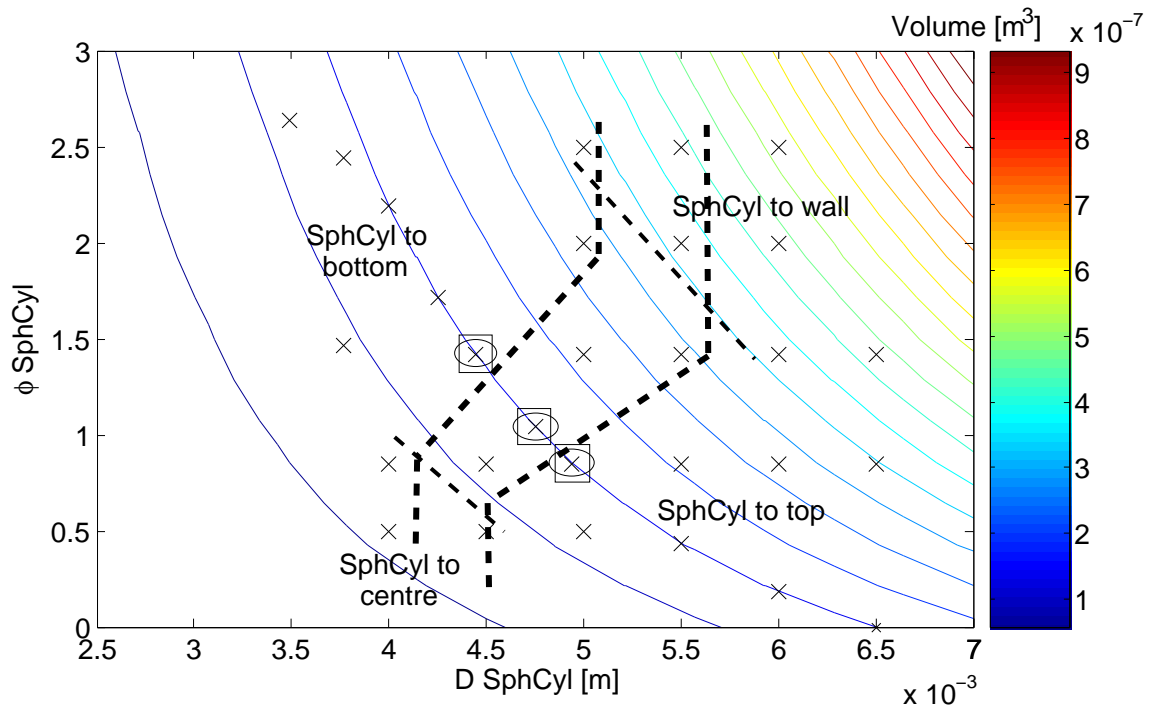


Figure 4.4: Shape segregation of spherocylinders of different elongations from 6 mm spheres in a vibrated cylinder. Friction = 0.75. Dashed lines suggest boundaries between the different segregation patterns observed.

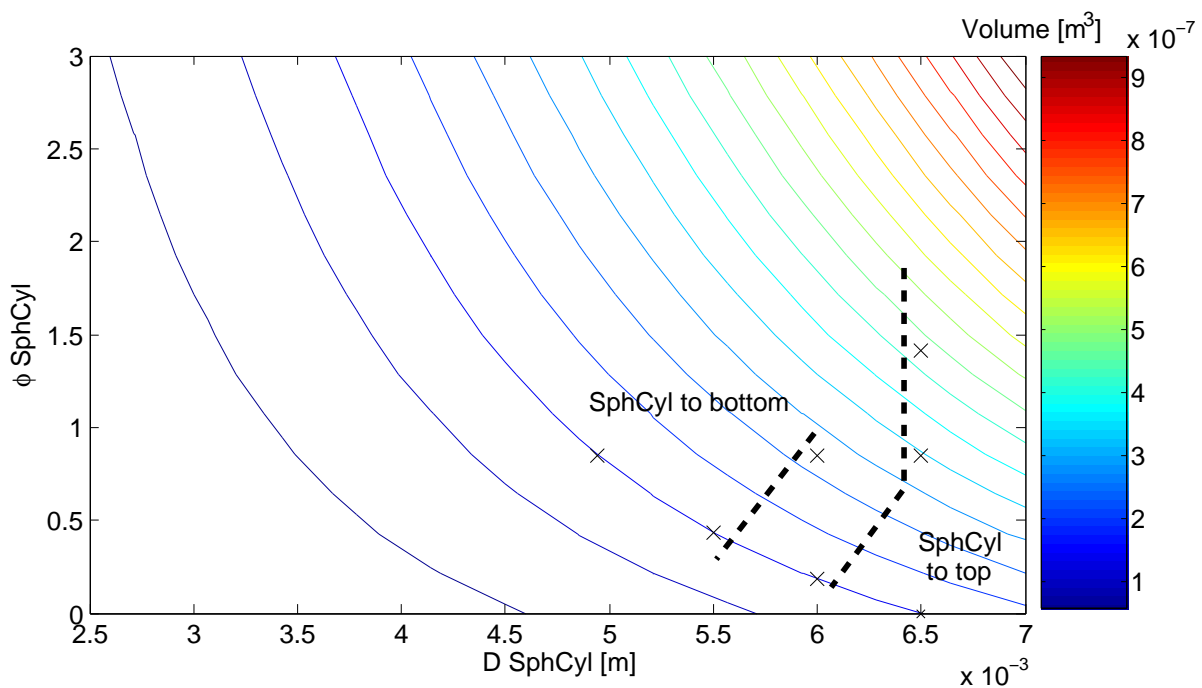


Figure 4.5: Shape segregation of spherocylinders of different elongations from 6 mm spheres in a vibrated cylinder. No friction. Dashed lines suggest boundaries between the different segregation patterns observed.

4.4 Simulation of the shape segregation of particles of different volumes.

It is natural to extend the study presented in the previous paragraph to mixtures of particles of different volumes. A systematic segregation study of mixtures of 6.5mm spheres and rods of different diameters and elongations was undertaken under the same vibration conditions as the previous paragraph. Figure 4.4 presents a phase diagram summarizing the long-term segregation of the mixtures. Iso-volume lines are plotted as continuous colored level curves. A x-mark on the phase diagram represents the mixture of the corresponding rod geometry with 6.5mm spheres. The mixtures on the iso-volume line intercepting the abscissae at 6.5mm represents the iso-volume mixtures described in the previous paragraph.

A mixture is considered segregated vertically when VSR is lower than 0.9 (rods migrate to the bottom) or VSR is higher than 1.1 (rods migrate to the top). Dashed lines sketch some approximate boundaries between different segregation patterns. Five regions can be identified. Within the central region of the plot no segregation occurs. In the south-east part rods migrate to the top of iso-volume spheres. In the north-west region rods migrate to the bottom. Some radial segregation bringing rods to the sidewall is observed in the north east region, while in the south-west radial segregation brings rods to the centre. Vertical and radial segregation can coexist. To verify the robustness of the simulation results, three simulations were repeated by decreasing ten times the time-step from $6 \cdot 10^{-4}$ to $6 \cdot 10^{-5}$. These simulations are highlighted by adding a rectangle around the x-mark. Similarly, the segregation of some mixtures was tested also while vibrating also the sidewall of the cylinder. These simulations are highlighted by adding an ellipse around the x-mark. In both cases the boundaries between absence of segregation and segregation toward the top or the bottom were not altered. The impact of friction among particles and among particles and walls was also tested for some mixtures, by setting friction coefficients to zero. Results are reported in 4.5 and show a significant shift of segregation boundaries toward "south-east", i.e. lower diameter and lower elongation. It can be argued that a lower friction makes it easier also for shorter rods to align vertically and therefore to segregate to the bottom of the mixture. Further confirmations to this hypothesis should be sought.

4.5 Comparison with experiments

4.5.1 Experimental setup

Figure 4.6 shows the experimental setup. All experiments are started from a mixed granular bed. All particles have same density ($\rho = 2500 \text{ kg/m}^3$). The mixture is prepared in two separate halves, which are poured one after the other into a Plexiglass cylindrical container, whose internal diameter is 50mm. A TIRA electromechanical shaker (model TIRAvib51075) is then used to vibrate vertically a cylinder with a sinusoidal vibration of amplitude $A = 1.99\text{mm}$ and frequency $\nu = 25 \text{ Hz}$. The adimensional acceleration $\Gamma = A(2\pi\nu)^2/g = 5$, where g is the gravity acceleration. At the end of the experiment, lateral pictures are taken, to record whether ordering has taken place at wall, and the mixture is carefully separated into horizontal halves (unless the experiment conditions mention more layers) by inserting two horizontal metallic spacers

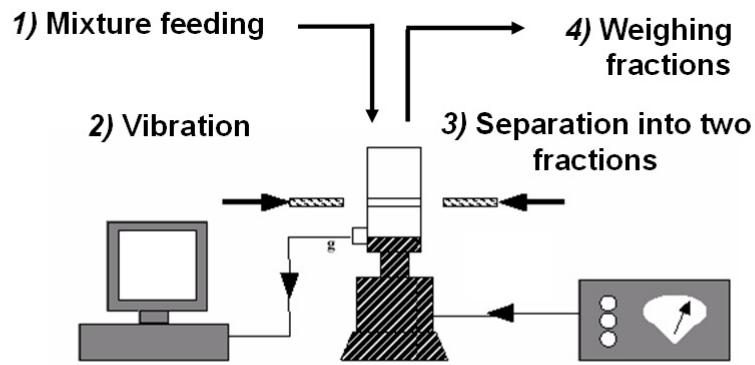


Figure 4.6: Setup for shape segregation experiments.

through appropriate slits in the sidewall. Each half is then sieved to measure its composition. The experiments are repeated three times and the variability of the initial mixture is measured three times without applying vibrations, following the same procedure.

The left part of Table 1 reports the size of the glass particles used in the experiments and the right part of Table 1 reports the composition of the binary mixture used in each experiment.

Table 4.2: Geometry of the particles used in the shape segregation experiments. Abbreviations: SCylN = Spherocylinders of diameter N mm, SphN = sphere of diameter N mm.

Part.	Diameter [mm]	Length [mm]
Sph6	6.0	—
SCyl5	5.0	7.43
SCyl4	4.0	10.3
Sph8	8.0	—
Sph5	5.0	—
Sph4	4.0	—

Table 4.3: Composition of the mixtures used in the shape segregation experiments.

Exp.	Longer Particle	Shorter Particle
Exp.SHS1	SCyl5	Sph6
Exp.SHS2	SCyl4	Sph6
Exp.SHS3	SCyl4	SCyl5
Exp.SHS4	SCyl4	Sph4
Exp.SHS5	SCyl5	Sph5
Exp.SHS6	SCyl4	Sph5
Exp.SHS7	Sph6	Sph4
Exp.SHS8	SCyl4	Sph8
Exp.SHS9	Sph8	SCyl5

4.5.2 DEM simulations setup

The same mixtures used in the experiments 4.3 were simulated in simulations 1 to 9. Further iso-volume mixtures, which could not be studied experimentally, were also simulated as summarized in 4.4 and 4.5. Particle restitution coefficient is set to 0.95, friction is 0.95 and contact time is $2e-5$ s. The simulations are started by generating the particles with random orientations, uniformly distributed in a box above the cylinder and by letting them fall into the cylinder. The cylinder is then vibrated as in the experiments.

Table 4.4: Geometry of the particles used in the shape segregation simulations (further to those reproducing experiments in Table 4.3). Abbreviations: SCylN = Spherocylinders of diameter N mm, SphN = sphere of diameter N mm.

	Part. Diameter [mm]	Length [mm]
<i>SCyl5.54</i>	5.54	6.54
<i>SCyl4.42</i>	4.42	8.84
<i>SCyl3.5</i>	3.4	12.92
<i>SCyl3</i>	3.0	17.00

Table 4.5: Composition of the mixtures used in the shape segregation simulations (further to those reproducing experiments in Table 4.3).

	Exp. Longer Particle	Shorter Particle
Sim.SHS10	<i>SCyl5.54</i>	<i>Sph6</i>
Sim.SHS11	<i>SCyl4.42</i>	<i>Sph6</i>
Sim.SHS12	<i>SCyl3.5</i>	<i>Sph6</i>
Sim.SHS13	<i>SCyl3</i>	<i>Sph6</i>

4.5.3 Results

Experiments 1 to 3 focus on the segregation occurring in mixtures of particles with same volume and different elongations. The picture included in figure 4.7 are taken from a side of the cylindrical container after 20 min. of vibrations. Experiment 1, where short spherocylinders are initially mixed with spheres results in a moderate vertical segregation of spheres to the bottom, where they partially order. Experiment 2, where longer spherocylinders are initially mixed with spheres, gave rise to a moderate vertical segregation of spherocylinders to the bottom, where they order vertically. Experiment 3, where longer spherocylinders are initially mixed with short spherocylinders, shows a strong vertical segregation of longer spherocylinders to the bottom, where they order vertically. Indeed, a hierarchy is therefore found among iso-volume particles: long spherocylinders tend to migrate to bottom more strongly than iso-volume spheres and even more strongly than short iso-volume spherocylinders. A quantitative confirmation of this phenomenon can be found in the plot within figure 4.7, where the concentration of longer particles in the top half of the mixture is plotted as function of time. Experiments and simulations are found to agree well after 20 min. of vibrations. This agreement consolidates the confidence in DEM simulation versus the MC simulations reported in (ATC03). We believe that this discrepancy stems from the limitations of MC methods: i.e. the absence of mechanics in the dynamic evolution and the absence of simultaneous movement of more particles.

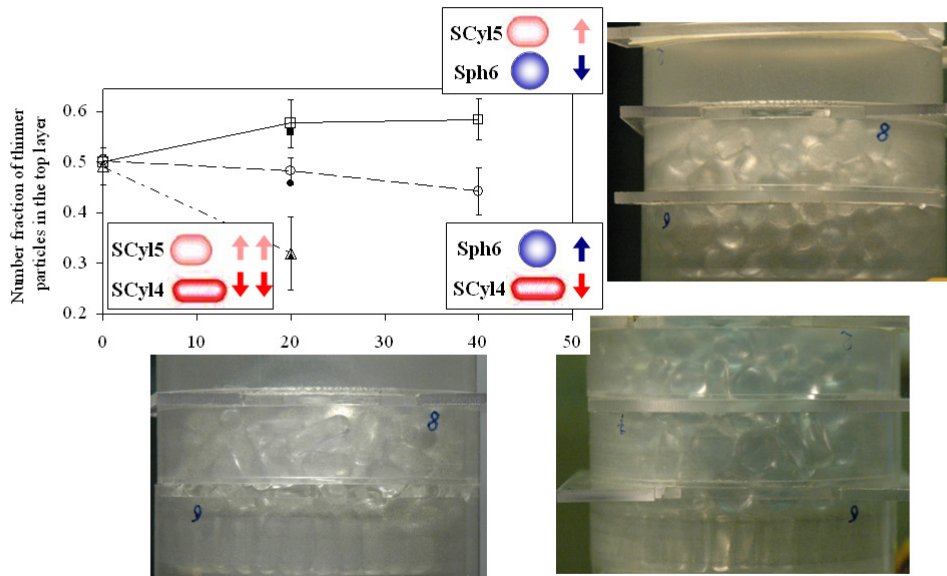


Figure 4.7: Shape segregation experiments: Number fraction of thinner particles in iso-volume mixtures during experiment 1 to 3 and corresponding simulations 1 to 3. Filled dots = experiments, Empty dots = simulations. Pictures are taken after 20min. of vibrations.

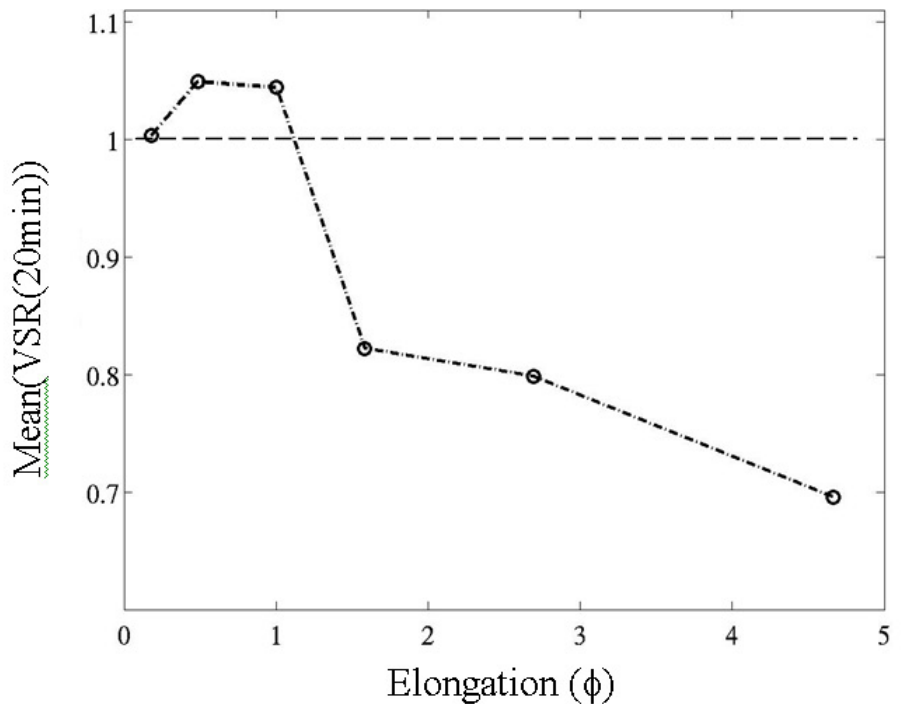


Figure 4.8: DEM Simulations (Sim. 1,2,10,11,12,13) of binary mixtures of 6mm spheres with iso-volume spherocylinders of increasing elongations. VSR averaged over 2 min. around 20min. VSR respectively higher/lower than one means that spherocylinders migrate at top/bottom.

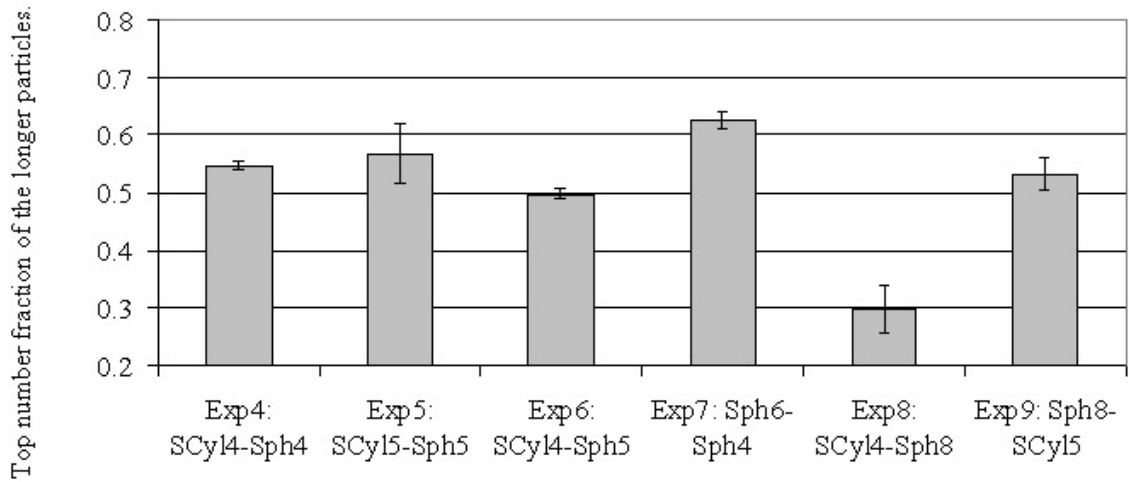


Figure 4.9: Segregation of binary mixtures of particles differing by shape and volume after 20min. of vibration. Y-axis: Top number fraction of the longer particles.

Using DEM simulations we can investigate a broader range of iso-volume mixtures, beyond the particles available in the experiments, as summarized in 4.5. Having access to the position of all particles, we can quantify segregation through the vertical segregation ratio (VSR), as done already earlier in this chapter. This measure has the advantage of being independent of the position chosen to separate the mixture into horizontal fractions. Quantifying segregation through VSR (Figure 4) confirms once more that long spherocylinders migrate below iso-volume spheres, whereas short spherocylinders migrate above them.

As a preliminary investigation of the behavior of mixtures of particle differing both by shape and volume, we report in Figure 4.9 the segregation observed during experiments 4 to 9, described in Table 2. Coherently with the mechanism sketched above, spheres mixed with isodiameter spherocylinders tend to segregate to the bottom of the mixture. Rods of 4mm/5mm diameter are found to be similar enough in shape to respectively spheres of diameter 5mm/8mm to give rise to very limited segregation. On the contrary 4mm spherocylinders migrate to the bottom of a mixtures with 8mm spheres and order vertically similarly to what reported in Figure 4.7.

4.6 Conclusions

We study the effect of particle elongation on segregation by coupling for the first time experiments and numerical simulations. Elongation does condition segregation. When vibrated vertically in a cylinder, short spherocylinders tend to segregate above iso-volume spheres, while long spherocylinders tend to migrate to the bottom. More generally short spherocylinders tend to migrate to the top of long spherocylinders. Moreover, in the conditions tested in this study, the particles migrating to the bottom tend to arrange in an ordered state. This ordering and segregation pattern can be interpreted thanks to the understanding of rod vertical ordering gained in the previous chapter. If the medium is driven with an amplitude and acceleration sufficient to orient vertically long rods, shorter rods will tend to a random orientation. Since particles have same volume, short rods will therefore offer a characteristic size for segregation which is

higher than spheres and long rods. Our discrete element model captures the direction and extent of elongation-driven segregation and can be trusted as predictive tool, contrarily to previous MC simulations. Predicting segregation while neglecting particle shape and considering only volume-equivalent spheres, is a valid assumption only when elongation is close to 0 or to 1.1 (i.e. particles length is about two times its diameter). Otherwise such a simplification leads to overlook elongation-driven segregation. Part of this work was published in (RPL06).

Chapter 5

Flow in vending machine canisters and dosage

5.1 Summary

Dosing experiments using a vending machine canister are performed using a cohesive beverage powder and a mixture of glass beads. The effect of the dosing screw design on the flow in the canister is measured and a coil improving the powder withdrawal across the canister length is designed and successfully tested.

A dosing experiment using glass beads is successfully compared with a three dimensional DEM simulation, which is made possible by the development of an algorithm to detect the collisions between spherical grains and the helix auger. The comparison shows a good agreement both in terms of the shape of the surface and the dosed mass.

The flow in the canister simulation is studied. This study highlights the presence of a shearing layer above the dosing coil and its role in conveying beads from the back to the front of the canister. These beads then merge with the beads transported inside the coil to form the stream of beads leaving the canister during dosage. The dosed mass decreases progressively over time. Contrary to intuition, it is shown that the mass of beads conveyed by the screw is almost constant over time and cannot be held responsible for the overall dose variation. The decreasing contribution of the free flow from the layer of beads above the screw is identified as the main source of the overall dose variation. Some next steps to continue the investigation are proposed.

5.2 Introduction

Vending machines allows the consumption "on-the-go" of hot and cold drinks. Many commercial vending machines contain dehydrated powder beverages, which are dosed and dissolved in water upon consumer's demand. To continuously improve the quality of the beverages served,

it is important to understand and improve the design of all the components and namely the machine canister which stores and doses the powder. The aim of this work is to:

1. Study experimentally the flow and dosage of a beverage powder and a reference mix of glass beads from a particular canister configuration, showing the impact of the dosing auger geometry.
2. Compare with Discrete Element Modelling (DEM) simulations using glass beads.

This application involves many classical phenomena studied in the granular flow literature. The characteristics of the different angles of repose of a granular medium are reviewed among others in (GH97) and (Dur00b). Zhou et al. (ZXYZ02) and Li et al. (LXT05) compare experiments and DEM simulations. Albert (AAH⁺97), Nowak (NSK05) and many others (e.g. (AAH⁺97)) extend these considerations including the impact of water addition or other sources of cohesion. Barton (BB03) studies more particularly the shape of sandpiles built of small platforms. Alonso (AHH98) proposes a discrete model to compute the angle of repose. Later Grasselli (GHOZ00) proposes a continuous extension, used to estimate the impact of falling grain energy on the shape and angle of the pile. Ancy (AEC96) studies the dynamics of a bead falling on a row of identical beads. A collective article by the GdR MIDI (MiD04) considers the onset of motion and kinematic profiles in different flow configurations.

The stress field in silos and hoppers and the hourglass flow rate are also classical topics relevant for this application. Ristow (Ris00b) provides a good summary of the classical theories and an excellent repository of references.

5.3 Flow and dosage experiments.

5.3.1 Experimental set-up

Two different granular media were used in this series of experiments. A fine cohesive food powder that has Rosin Rammler mean diameter $265 \mu\text{m}$ and $n=2.4$, poured bulk density 224 kg/m^3 , tapped density 276 kg/m^3 . This product was conditioned for two days in a conditioning chamber at 20°C , 43% RH, conditions close to its glass transition temperature. It was verified that the product humidity does not change significantly during the test. A mixture of glass beads was also used having the composition reported in table 5.1.

	P1	P2	P3	P4	P5
<i>Radius(mm)</i>	2.25	1.75	1.25	0.968	0.75
<i>Number fraction</i>	0.0161	0.0521	0.1053	0.1737	0.6528

Table 5.1: Composition of the glass mixture.

The geometry of the canister used for the experimental tests is sketched in figure 5.1. The canister is composed of a storage body, with two shoulders at 50° angle, a throat with a dosing

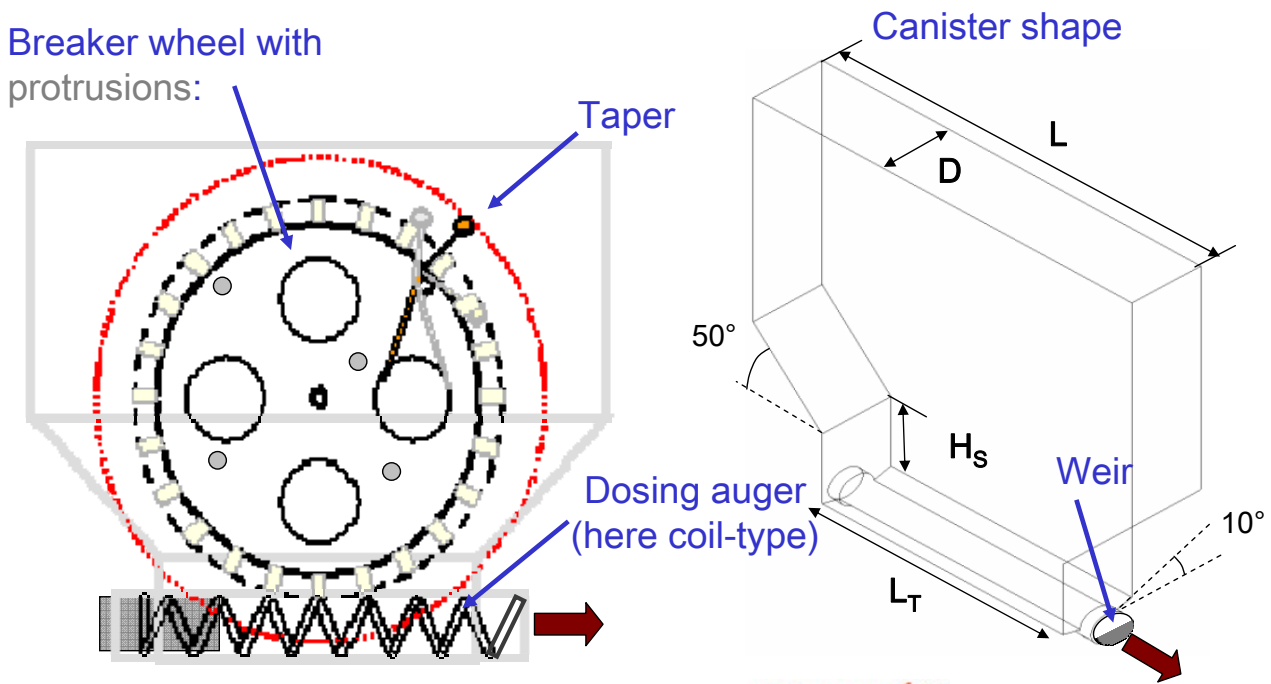


Figure 5.1: Schematics of the canister used for the dosage experiments. Only tests without breaker wheel are reported in this thesis.

auger and a weir. A breaker wheel can also be used but only tests without breaker wheel are reported in this thesis. The canister dimensions are summarized in table 5.2.

Three different screws were tested, their picture is reported in figure 5.2. Note that the upstream section of all the screws is filled by a full cylinder whose length is 27 mm.

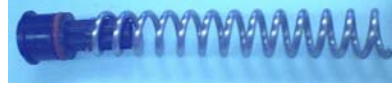
Table 5.2: Canister dimensions.

Dimension	Length (mm)
Length	220
Height	182
Depth	48
Throat diameter	23
Throat length (L_T)	124
Dosing auger length	134
Outlet cyl. length (L_{OC})	17
Weir height	8
Shoulders' height (H_S)	15

A dosing test starts by filling the canister with the weir closed, letting the mixture fall into the canister and moving the point of insertion of the particle to obtain an initial surface as flat as possible. After a calibration the dosing tests are run by turning the dosing auger for 3.36 turns per dose, letting the system rest for 5 seconds and restart again until no more mass is poured from the canister.

A typical way to characterise canister performance is to assess its dose mass sequence as function of the number of doses. In order to compare different setups the mass of a dose is expressed

Screw 1: Standard 9.5-mm-pitch coil. A 27mm cylinder fills up the first pitches.



Screw 2: 9.5-mm-pitch coil with conical insert. A 27mm cylinder fills up the first pitches.



Screw 3: 9.5-mm-pitch coil with an insert designed to obtain a transport volume linearly increasing with coil length.



Figure 5.2: Schematics of the three dosing augers used for the dosing experiments.

in a normalized form as:

$$\frac{\text{Dose Mass}}{\text{Average Dose Mass}} \quad (5.1)$$

where the average dose mass is computed as the mass that maximises the number of doses belonging to the interval bounded by the average dose mass \pm a prescribed tolerance, that depends on the powder used. Dose number can also be substituted by the (cumulative) Normalized Poured Mass, defined by the ratio:

$$NPM = \frac{\text{Cumulative mass of powder poured until the current dose}}{\text{Total mass initially in the canister}} \quad (5.2)$$

5.3.2 Experimental results using a cohesive beverage powder

Only the experimental results obtained with the cohesive beverage powder are reported in this section. The results obtained using glass beads are reported directly in paragraph 5.5.3, where they are compared with DEM simulations. A normalized dosing profile obtained with dosing screw 1 is reported in figure 5.3. The dosage decreases slightly with time; it starts decreasing more markedly after 80 % of the total weight has been poured.

Several lateral snapshots of the canister lateral surface were taken and analysed to identify the shape of the surface of the powder during dosage. The successive positions of the powder surface over time are plotted in a graph (one curve each 10% poured capacity). A constant pitch coil like screw 1 does not result in uniform product withdrawal from the canister, with a stronger withdrawal at the back of the screw as can be seen in 5.4. The product is filled only to the back of the screw. The rest of the screw only transports the powder toward the exit.

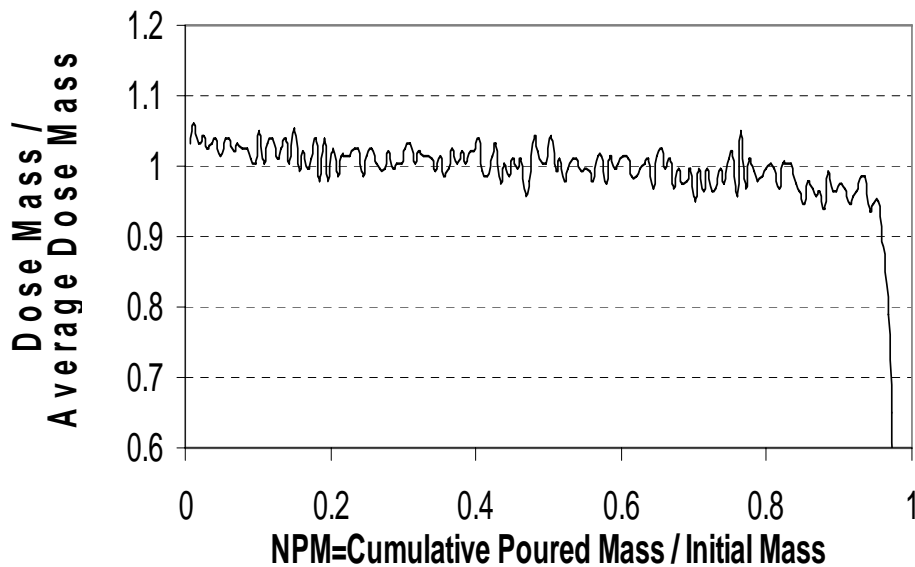


Figure 5.3: Typical dosage pattern of the cohesive powder using screw 1.

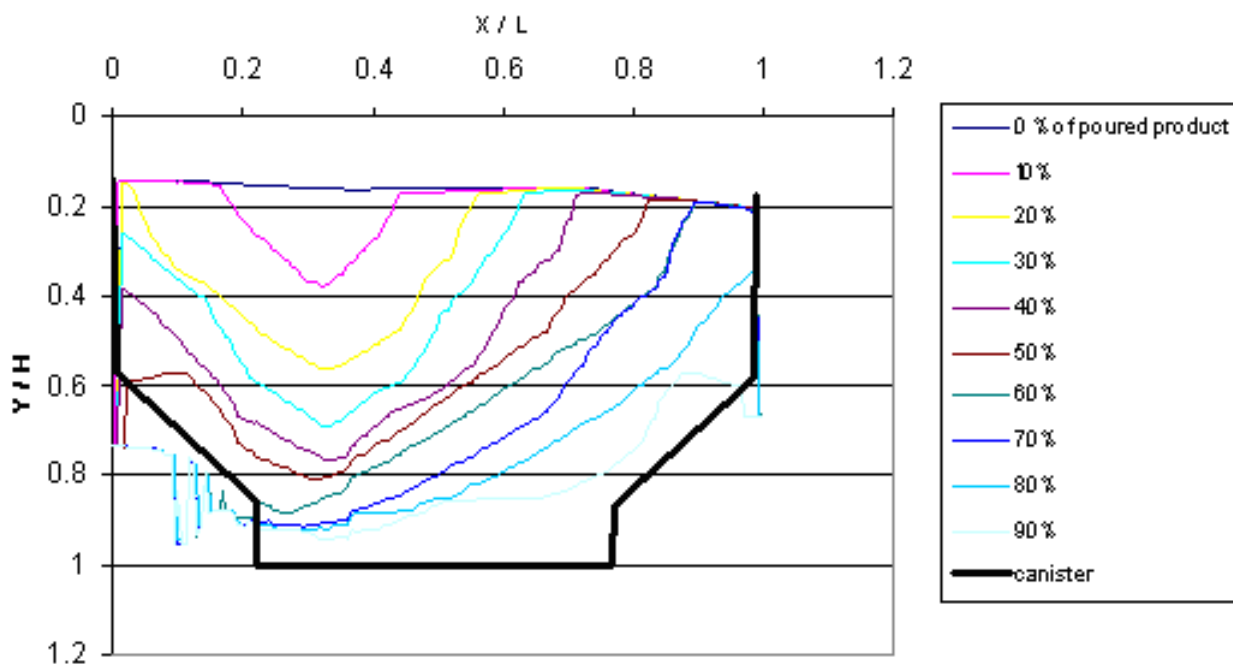


Figure 5.4: Powder flow during a dosing experiment using screw 1.

Screw 2 presents a conical insert and an increasing transport volume along the screw length. It improves partially the powder flow as shown in figure 5.5, emptying better also the front of the canister.

Screw 3 presents a linearly increasing transport volume along the screw length. This is obtained through an appropriate design of the insert. An alternative natural way to obtain a transport volume linearly increasing with coil length would be to increase the pitch of the coil. However,

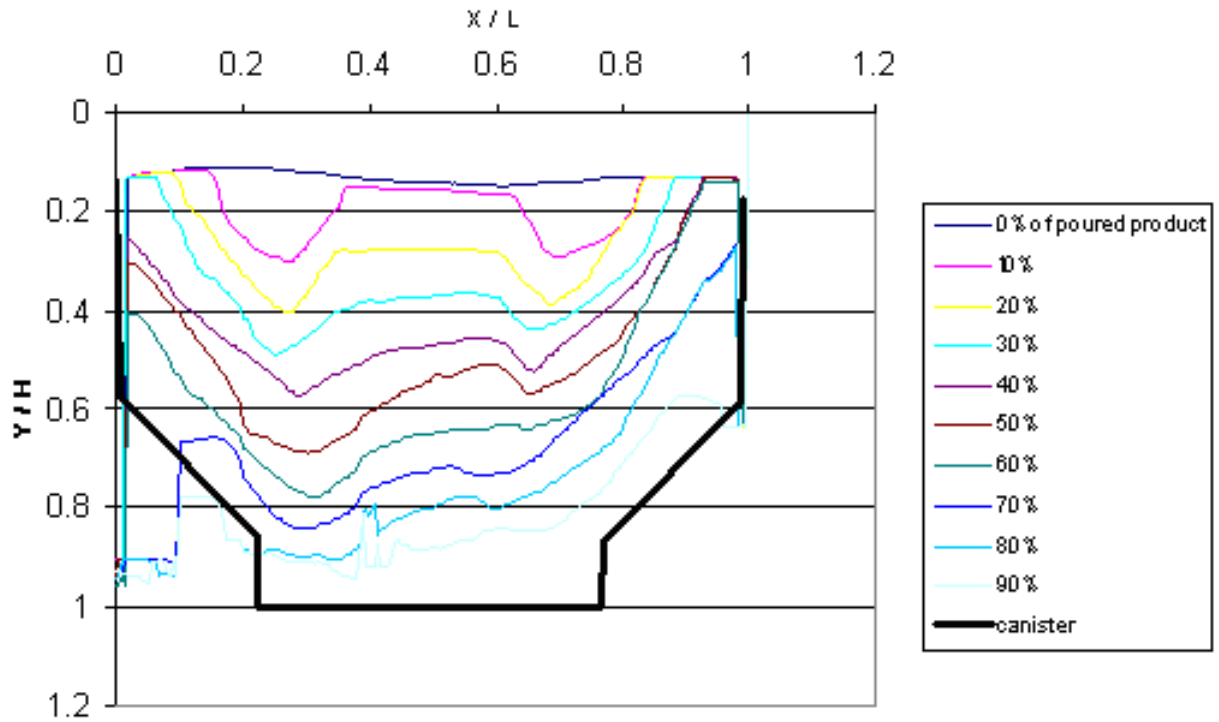


Figure 5.5: Powder flow during a dosing experiment using screw 2.

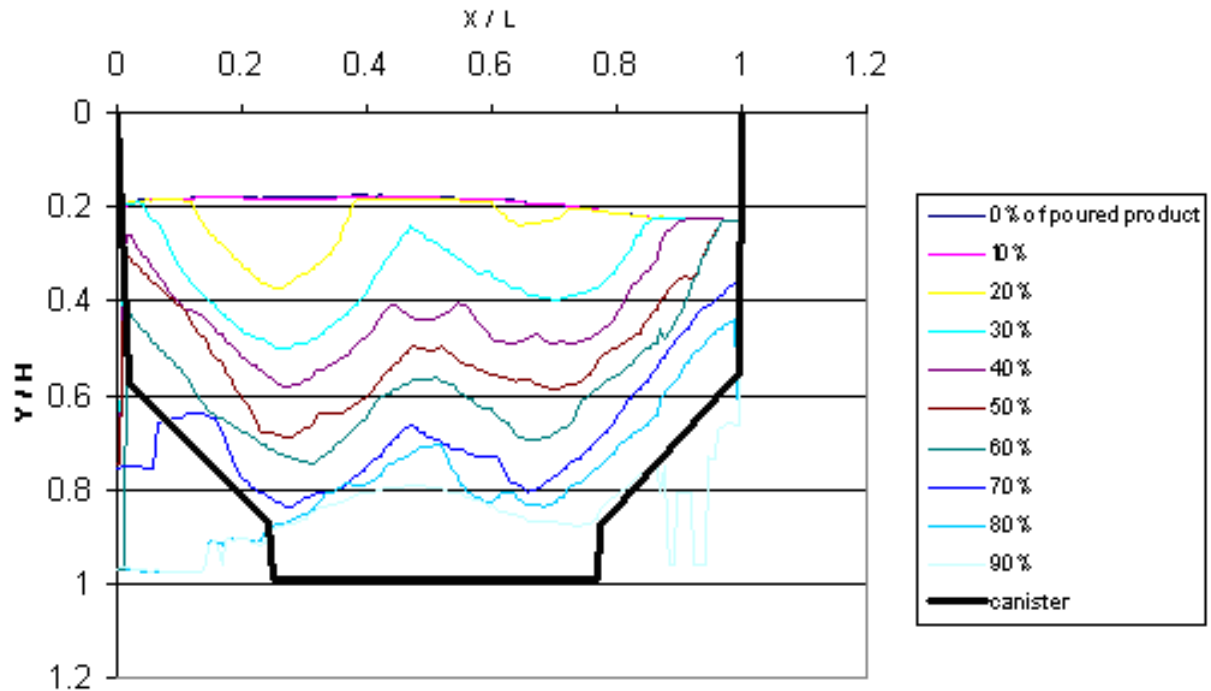


Figure 5.6: Powder flow during a dosing experiment using screw 3.

when varying pitch two constraints must be satisfied: pitch should not be too small to avoid local blockages that would make screw load irregular; nor too wide at outlet to avoid the risk of increasing the dosage variability. These reasons led the author to prefer screw 3 design over a variable pitch. This screw design allows uniform feeding along the doser length and reflects in a fairly uniform powder surface depression until the canister is almost empty as can be seen in figure 5.6.

5.4 Angle of repose test and its relevance to the canister dosage

The cohesive powder angle of repose was measured using the angle of repose setup sketched in figure 5.7. Standard angle of repose tests, measuring the angle formed by a powder depositing on a surface, provide a result which is conditioned by the energy of the grains poured on the pile (GHOZ00). The test designed and used in this work tries to circumvent this undesired effect by a two- step approach. The powder is poured on a cylindrical base forming a first heap. Around the base there is a cylindrical ring which is initially in the highest position as in picture 5.7 (b). The cylindrical ring is then lowered and the first powder heap partly collapse forming a second steeper heap as in picture 5.7 (c). This second heap is believed by the author to be less sensitive to the energy of the falling grains and closer to the situation of the canister throat. Some detail on the geometry: the 15mm radius of the base is chosen on purpose close to the canister outlet cylinder length to have similar finite size effect (BB03). At its final position (c), the cylindrical ring top edge is higher than the cylindrical base by 4.5mm to avoid any possible (although unlikely) influence of the friction among the grain and the base on the measurement.

Following such a procedure, the angle of repose of the cohesive powder is estimated in $50.6^{\circ} \pm 2.5^{\circ}$ over six repetitions, while the glass bead mixture's one in $28.8^{\circ} \pm 1.5^{\circ}$. The glass beads do not show a surface as flat as the (finer) cohesive powder, due to finite size effects due to their bigger grain size. The glass bead measured angle of repose is nevertheless computed assuming a conical geometry. The results are slightly higher than values reported in the literature (LXT05), (AAH⁺97). More extensive investigations are necessary to ascertain whether this is simply due to the low precision of the procedure for low angle (low height) heaps built using beads that are big with respect to the size of the heap base, or whether humidity is also playing a role.

The angle of repose is relevant for the canister design. Indeed the inclination taken by the powder at rest conditions whether and how easily the flow in the canister can be blocked in the outlet cylinder, upon interruption of the coil movement. Considering the 8mm weir height, the outlet cylinder diameter of 23mm and its length of 15mm, the geometric critical value of the AOR for a product to block is 41.4° . Products whose angle of repose is lower than such threshold, can still block, but need some form of arching. The presence of the static coil which reduces the open section can provide a support for making arching easier. Being the angle of repose vary sensitive to the shape of the heap, the relevant angle of repose should be measured in a cylindrical geometry similar to the outlet cylinder geometry. The measurements above therefore should be taken only as an approximation. The effect of both the geometric parameters and the stress acting from upstream requires a study per-se and goes beyond the scope of this work.

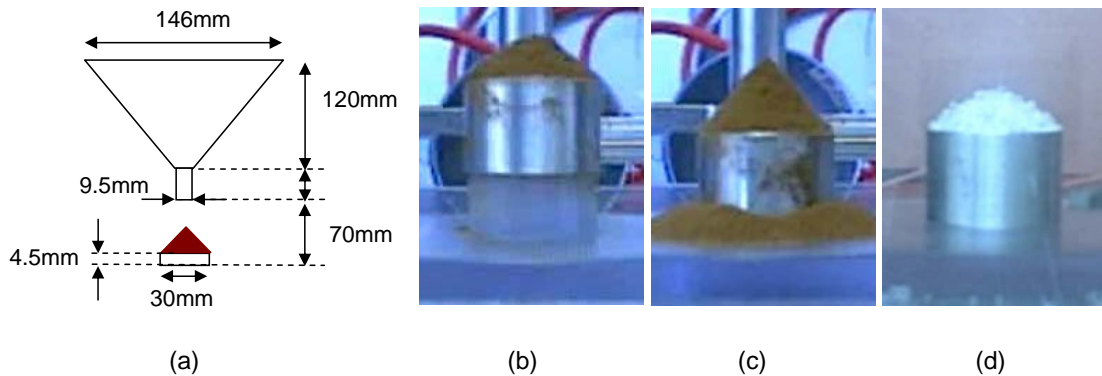


Figure 5.7: Angle of Repose setup. (a) Geometry (b) Cohesive powder: initial picture (c) Cohesive powder: final picture (d) Glass beads: final picture

5.5 Flow and dosage simulations

5.5.1 Contact detection between the dosing coil and spherical grains

Simulating such an experiment with at least 50000 particles requires an efficient algorithm to detect contacts between the spherical particles and the dosage coil.

The dosage coil can be modelled as a wire folded on a cylinder, following the shape of a helix. It is characterised by four geometrical parameters: the coil length (L), the coil radius (CR), the wire radius (WR) and the coil pitch (P). From a geometrical point of view, one could alternatively define the coil as a helix and the locus of the points whose distance from the helix is lower than WR .

Detecting a contact between such a coil and a spherical grain corresponds to finding the closest point of the helix with respect to the centre of the grain. In practice, instead of always correctly calculating this point, it is more effective to evaluate quickly a lower bound of its distance from the centre of the grain and continue computing accurately the distance and the direction only if this lower bound is compatible with a contact. The coil geometry allows this, since an easy-to-compute lower bound of the distance from the coil is the distance from the cylinder to which the helix belongs.

The algorithm therefore follows these steps:

1. Find the closest point (CC) of the cylinder to which the helix belongs (blue segment in fig. 5.8). Its distance from the sphere is a lower bound for the distance from the helix. If it is compatible with a contact, then continue to the next step; else exit answering that no contact exists.
2. Find the point on the helix that is closer to CC (green segment in fig. 5.8). This is done by moving from cartesian to cylindrical coordinates and thus unfolding the helix into a segment. Find the closest point (CH) to CC on the segment and finally obtain CH coordinates in the original frame of reference.

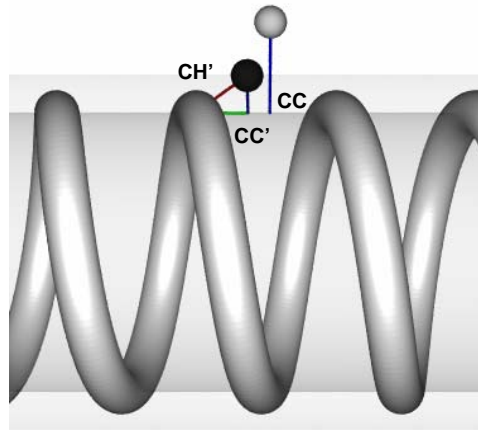


Figure 5.8: Detecting the contact between a sphere and the dosage coil.

3. Add the two vectors found at steps 1 and 2 to obtain the vector joining the centre of the sphere and the closest point on the coil (red segment in fig. 5.8).

Fig. 5.8 shows two examples of contact detection. In the case of the grey sphere only step 1 of the algorithm is completed, because the lower bound of the distance is incompatible with the existence of a contact. In the case of the black sphere all three steps of the algorithm are completed.

5.5.2 Simulation set-up

The canister shape is simplified in simulations by reducing the distance between the longer sidewalls from the real depth of 49mm to 23mm, i.e. same as the throat diameter. This way the canister volume is decreased and with it the number of particles to simulate. This simplification is adopted having empirically observed that the flow in the canister appears essentially bi-dimensional. This simplification makes the longer sidewalls straight, whereas the real canister sidewalls converge to the throat with a 10° angle as depicted in figure 5.1.

The throat and the weir are faithfully reproduced. The dosing auger is almost identical to the one depicted on the top of figure 5.2, except for the fact that the coil covers the whole throat length in simulation, whereas in the dosing screw 1 of figure 5.2 the coil starts only at one pitch (9.5 mm) from the back of the throat.

Grains are generated inside the canister, uniformly along the canister length. During the filling the exit of the canister is closed. A dose consists of a period of 2.24s rotation at 90 rpm followed by 0.32s rest. The rest delay is reduced significantly with respect to the experiment, to reduce the computation time. After each dose the particles that are poured from the canister are deleted from the simulation.

5.5.3 Comparing experiments using glass beads and simulations

Dosage experiments and simulation using glass beads were performed as described in table 5.3.

Table 5.3: Experiments and simulations using glass beads. (*) Dosing screw 1 and 2 are depicted in figure 5.2. Dosing screw 4 is a 9.5mm pitch coil with a conical insert spanning the throat length and without the 27mm cylinder present in screw 1 and 2.

	Dosing screw (*)	Initial weight (g)
Exp.DosG11	Dosing screw 1	1177
Exp.DosG12	Dosing screw 2	1044
Sim.DosG11	Dosing screw 1	479
Sim.DosG12	Dosing screw 2	548
Sim.DosG13	Dosing screw 4	547

To compare flow and dosage from simulations with experiments one needs to apply an appropriate scaling. The ratio of the real to simulated canister depth is $48/23=2.09$. It is therefore necessary to pour slightly over twice the weight in the experiments than in simulations, to obtain the same decrease in surface level.

Figure 5.9 shows the comparison of the shapes of the surface of the beads in the canister for Exp.DosG11 and Sim.DosG11, at different bead weights in the canister. The agreement is quite good although the initial conditions could not be matched exactly. In the simulation we can see a slightly higher withdrawal from the back of the canister, evident for instance in the fourth picture from the top. Two possible explanations for this difference are proposed at the end of the next section.

Figure 5.10 shows the mass dosed versus the Normalized Poured Mass for both Exp.DosG11 and Sim.DosG11. The average dosed weight are close, both start by dosing higher than the average and both decrease sharply when almost all the beads are poured. However the pouring patterns of the experiment and the simulation have a different qualitative behaviour with the simulation decreasing progressively all along the dosage, while the experiment delivers a more constant dosage. The higher value of the first dose is attributed to the fact that the canister is filled by keeping the weir closed. The beads falling in the empty canister can fill the outlet throat almost entirely, without having to respect the limit of the maximum angle of stability at the outlet, as beads have to at the following doses.

The comparison among Exp.DosG112 and Sim.DosG12 cannot be reported in as much detail as for the previous configuration, because repeated experimental issues biased both the dose versus time profile and the lateral images. The feeling that the author got from the approximate comparison of Exp.DosG112 and Sim.DosG12 is that the last experiment shows a more uniform withdrawal across the throat length than the corresponding simulation and with respect also to the previously considered Exp.DosG111. Further experiments are necessary, however, to allow a comparison and to draw a robust conclusion.

The dosage profile of the three simulations using different screws are compared in figure 5.11. Both Sim.DosG12 and Sim.DosG13 show a progressive decrease of the dosed weight along NPM similar to Sim.DosG11. These last two simulations however deliver a better dosage profile, with lower overall variation as the dosing progresses.

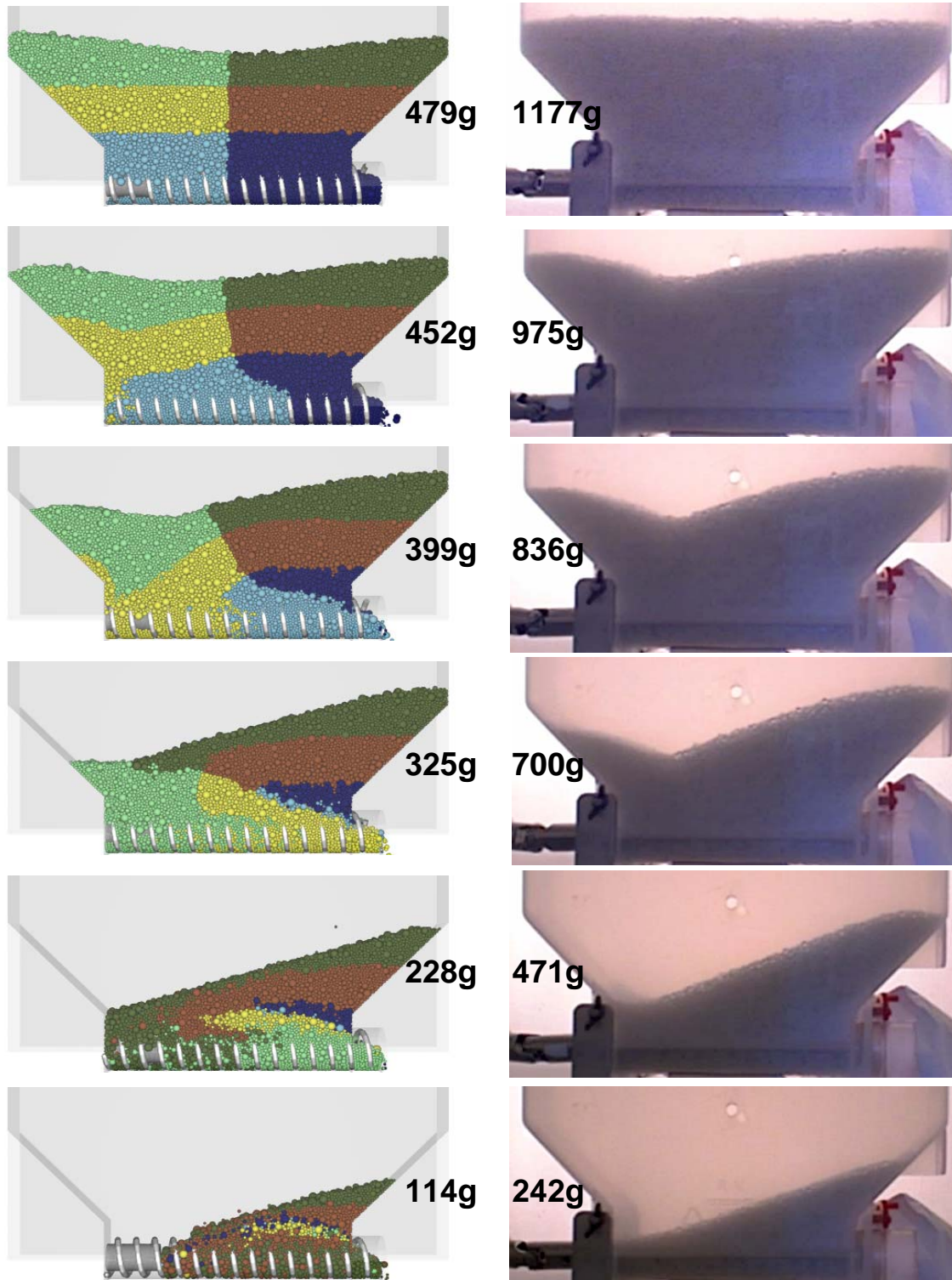


Figure 5.9: Lateral snapshot of the dosage simulation Sim.DosG11 and the experiment Exp.DosG11 using dosing screw 1. Pictures are matched using the weight of beads in the canister. Due to the different canister depth, a 2.09 scaling applies. Initial conditions do not match precisely because of the higher initial weight in the experiment with respect to the simulation (top pictures).

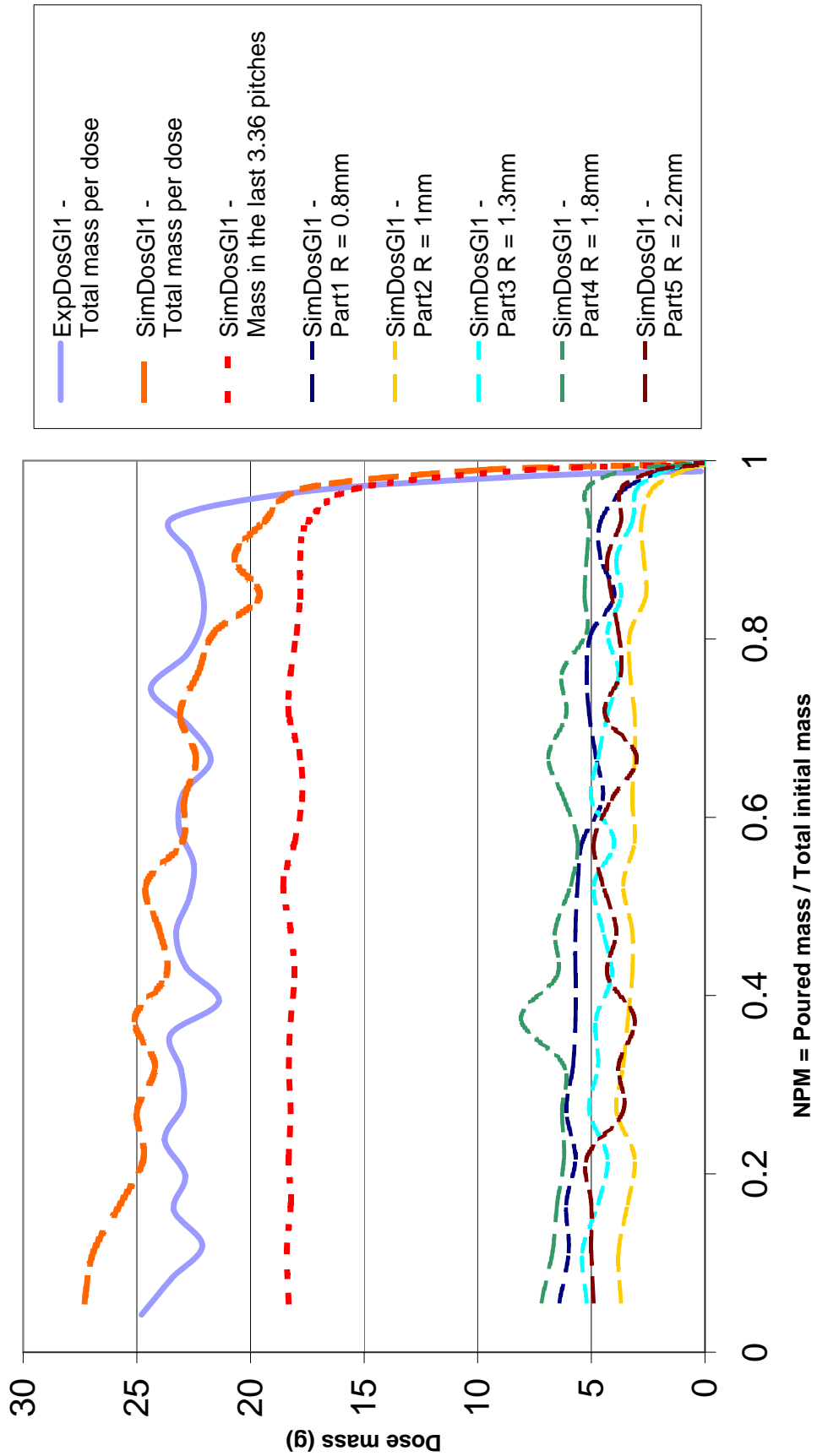


Figure 5.10: Dosed mass versus normalized poured mass for Exp.DosG11 and Sim.DosG11. The curves on the bottom represent the dosed weight of each of the species constituting the simulated glass mixture.

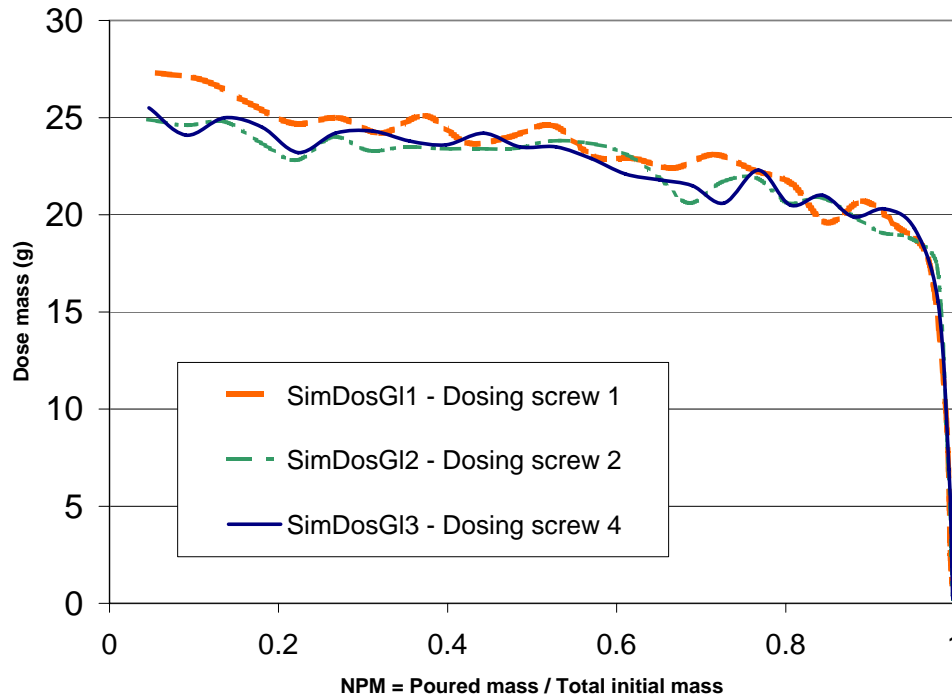


Figure 5.11: Dosed mass versus normalized poured mass for Sim.DosG11, Sim.DosG12 and Sim.DosG13.

5.5.4 What more can simulation tell us?

In this section a closer look is given to simulation Sim.DosG11 results, to extract further insight on the phenomena taking place and their influence on dosing.

What is the flow pattern in the canister?

The top-left three colour images within figure 5.9 show that at the beginning of the dosage, the light green grains at the back shoulder of the canister slide along the inclined wall without much relative rearrangement and the dark green and gold layers initially stretch and bend. Both movements take place to fill the room left empty by the light blue and yellow beads fed to the back of the coil. The upper junction (or "cross") between grains of different colours progressively rotates counter-clockwise and slightly moves toward the back of the screw.

The stretching and progressive inclination of the dark green and gold layers takes place until locally the angle of the surface reaches the angle of maximal stability of about 24° . This is similar to what is reported in the literature for dry glass beads (AAH⁺97), (NSK05). The left side of figure 5.12 provides a visual snapshot of the medium, just before the critical stability angle is reached and before avalanching occurs at the top surface in proximity of the boundary between dark and light green beads. Progressively the surface angle becomes uniform throughout the slope and close to 16° , i.e. significantly below the critical angle.

Grains are fed to the screw preferentially at the first pitch and after the end of the internal cylinder, i.e. around the fourth pitch. The shape of the dark green layer being fed to the screw on the right side of figure 5.12 provides a clear visual evidence of this feeding pattern. More

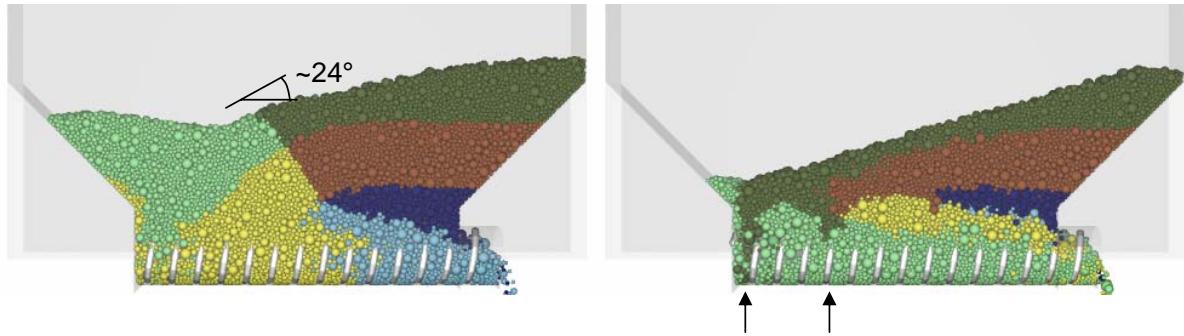


Figure 5.12: Two snapshots of simulation Sim.DosG11 that show the onset of avalanching on the bead surface (left) and the preferential feeding of dark green beads at the first and fourth pitch (right).

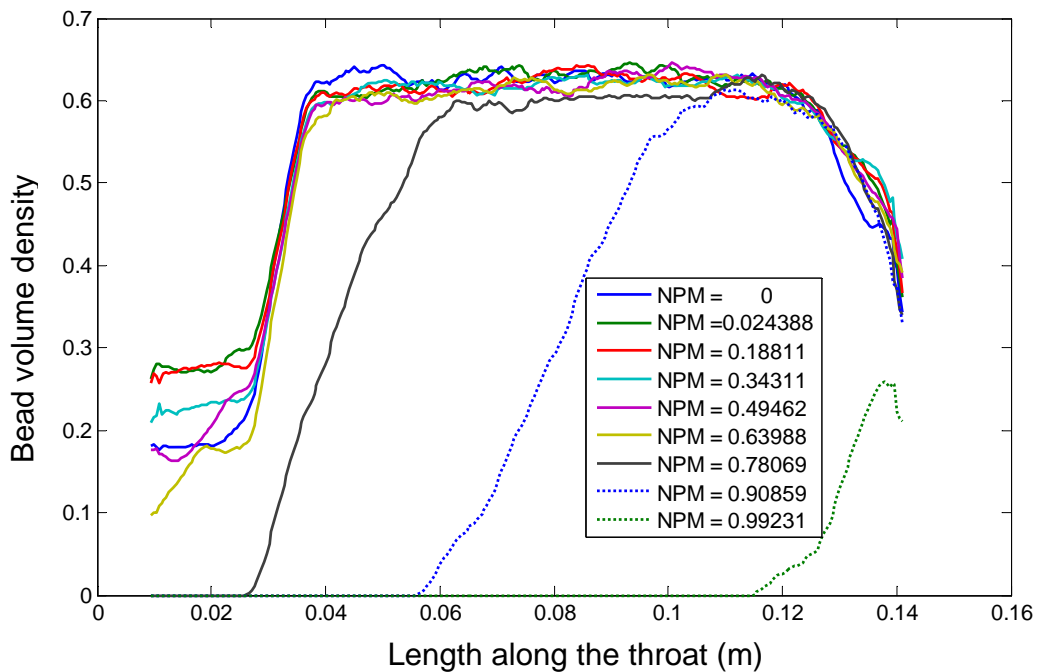


Figure 5.13: Sim.DosG11: Evolution of bead volume density along the coil length averaged on one pitch length. Different curves corresponds to different time and Normalized Poured Mass (NPM).

quantitatively, figure 5.13 shows the evolution of the bead volume density in the coil and along the coil length. The density is measured at half the dosing time on one pitch length (upstream) and is computed on the volume left free in the throat by the coil wire. The cylinder is not considered to emphasize the progressive filling of the coil. Once more it is evident that some mass is fed at the first pitch on the back of the coil and some more at the fourth pitch, when the internal volume of the coil is not filled by the internal cylinder anymore. The different curves correspond to different dosing time and Normalized Poured Mass. The density in the throat decreases only slightly with the NPM. Especially before the end of the throat (0.124m), only the two last profiles show a significantly lower density. At NPM close to one, the coil is

partly empty. At the exit of the coil the density decreases along the coil length, because the avalanching inclined region above the weir has a partially empty headspace.

The coil convects the beads at its interior toward the exit of the canister. It also creates a region of strong shear in the layers above, where grains are entrained from the back to the front of the canister. The grains flowing toward the exit in this shear region find on their way the front wall of the canister that prevents all the grains outside the circumference of the outlet cylinder from exiting. During dosage, close to the exit of the throat into the outlet, cylinder avalanching occurs. There is there room for the sheared layer to join the beads transported in the screw and merge into the final dose of grain exiting the canister.

The coil orientation (see bottom left image of figure 5.9) can be a source of non uniform feeding along the canister depth. This could favor bead feeding to the coil along the bigger wall closer to the reader in figure 5.9. Comparing the flow on both sides of the canister allows us to conclude that this effect is negligible in this configuration. A longer pitch and the resulting higher inclination of the coil wire, could however make this effect relevant in other configurations. This effect can be probably partly counterbalanced by a rotation of the internal cylinder together with the coil.

An interesting question for all types of silo is the residence time distribution of a powder product within the silo. The colouring in figure 5.9 helps identifying the order in which the different layers are dosed, namely: dark blue, light blue, yellow, light green, dark green, followed by a mix with a prevalence of brown. Considering the initial position of each colour, it is evident that this configuration does not pour first what is fed first into the canister (i.e. it is not a FIFO silo).

Why does dosage decrease with time?

This question is important to improve the performance of the dosing canister.

The evolution of the dosed weight *within a dose* is reported in figure 5.14. In order to understand better the way a single dose is poured, the overall dosing and rest duration are divided into eight consecutive intervals. A dose at the beginning of the simulation and a dose toward the end of the decreasing dosing plateau are compared. Both show a "M" like shape. Initially the poured mass per unit time is lower due to the initiation of the movement. During the last interval the coil is at rest and the bead motion is also slowing down toward rest. Beside confirming the quantitative difference of the dosed weight, these qualitatively similar plots do not shed unfortunately any light on the mechanism leading to the dose decrease with time.

At first glance, two intuitive explanations occurred to the author: either a segregation within the canister, which is varying the composition and as a consequence the volume density of the doses, or simply the fact that packing into the coil becomes looser over time due to a decrease in the stresses transferred to the beads being filled to the two filling zones of the coil from the decreasing mass of beads in the canister. Neither of these two explanations turned out to be the main cause of the decreasing dosage with time as we now explain.

The composition of each dose and the fraction of each constituent can be obtained easily from DEM simulations. The dashed lines on the bottom of figure 5.10 show such a composition versus the normalized poured weight for simulation Sim.DosG11. Some sporadic non-uniformities

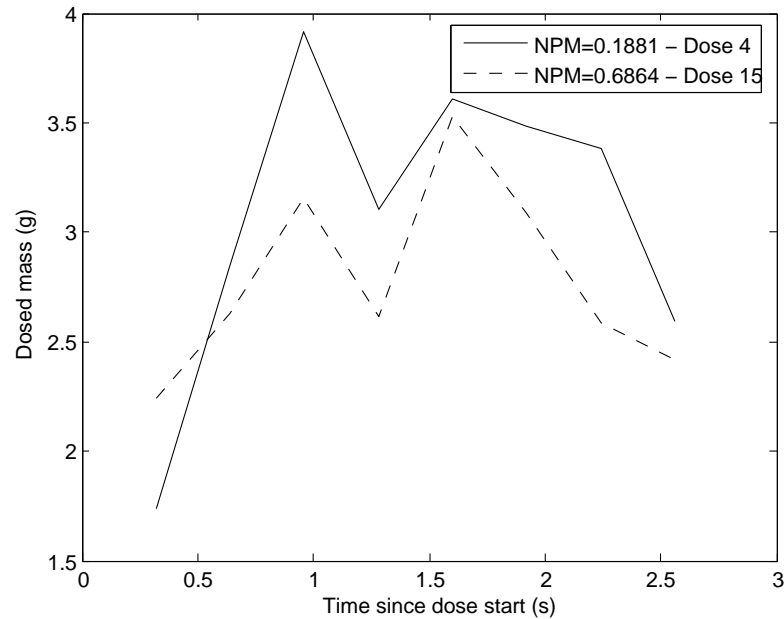


Figure 5.14: Sim.DosG11: Dosed mass versus time *within each dose*

can be spotted, but no clear overall segregation can be identified among subsequent doses. More generally, one can compute the mass of beads which is contained in the coil just upstream from the exit and just before the start of a new dose. It is relevant to consider the mass contained in 3.36 pitch, because the coil travels such a distance during each dose. The evolution of such mass is reported in figure 5.10 using a dotted line. It decreases only slightly with NPM, much less than the dose weight that is plotted above with a dashed line. Surprisingly, this mass is significantly lower than the dosed mass. The difference comes from the beads conveyed by the shearing layer on the top of the coil, which enters the coil close to the outlet of the throat. During dosage the canister thus partly behaves like an hourglass, where arching at the outlet is prevented by the motion of the coil. The mass convected within the coil represent a large majority of the mass dosed. The variation of this contribution is negligible. The reason of the decrease of the dosage with time rather stems from the decrease of the "hourglass-like" contribution. It can be argued that the progressive decrease is caused by a decrease in the stresses transferred to the sheared layer in proximity of the throat outlet. Naturally the friction at the wall modulates such variation through the Janssen's effect and stresses become independent of the height of material above, but only when this height is sufficiently high.

Further elements about the comparison between simulations and experiments.

Having better understood the flow pattern also helps proposing interpretations for the slightly higher withdrawal from the back of the canister in the simulation with respect to the experiment. Two main simplifications of the model geometry with respect to the experimental geometry are described in paragraph 5.5.2. The apparent minor difference in the dosing coil design, i.e. the extra pitch at the rear of the coil present in the simulation compared to the experiment does certainly contribute to move the first feeding zone toward the back of the coil. This contributes to a faster emptying of the canister rear shoulder in the simulation with respect to the experiment. The possible contribution of the second geometrical difference, i.e. the decrease in

canister depth from 48 to 23mm, is more subtle. In the experiment the existence of a different depth between the body of the canister and the throat reduces the importance of the shear band generated by the coil which does not span the whole depth of the canister as it does in the simulation. Furthermore the 10° convergent walls oblige the beads around the coil to a convergent flow in the direction orthogonal to the plane of figure 5.9). This convergent flow is absent in the simulation and could further reduce the entrainment of beads in the high shear area above the coil. The same elements can also be invoked to interpret the "still-to-confirm" difference between simulation Exp.DosG12 and Sim.DosG12, but it appears too early to venture in such a discussion.

A few final words go to the flow of the cohesive powder which is studied experimentally at the beginning of this chapter. As described in paragraph 5.4, the higher angle of repose certainly conditions the likelihood of the powder to stop flowing upon interruption of the coil movement. It seems natural to imagine that it will also condition the depth of the avalanching layer within the outlet cylinder. And thus most probably the flow field during dosage and the relative contribution to the total dosed mass of the mass of powder transported in the screw and of the mass free flowing from above into the canister outlet.

5.6 Next steps

This work has only lifted the lid covering the richness of the flow within such a complex geometry and much can still be done to continue this investigation. Some interesting steps would be:

- Further investigate experimentally the flow of glass beads with different dosing screw and compare with simulations, while ensuring that both setups have comparable initial conditions.
- Explore the effect of the beads' properties and of macroscopic properties as the angle of repose.
- Simulate the true canister geometry to highlight the effect of the real canister depth and convergent movement of the beads toward the throat.
- Identify a suitable cohesive contact model to reproduce the static and dynamic behaviour of the cohesive beverage powder used for the first series of experiments.
- Elaborate a strategy to simulate the flow of the cohesive product. The computational cost is too high when trying to simulate the real particle population, with the further complication of cohesion. A strategy that was started, but not yet fully developed, is to downscale to 2D simulations. This strategy might be promising, although it is not straightforward. A necessary but difficult step is to elaborate realistic scaling to transfer the simulation conditions and the results across the dimensions.

5.7 Conclusions

Dosing experiments using a vending machine canister are performed using a cohesive beverage powder and a mixture of glass beads. A coil improving the powder withdrawal across the canister length is designed and successfully tested.

An algorithm to detect the collisions between spherical grains and the helix auger is developed, which allows a three dimensional simulation of dosage and flow of glass beads in the canister. A dosing experiment using glass beads is successfully compared with the simulation by looking at the shape of the surface and the dosed mass. A good agreement is reached. Simulations show a slightly higher withdrawal from the back of the canister than the experiment and a slightly higher decrease in the dosed mass with time.

The feeding pattern of the coil, the order in which different layers are poured and the very little importance of segregation are discussed. The flow in the canister simulation is studied, highlighting the presence of a shearing layer above the dosing coil and its role in conveying beads from the back to the front of the canister. These beads then merge in with the beads transported inside the coil to form the stream of beads leaving the canister during dosage. Indeed, in average, only three quarters of the dosed mass is constituted of beads transported inside the coil, while the rest comes from free flow of the shearing layer.

The dosed mass decreases progressively over time. Contrary to intuition, it is shown that the mass of beads conveyed by the screw is almost constant over time and cannot be held responsible for the overall dose variation. The decreasing contribution of the free flow from the layer of beads above the screw is identified as the main source of the overall dose variation.

The insight gained by simulating the flow and dosage in the canister clearly confirms the potential of DEM in unveiling the mechanisms driving granular flows in systems of interest to the food industry. Some next steps to continue the investigation are proposed.

Conclusions

A main contribution of this thesis is an in-depth quantitative comparison of experiments and simulations, confirming DEM's capability to shed light on granular processes relevant to the food industry.

A novel explanation in terms of threshold energy barriers for the vertical ordering of elongated grains is introduced, which encompasses the observed influence of particle elongation and vibration acceleration. This phenomenon is then related to the segregation driven by different elongations. We are the first to succeed in quantifying experimentally such segregation and obtain good agreement with simulations. Both ordering of elongated particles and elongation segregation are extensions of the size segregation of spherical cereals, that is studied in a vertically vibrated cereal box. Three configurations are tested experimentally. A qualitative comparison with simulations is achieved for one of them. Convection in cereals of uniform size is also studied numerically and experimentally, illustrating the role of friction in conditioning whether a two-dimensional or three-dimensional convection occurs.

The second food application concerns the flow and dosing from vending machine canisters. An algorithm to detect the collisions between spherical grains and the helix dosing screw is developed, which allows performing three-dimensional DEM simulations of the granular flow in the canister. A dosing experiment using glass beads is successfully compared with a simulation in terms of the evolution of both the shape of the surface and the dosed mass. The flow in the canister simulation is studied, uncovering an explanation for the decreasing dose mass over time, which goes beyond what the first intuition would suggest. Dosing experiments are also performed using a cohesive beverage powder. The effect of the dosing screw design on the flow in the canister is measured and a coil improving the powder withdrawal across the canister length is designed and successfully tested.

The benefit for the food industry stemming from a coupled use of DEM simulations and experiments is clearly shown by the results of this work. We thus provide a basis for the necessary future developments to turn DEM into a predictive tool mature for a daily use in food process design. Experiments to quantify food product cohesion and friction should be developed and a direct link with the parameters of appropriate DEM contact models established. While in this work we did not put emphasis on speeding up computations, simulating industrial scale granular flows also requires faster algorithms, beside relying on the growing computing power. Finally, we consider what was done in this thesis a first step in the important direction of setting up a series of validation benchmarks, similar to that established for computational fluid dynamics some decades ago.

Bibliography

- [AA98] K. M. Aoki and T. Akiyama. Control parameter in granular convection. *Physical Review E*, 58(4):4629–4637, 1998. Times Cited: 4 Article English Cited References Count: 16 130rd.
- [AAH⁺97] R. Albert, I. Albert, D. Hornbaker, P. Schiffer, and A. L. Barabasi. Maximum angle of stability in wet and dry spherical granular media. *Physical Review E*, 56(6):R6271–R6274, 1997. 21 AMERICAN PHYSICAL SOC.
- [AAMW96] K. M. Aoki, T. Akiyama, Y. Maki, and T. Watanabe. Convective roll patterns in vertically vibrated beds of granules. *Physical Review E*, 54(1):874–883, 1996. Times Cited: 32 Article English Cited References Count: 29 Uy734.
- [AEC96] C. Ancey, P. Evesque, and P. Coussot. Motion of a single bead on a bead row: Theoretical investigations. *Journal De Physique I*, 6(5):725–751, 1996. 58 EDITIONS PHYSIQUE.
- [AHH98] J. J. Alonso, J. P. Hovi, and H. J. Herrmann. Lattice model for the calculation of the angle of repose from microscopic grain properties. *Physical Review E*, 58(1):672–680, 1998. 27 AMERICAN PHYSICAL SOC.
- [AKR01] S. Aumaitre, C. A. Kruelle, and I. Rehberg. Segregation in granular matter under horizontal swirling excitation. *Physical Review E*, 6404(4):4, 2001. 17 AMERICAN PHYSICAL SOC Part 1.
- [ATC03] C. R. A. Abreu, F. W. Tavares, and M. Castier. Influence of particle shape on the packing and on the segregation of spherocylinders via monte carlo simulations. *Powder Technology*, 134(1-2):167–180, AUG 5 2003.
- [BB03] J. M. H. Barton and S. G. Buchberger. Geometrical analysis of sand piles on small platforms. *Physical Review E*, 68(1):11, 2003. 15 AMERICAN PHYSICAL SOC Part 1.
- [BEKR03] A. P. J. Breu, H. M. Ensner, C. A. Kruelle, and I. Rehberg. Reversing the brazil-nut effect: Competition between percolation and condensation. *Physical Review Letters*, 90(1):–, 2003.
- [BKS02] N. Burtally, P. J. King, and M. R. Swift. Spontaneous air-driven separation in vertically vibrated fine granular mixtures. *Science*, 295(5561):1877–1879, 2002. 25 AMER ASSOC ADVANCEMENT SCIENCE.

- [BNK03] D. L. Blair, T. Neicu, and A. Kudrolli. Vortices in vibrated granular rods. *Physical Review E*, 67(3):031303–1/6, 2003.
- [BSSK03] P. Biswas, P. Sanchez, M. R. Swift, and P. J. King. Numerical simulations of air-driven granular separation. *Physical Review E*, 68(5):4, 2003. 27 AMERICAN PHYSICAL SOC Part 1.
- [Cam06] C. S. Campbell. Granular material flows - an overview. *Powder Technology*, 162(3):208–229, 2006.
- [Cle04] P. W. Cleary. Large scale industrial dem modelling. *Engineering Computations*, 21(2-4):169–204, 2004. 42 EMERALD GROUP PUBLISHING LIMITED.
- [CS79] P. A. Cundall and O. D. L. Strack. Discrete numerical-model for granular assemblies. *Geotechnique*, 29(1):47–65, 1979. 14 THOMAS TELFORD SERVICES LTD.
- [CS02] P. W. Cleary and M. L. Sawley. Dem modelling of industrial granular flows: 3d case studies and the effect of particle shape on hopper discharge. *Applied Mathematical Modelling*, 26(2):89–111, 2002. 26 ELSEVIER SCIENCE INC Sp. Iss. SI.
- [CSM06] P. W. Cleary, M. Sinnott, and R. Morrison. Analysis of stirred mill performance using dem simulation: Part 2 - coherent flow structures, liner stress and wear, mixing and transport. *Minerals Engineering*, 19(15):1551–1572, 2006. Cleary, Paul W. Sinnott, Matt Morrison, Rob 18 PERGAMON-ELSEVIER SCIENCE LTD.
- [CVF⁺06] Massimo Pica Ciamarra, Maria Domenica De Vizia, Annalisa Fierro, Marco Tarzia, Antonio Coniglio, and Mario Nicodemi. Granular species segregation under vertical tapping: Effects of size, density, friction, and shaking amplitude. *Physical Review Letters*, 96(5), 2006.
- [CWHB96] W. Cooke, S. Warr, J. M. Huntley, and R. C. Ball. Particle size segregation in a two-dimensional bed undergoing vertical vibration. *Physical Review E*, 53(3):2812–2822, 1996. 30 AMERICAN PHYSICAL SOC.
- [DFL89] S. Douady, S. Fauve, and C. Laroche. Subharmonic instabilities and defects in a granular layer under vertical vibrations. *Europhysics Letters*, 8(7):621–627, 1989. 6 EDITIONS PHYSIQUE.
- [dG99] P. G. de Gennes. Granular matter: a tentative view. *Reviews of Modern Physics*, 71(2):S374–S382, 1999. 74 AMERICAN PHYSICAL SOC Sp. Iss. SI.
- [DRC93] J. Duran, J. Rajchenbach, and E. Clement. Arching effect model for particle-size segregation. *Physical Review Letters*, 70(16):2431–2434, 1993. 8 AMERICAN PHYSICAL SOC.
- [Dur00a] J. Duran. Sands, powder and grains - chap.1 - introduction. In Springer, editor, *Sands, Powder and Grains*. Springer, 2000.

- [Dur00b] J. Duran. Sands, powder and grains - chap.4 - granular media in a state of flow. In Springer, editor, *Sands, Powder and Grains*. Springer, 2000.
- [Dur00c] J. Duran. Sands, powder and grains - chap.5 - mixing and segregation. In Springer, editor, *Sands, Powder and Grains*. Springer, 2000.
- [ESD90] P. Evesque, E. Szmatura, and J. P. Denis. Surface fluidization of a sand pile. *Europhysics Letters*, 12(7):623–627, 1990. 15 EDITIONS PHYSIQUE.
- [FL02] J. A. Ferrez and T. M. Liebling. Dynamic triangulations for efficient detection of collisions between spheres with applications in granular media simulations. *Philosophical Magazine B-Physics of Condensed Matter Statistical Mechanics Electronic Optical and Magnetic Properties*, 82(8):905–929, 2002.
- [FLCA94] S. F. Foerster, M. Y. Louge, A. H. Chang, and K. Allia. Measurements of the collision properties of small spheres. *Physics of Fluids*, 6(3):1108–1115, 1994. 14 AMER INST PHYSICS.
- [FW03] D. N. Fernando and C. R. Wassgren. Effects of vibration method and wall boundaries on size segregation in granular beds, NOV 2003.
- [GH97] Y. Grasselli and H. J. Herrmann. On the angles of dry granular heaps. *Physica A*, 246(3-4):301–312, 1997. 12 ELSEVIER SCIENCE BV.
- [GHOZ00] Y. Grasselli, H. J. Herrmann, G. Oron, and S. Zapperi. Effect of impact energy on the shape of granular heaps. *Granular Matter*, 2(2):97–100, 2000. 20 SPRINGER VERLAG.
- [GHS92] J. A. C. Gallas, H. J. Herrmann, and S. Sokołowski. Convection cells in vibrating granular media. *Phys. Rev. Lett.*, 69(9):1371–1374, Aug 1992.
- [GHS⁺06] J. Galanis, D. Harries, D.L. Sackett, Losert W., and R. Nossal. Spontaneous patterning of confined granular rods. *Physical Review Letters*, 96:028002–1/4, 2006.
- [Gro97] E. L. Grossman. Effects of container geometry on granular convection. *Phys. Rev. E*, 56(3):3290–3300, Sep 1997.
- [GRVM03] D. Gelosa, M. Ramaioli, G. Valente, and M. Morbidelli. Chromatographic reactors: Esterification of glycerol with acetic acid using acidic polymeric resins. *Industrial & Engineering Chemistry Research*, 42(25):6536–6544, 2003. 15 AMER CHEMICAL SOC.
- [HL98] H. J. Herrmann and S. Luding. Modeling granular media on the computer. *Continuum Mechanics and Thermodynamics*, 10(4):189–231, 1998. 232 SPRINGER VERLAG.
- [Hon99] Daniel C. Hong. Condensation of hard spheres under gravity. *Physica A: Statistical Mechanics and its Applications*, 271(1-2):192–199, 1999. TY - JOUR.

- [HQL01] D. C. Hong, P. V. Quinn, and S. Luding. Reverse brazil nut problem: Competition between percolation and condensation. *Physical Review Letters*, 86(15):3423–3426, 2001. Times Cited: 47 Article English Cited References Count: 35 421cz.
- [HRS04] D. A. Huerta and J. C. Ruiz-Suarez. Vibration-induced granular segregation: A phenomenon driven by three mechanisms. *Physical Review Letters*, 92(11):–, 2004.
- [HY97] S. S. Hsiau and H. Y. Yu. Segregation phenomena in a shaker. *Powder Technology*, 93(1):83–88, 1997. 28 ELSEVIER SCIENCE SA LAUSANNE.
- [JN92] H. M. Jaeger and S. R. Nagel. Physics of the granular state. *Science*, 255(5051):1523–1531, 1992. 122 AMER ASSOC ADVANCEMENT SCIENCE.
- [JN96] H. M. Jaeger and S. R. Nagel. Granular solids, liquids, and gases. *RevModPhys*, 68:1259, 1996.
- [KEK⁺96] J. B. Knight, E. E. Ehrichs, V. Y. Kuperman, J. K. Flint, H. M. Jaeger, and S. R. Nagel. Experimental study of granular convection. *Physical Review E*, 54(5):5726–5738, 1996.
- [Kni97] J. B. Knight. External boundaries and internal shear bands in granular convection. *Physical Review E*, 55(5):6016–6023, 1997.
- [Kud04] A. Kudrolli. Size separation in vibrated granular matter. *Reports on Progress in Physics*, 67(3):209–247, 2004. 117 IOP PUBLISHING LTD.
- [LCB⁺94] S. Luding, E. Clement, A. Blumen, J. Rajchenbach, and J. Duran. Onset of convection in molecular-dynamics simulations of grains. *Physical Review E*, 50(3):R1762–R1765, 1994. 26 AMERICAN PHYSICAL SOC.
- [Lee94] J. Lee. Heap formation in two-dimensional granular media. *Journal of Physics a-Mathematical and General*, 27(9):L257–L262, 1994. 20 IOP PUBLISHING LTD.
- [LHB94] S. Luding, H. J. Herrmann, and A. Blumen. Simulations of two-dimensional arrays of beads under external vibrations: Scaling behavior. *Phys. Rev. E*, 50(4):3100–3108, Oct 1994.
- [LR97] Y. Lan and A. D. Rosato. Convection related phenomena in granular dynamics simulations of vibrated beds. *Phys. Fluids*, 9(12):3615–3624, 1997.
- [Lum85] V. J. Lumelsky. On fast computation of distance between line segments. *Information Processing Letters*, 21, 1985.
- [LV04] G. Lumay and N. Vandewalle. Compaction of anisotropic granular materials: Experiments and simulations. *Physical Review E*, 70(5):051314–1/5, 2004.

- [LXT05] Y. J. Li, Y. Xu, and C. Thornton. A comparison of discrete element simulations and experiments for 'sandpiles' composed of spherical particles. *Powder Technology*, 160(3):219–228, 2005. 20 ELSEVIER SCIENCE SA.
- [M96] D. Müller. Techniques informatiques efficaces pour la simulation de milieux granulaires par des méthodes d'éléments distincts. *Thèse EPFL*, (1545), 1996.
- [MiD04] G. D. R. MiDi. On dense granular flows. *European Physical Journal E*, 14(4):341–365, 2004. 104 SPRINGER.
- [MK02] T. Mullin and Kw. Mixing and de-mixing. *Science*, 295(5561):1851–1851, 2002. 4 AMER ASSOC ADVANCEMENT SCIENCE.
- [MLNJ01] M. E. Mobius, B. E. Lauderdale, S. R. Nagel, and H. M. Jaeger. Brazil-nut effect - size separation of granular particles. *Nature*, 414(6861):270–270, 2001.
- [MYOK00] A. J. Matchett, T. Yanagida, Y. Okudaira, and S. Kobayashi. Vibrating powder beds: a comparison of experimental and distinct element method simulated data. *Powder Technology*, 107(1-2):13–30, 2000.
- [NKBN⁺98] E. R. Nowak, J. B. Knight, E. Ben-Naim, H. M. Jaeger, and S. R. Nagel. Density fluctuations in vibrated granular materials. *Physical Review E*, 57(2):1971–1982, 1998.
- [NKP⁺97] E. R. Nowak, J. B. Knight, M. L. Povinelli, H. M. Jaeger, S. R. Nagel, and Ye. Reversibility and irreversibility in the packing of vibrated granular material. *Powder Technology*, 94(1):79–83, 1997. 38 ELSEVIER SCIENCE SA LAUSANNE.
- [NMCCRS03] Y. Nahmad-Molinari, G. Canul-Chay, and J. C. Ruiz-Suarez. Inertia in the brazil nut problem, OCT 2003.
- [NMR06] V. Narayan, N. Menon, and S. Ramaswamy. Nonequilibrium steady states in a vibrated-rod monolayer: tetratic, nematic, and smectic correlations. *Journal Of Statistical Mechanics - Theory and experiments*, page 01005, Jan 2006.
- [NSK05] S. Nowak, A. Samadani, and A. Kudrolli. Maximum angle of stability of a wet granular pile. *Nature Physics*, 1(1):50–52, 2005. 11 NATURE PUBLISHING GROUP.
- [PL05] L. Pournin and Th. M. Liebling. A generalization of discrete element method to tridimensional particles with complex shapes. *Proc. Powder and Grains conference, Stuttgart*, 2:1375, 2005.
- [PLM02] L. Pournin, T. M. Liebling, and A. Mocellin. Molecular-dynamics force models for better control of energy dissipation in numerical simulations of dense granular media. *Physical Review E*, 65(1):7, 2002. 8 AMERICAN PHYSICAL SOC Part 1.
- [Pou05] L. Pournin. On the behaviour of spherical and non-spherical grain assemblies, its modeling and numerical simulation. *Thèse EPFL*, (3378), 2005.

- [PRFL07] L. Pournin, M. Ramaioli, P. Folly, and T. M. Liebling. About the influence of friction and polydispersity on the jamming behavior of bead assemblies. *European Physical Journal E*, 23(2):229–235, 2007. Pournin, L. Ramaioli, M. Folly, P. Liebling, Th. M. 18 SPRINGER.
- [PSO⁺06] N. A. Pohlman, B. L. Severson, J. M. Ottino, R. M. Lueptow, and Dr. Surface roughness effects in granular matter: Influence on angle of repose and the absence of segregation. *Physical Review E*, 73(3):9, 2006. 35 AMERICAN PHYSICAL SOC Part 1.
- [PVB95] H. K. Pak, E. Vandoorn, and R. P. Behringer. Effects of ambient gases on granular-materials under vertical vibration. *Physical Review Letters*, 74(23):4643–4646, 1995. 26 AMERICAN PHYSICAL SOC.
- [PWT⁺05] L. Pournin, M. Weber, M. Tsukahara, J. A. Ferrez, M. Ramaioli, and Th. M. Liebling. Three dimensional distinct element simulation of spherocylinders crystallisation. *Granular Matter*, 7:119, 2005.
- [QH00] P. V. Quinn and D. C. Hong. Liquid-solid transition of hard spheres under gravity. *Physical Review E*, 62(6):8295–8298, 2000. 39 AMERICAN PHYSICAL SOC Part B.
- [RBZL02] A. D. Rosato, D. L. Blackmore, N. H. Zhang, and Y. D. Lan. A perspective on vibration-induced size segregation of granular materials. *Chemical Engineering Science*, 57(2):265–275, 2002.
- [RGLB06] C. H. Rycroft, G. S. Grest, J. W. Landry, and M. Z. Bazant. Analysis of granular flow in a pebble-bed nuclear reactor. *Physical Review E*, 74(2):16, 2006. Rycroft, Chris H. Grest, Gary S. Landry, James W. Bazant, Martin Z. 50 AMERICAN PHYSICAL SOC Part 1.
- [Ris00a] G. H. Ristow. Pattern formation in granular material - chap.3 - vertical shaking. In *Pattern formation in granular material*, page 161. Springer, 2000.
- [Ris00b] G. H. Ristow. Pattern formation in granular material - chap.6 - conical hopper. In *Pattern formation in granular material*, page 161. Springer, 2000.
- [RLNM06] G. M. Rodriguez-Linan and Y. Nahmad-Molinari. Granular convection driven by shearing inertial forces. *Physical Review E*, 73(1):6, 2006. 21 AMERICAN PHYSICAL SOC Part 1.
- [RND⁺05a] P. Richard, M. Nicodemi, R. Delannay, P. Ribiere, and D. Bideau. Slow relaxation and compaction of granular systems. *Nature Materials*, 4(2):121–128, 2005. 60 NATURE PUBLISHING GROUP.
- [RND⁺05b] P. Richard, M. Nicodemi, R. Delannay, P. Ribiere, and D. Bideau. Slow relaxation and compaction of granular systems. *Nature materials*, 4:121–128, Feb 2005.

- [RPL05] M. Ramaioli, L. Pournin, and Th. M. Liebling. Numerical and experimental investigations of alignment and segregation of vibrated granular media composed of rods and spheres. *Proc. Powder and Grains conference, Stuttgart,*, 2:1359, 2005.
- [RPL06] M. Ramaioli, L. Pournin, and T. M. Liebling. Brazil's nut effect beyond spherical grains: elongation matters! *Proc. of World Conference Particle Technology 5, Orlando, USA,* 2006.
- [RPL07] M. Ramaioli, L. Pournin, and T. M. Liebling. Vertical ordering of rods under vertical vibration. *Physical Review E*, 76(2):6, 2007.
- [RPSS86] A. Rosato, F. Prinz, K. J. Standburg, and R. Swendsen. Monte-carlo simulation of particulate matter segregation. *Powder Technology*, 49(1):59–69, 1986. Times Cited: 80 Article English Cited References Count: 35 F5616.
- [RRCV00] R. Ramirez, D. Risso, P. Cordero, and Vn. Thermal convection in fluidized granular systems. *Physical Review Letters*, 85(6):1230–1233, 2000. 21 AMERICAN PHYSICAL SOC.
- [RRDB05] P. Ribière, P. Richard, R. Delannay, and D Bideau. Importance of convection in the compaction mechanisms of anisotropic granular media. *Physical Review E*, 71:011304–1/4, 2005.
- [RRP⁺07] P. Ribiere, P. Richard, P. Philippe, D. Bideau, and R. Delannay. On the existence of stationary states during granular compaction. *European Physical Journal E*, 22(3):249–253, 2007. Ribiere, Ph. Richard, P. Philippe, P. Bideau, D. Delannay, R. 20 SPRINGER.
- [RSG⁺05] D. Risso, R. Soto, S. Godoy, P. Cordero, and Vr. Friction and convection in a vertically vibrated granular system. *Physical Review E*, 72(1):6, 2005. 28 AMERICAN PHYSICAL SOC Part 1.
- [RSPS87] A. Rosato, K. J. Strandburg, F. Prinz, and R. H. Swendsen. Why the brazil nuts are on top - size segregation of particulate matter by shaking. *Physical Review Letters*, 58(10):1038–1040, 1987.
- [RvRA⁺02] R. Roth, R. van Roij, D. Andrienko, K. R. Mecke, and S. Dietrich. Entropic torque. *Phys. Rev. Lett.*, 89(8):088301, Jul 2002.
- [Sab] Sable. *Muséum d'histoire naturelle, Neuchatel, Switzerland*, pages 24.08.02–08.01.03.
- [SBKR05] T. Schnautz, R. Brito, C. A. Kruelle, and I. Rehberg. A horizontal brazil-nut effect and its reverse. *Physical Review Letters*, 95(2):4, 2005. 27 AMERICAN PHYSICAL SOC.
- [SCM06] M. Sinnott, P. W. Cleary, and R. Morrison. Analysis of stirred mill performance using dem simulation: Part 1 - media motion, energy consumption and collisional environment. *Minerals Engineering*, 19(15):1537–1550, 2006. Sinnott, Matt Cleary, Paul W. Morrison, Rob 17 PERGAMON-ELSEVIER SCIENCE LTD.

- [SDS03] K. Stokely, A. Diacou, and Franklin S.V. Two-dimensional packing in prolate granular materials. *Physical Review E*, 67(5):051302–1/5, 2003.
- [Shi04] T. Shinbrot. Granular materials - the brazil nut effect - in reverse. *Nature*, 429(6990):352–353, 2004. 13 NATURE PUBLISHING GROUP.
- [SM98] T. Shinbrot and F. J. Muzzio. Reverse buoyancy in shaken granular beds. *Physical Review Letters*, 81(20):4365–4368, 1998.
- [SUK⁺06] Matthias Schroter, Stephan Ulrich, Jennifer Kreft, Jack B. Swift, and Harry L. Swinney. Mechanisms in the size segregation of a binary granular mixture. *Physical Review E*, 74(1), 2006.
- [Tag92] Y-h. Taguchi. New origin of a convective motion: Elastically induced convection in granular materials. *Phys. Rev. Lett.*, 69(9):1367–1370, Aug 1992.
- [TH04] C. H. Tai and S. S. Hsiau. Dynamic behaviors of powders in a vibrating bed. *Powder Technology*, 139(3):221–232, 2004. 24 ELSEVIER SCIENCE SA.
- [TRDB03] E. Tijssens, H. Ramon, and J. De Baerdemaeker. Discrete element modelling for process simulation in agriculture. *Journal of Sound and Vibration*, 266(3):493–514, 2003. 105 ACADEMIC PRESS LTD ELSEVIER SCIENCE LTD.
- [TTV00a] J. Talbot, G. Tarjus, and P. Viot. Adsorption-desorption model and its application to vibrated granular materials. *Physical Review E*, 61(5):5429–5438, 2000.
- [TTV00b] J. Talbot, G. Tarjus, and P. Viot. Adsorption-desorption model and its application to vibrated granular materials. *Phys. Rev. E*, 61(5):5429–5438, May 2000.
- [USS07] S. Ulrich, M. Schroter, and H. L. Swinney. Influence of friction on granular segregation. *Phys. Rev. E*, 76(4):2301–2304, Oct 2007.
- [vB97] E. vanDoorn and R. P. Behringer. Dilation of a vibrated granular layer. *Europhysics Letters*, 40(4):387–392, 1997. 24 EDITIONS PHYSIQUE.
- [VKT04] D. Volfson, A. Kudrolli, and L. S. Tsimiring. Anisotropy-driven dynamics in vibrated granular rods. *Physical Review E*, 70(5):051312–1/12, 2004.
- [VL94] C. Vega and C. Lago. A fast algorithm to evaluate the shortest distance between rods. *Computers and Chemistry*, 18(1), 1994.
- [VLMJ00] F. X. Villarruel, B. E. Lauderdale, D. M. Mueth, and H. M. Jaeger. Compaction of rods: Relaxation and ordering in vibrated, anisotropic granular material. *Physical Review E*, 61(6):6914–6921, JUN 2000.
- [VRD97] L. Vanel, A. D. Rosato, and R. N. Dave. Rise-time regimes of a large sphere in vibrated bulk solids. *Physical Review Letters*, 78(7):1255–1258, FEB 17 1997.

- [vZTD⁺06a] A. van Zeebroeck, E. Tijskens, E. Dintwa, J. Kafashan, J. Loodts, J. De Baeremaeker, and H. Ramon. The discrete element method (dem) to simulate fruit impact damage during transport and handling: Model building and validation of dem to predict bruise damage of apples. *Postharvest Biology and Technology*, 41(1):85–91, 2006. 20 ELSEVIER SCIENCE BV.
- [vZTD⁺06b] M. van Zeebroeck, E. Tijskens, E. Dintwa, J. Kafashan, J. Loodts, J. De Baeremaeker, and H. Ramon. The discrete element method (dem) to simulate fruit impact damage during transport and handling: Case study of vibration damage during apple bulk transport. *Postharvest Biology and Technology*, 41(1):92–100, 2006. 24 ELSEVIER SCIENCE BV.
- [WP03] S. R. Williams and A. P. Philipse. Random packings of spheres and spherocylinders simulated by mechanical contraction. *Phys. Rev. E*, 67(5):051301, May 2003.
- [YSH⁺03] X. Yan, Q. Shi, M. Hou, K. Lu, and C. K. Chan. Effects of air on the segregation of particles in a shaken granular bed. *Physical Review Letters*, 91(1):–, 2003. Times Cited: 3 Article English Cited References Count: 23 696yp.
- [ZRV04] N. H. Zhang, A. D. Rosato, and Vu. Analysis of instantaneous dynamic states of vibrated granular materials. *Mechanics Research Communications*, 31(5):525–544, 2004. 56 PERGAMON-ELSEVIER SCIENCE LTD.
- [ZXYZ02] Y. C. Zhou, B. H. Xu, A. B. Yu, and P. Zulli. An experimental and numerical study of the angle of repose of coarse spheres. *Powder Technology*, 125(1):45–54, 2002. 32 ELSEVIER SCIENCE SA.



Marco Ramaioli – Curriculum Vitae

Nov. 6th 2007

Born on April 21st, 1974 in Milan (Italy).
Italian nationality.
marco.ramaioli@gmail.com

Working experience:

- Jan.'08 – **Research Scientist** at Nestlé Research Centre, Lausanne, Switzerland.
- Oct.'99 – **Process Modelling specialist** at Nestlé PTC Orbe, Switzerland.
Dec.'07
Food process analysis, design, scale up and optimisation through modelling and experiments, both at laboratory and pilot scale.
- Mar.'99- **Research consultant** with Prof. Servida at Genova University, Italy on the control of pollutant emission from industrial burners through artificial neural networks.
Sept.'99
- Feb.'98- **Research internship** in Prof.M.Morbidelli group at Politecnico di Milano, Italy. Experimental and modelling study of the esterification of glycerol through reactive chromatography (master project).
Feb.'99

Education:

- May '03– **PhD** at EPFL under the supervision of Prof. Th.M.Liebling: Granular flow simulations and experiments for the food industry.
Dec '07
- Sept '93- **Chemical Engineering “Laurea Specialistica”** obtained from Politecnico di Milano in Feb.'99 with Honours.
Feb. '99

Languages:

Italian mother tongue;
Fluent in French;
Fluent in English (CAE, TOEFL, TWE);
Advanced level in Spanish.

Peer-reviewed publications:

M. Ramaioli, L. Pournin and Th. M. Liebling, On the vertical ordering of rods under vertical vibration, *Physical Review E*, 76, 2, 2007.

L. Pournin, M. Ramaioli, P. Folly, and Th. M. Liebling, About the influence of friction and polydispersity on the jamming behavior of bead assemblies, *European Physical Journal E*, 23, 2, 229-235, 2007.

L. Pournin, M. Weber, M. Tsukahara, J.-A. Ferrez, M. Ramaioli and Th. M. Liebling, Three-dimensional distinct element simulation of spherocylinder crystallization, *Granular Matter*, 7, 2-3, 119-126, 2005.

M. Ramaioli, L. Pournin and Th. M. Liebling, Numerical and experimental investigation of alignment and segregation of vibrated granular media composed of rods and spheres, *Powders and Grains 2005, II, 1359-1363*, R. Garcia-Rojo, H. J. Herrmann and S. McNamara, A.A.Balkema Publishers, 2005.

D. Gelosa, M. Ramaioli, G. Valente and M. Morbidelli. Chromatographic Reactors: Esterification of Glycerol with Acetic Acid Using Acidic Polymeric Resins. *Ind. Eng. Chem. Res.*, 42,536-6544, 2003.

M. Ramaioli, R. Baratti, e A. Servida, Monitoring Pollutant Emissions through Neural-Based Software Sensors, in *Engineering Neural Network - Problem Solutions (D. Tsaptsinos, Editore)*, Abo Akademis tryckeri, Abo 2000, 207-212, 2000.

Communications to scientific conferences:

M. Ramaioli, L. Pournin and Th. M. Liebling, Brazil's nut effect beyond spherical grains: elongation matters!, *Proc. of World Conference Particle Technology 5, Orlando, USA*, 2006.

A. Servida, M. Ramaioli and R. Baratti, Parametric Monitoring of Pollutant Emissions through Neural Software Sensor, *3rd European IFS Workshop, 7-8 June 2000, Santorini (Greece)*.

M. Ramaioli, A. Servida e R. Baratti, Monitoring Pollutant Emissions through Neural-Based Software Sensors, *International Conference on Engineering Applications of Neural Networks EANN2000, 17-19 July 2000, Kingston (U.K.)*.